DIVERSITY IN STRUCTURAL AND SPECTRAL CHARACTERISTICS OF SOME TRANSITION METAL COMPLEXES DERIVED FROM ALDEHYDE BASED THIOSEMICARBAZONE LIGANDS

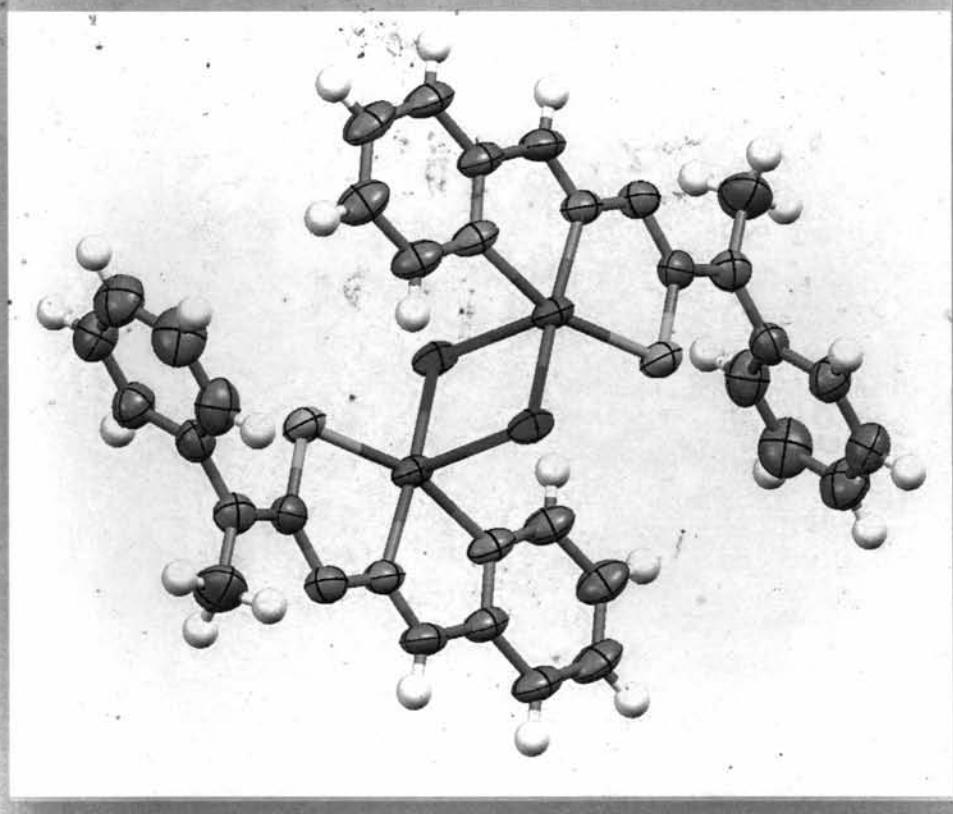

Thesis Submitted to the Cochin University of Science and Technology
in partial fulfillment of the requirements for the degree of

Doctor of Philosophy
in
Chemistry
by

Rapheal P. F.

Department of Applied Chemistry
Cochin University of Scince and Technology
Kochi 682 022

DIVERSITY IN STRUCTURAL AND SPECTRAL CHARACTERISTICS OF SOME TRANSITION METAL COMPLEXES DERIVED FROM ALDEHYDE BASED THIOSEMICARBAZONE LIGANDS

Thesis submitted to the
Cochin University of Science and Technology in partial fulfillment of the requirements for the award of the degree of

Doctor of Philosophy

in

Chemistry

by

RAPHEAL P.F.
(Reg. No. 2372)

Department of Applied Chemistry
Cochin University of Science and Technology
Kochi - 682 022
October 2006

Phone Off. 0484-2575804
Phone Res. 0484-2576904
Telex: 885-5019 CUIN
Fax: 0484-2577595
Email: mrp@cusat.ac.in
mrp_k@yahoo.com

DEPARTMENT OF APPLIED CHEMISTRY
COCHIN UNIVERSITY OF SCIENCE AND TECHNOLOGY
KOCHI - 682 022, INDIA

M.R. PRATHAPACHANDRA KURUP
Professor and Head

12 October 2006

CERTIFICATE

This is to certify that the thesis entitled "DIVERSITY IN STRUCTURAL AND SPECTRAL CHARACTERISTICS OF SOME TRANSITION METAL COMPLEXES DERIVED FROM ALDEHYDE BASED THIOSEMICARBAZONE LIGANDS" submitted by **Mr. RAPHEAL P.F.,** in partial fulfillment of the requirements of the degree of Doctor of Philosophy in Chemistry, to the Cochin University of Science and Technology, Kochi, is an authentic and bonafide record of the original research work carried out by him under my guidance and supervision. Further, the results embodied in this thesis, in full or in part, have not been submitted for award of any other degree.

M.R. Prathapachandra Kurup

(Supervising guide)

PREFACE

The work from which this thesis originated was carried out by the author in the Department of Applied Chemistry, Cochin University of Science and Technology, Kochi, during the period 2001-2006. In our laboratory, the development of new thiosemicarbazones and their metal complexes have been an active area of research during the past years because of the beneficial biological activities of these substances. Tridentate NNS and ONS thiosemicarbazone systems formed from heterocyclic and aromatic carbonyl compounds and their transition metal complexes are well-authenticated compounds in this field and their synthesis and characterization are well desirable. Hence, we decided to develop a research program aimed at the synthesis and characterization of novel thiosemicarbazones derived from pyridine-2-carbaldehyde and salicylaldehyde and their transition metal complexes. In addition to various physico-chemical methods of analysis, single crystal X-Ray diffraction studies were also used for the characterization of the ligands and complexes.

The thesis has been divided in to seven chapters carrying a detailed account of the novel ligands and their complexes with some first row transition metal ions. Chapter 1 is a review of applications and recent developments in the field of thiosemicarbazones and their metal complexes. Chapter 2 deals with the syntheses and characterization of the ligands. Crystal structures of two ligands and one intermediate compound is also discussed. Chapter 3 describes the syntheses and physico-chemical characterizations of binuclear and monomeric copper(II) complexes with the crystal structure of a binuclear square pyramidal complex. Chapter 4 deals with the syntheses and physico-chemical characterizations of octahedral manganese(II) complexes with the crystal structure of one complex. Syntheses and spectral characterizations of octahedral cobalt(III) complexes are discussed in Chapter 5. Crystal structures of two complexes are also included. Chapter 6 comprises syntheses and spectral characterizations of square planar and octahedral Ni(II) complexes with the crystal structures of two octahedral complexes. Chapter 7 describes the syntheses and physico-chemical characterizations of zinc(II) complexes with the crystal structure of a square pyramidal complex. Summary of the thesis is also given at the end.

CONTENTS

Chapter 1

Thiosemicarbazones – Biologically active materials, Analytical reagents and Coordinating agents

Chapter 2

Syntheses and characterization of the new thiosemicarbazone ligands

Chapter 7

Syntheses of zinc(II) complexes and studies on their structural and spectral characteristics

Thiosemicarbazones - Biologically active materials, Analytical reagents and Coordinating agents

1.1. Introduction

Chemical reactions were known to man long before chemistry had attained the status of science. It was found that substances changed their properties under certain external conditions, and this observation is a characteristic of chemical reactions. Thus the ancient Egyptians found that if malachite, a green ore, was fired with charcoal, a red metal was obtained, called copper. Medicinal application of metals can be traced back to almost 5000 years [1]. The development of modern medicinal inorganic chemistry, stimulated by the discovery of *cis*-dichlorodiammine platinum(II) [cisplatin] and its subsequent use as a drug in the treatment of several human tumors [2,3], has been facilitated by the inorganic chemist's extensive knowledge of the coordination and redox properties of metal ions. Metal centres, being positively charged, are favoured to bind to negatively charged biomolecules and the constituents of proteins and nucleic acids offer excellent ligands for binding to metal ions. The pharmaceutical use of metal complexes therefore has excellent potential.

Thiosemicarbazones (hydrazine carbothioamides) are a family of compounds with beneficial biological activity. They are very good ligands, and it has been shown that their biological activity is related to their ability to coordinate to metal centres in enzymes. One interesting thing is that the more pharmaceutically promising thiosemicarbazone derivatives possess additional functional groups that are not coordinated to their "primary" metal ion, suggesting that the biological activity may also depend on the non-coordinating groups.

1.2. Thiosmicarbazones in the biological field - a survey

Thiosemicarbazones and their metal complexes have been widely explored for nearly 50 years [4,5] because of their versatile biological activity and prospective use as drugs [6]. Owing to the interest they generate through a variety of biological properties ranging from anticancer [7], antitumour [8], antifungal [9] antibacterial [10]

antimalarial [11], antifilarial [12] antiviral [13] and anti-HIV [14] activities, thiosemicarbazones and their metal complexes have been extensively studied. The hypoxic selectivity of certain copper bis(thiosemicarbazones) and their use as vehicles for the delivery of radioactive copper isotopes to tumors [15] or leucocytes [16] has attracted much recent attention [17]. The hypoxic selectivity is strongly dependent on the substituents on the carbon backbone. Earlier studies on the biological properties of thiosemicarbazones and their metal complexes revealed that the biologically active thiosemicarbazone molecules were planar and a pyridine ring or a NNS tridentate system were present [18]. It is now well understood that the biological activity depends on the parent aldehyde or ketone [19, 20] and the presence of a bulky group at the terminal nitrogen considerably increases the activity [21]. Reports on N(4)-substituted thiosemicarbazones have concluded that, an additional potential bonding site together with the presence of bulky groups at the N(4) position of the thiosemicarbazone moiety greatly enhances biological activity [22-24].

The ability of thiosemicarbazone molecules to chelate with traces of metals in the biological system is believed to be a reason for their activity. By coordination, the lipophilicity, which controls the rate of entry into the cell, is modified, and some side effects may be decreased [25,26]. It has been proved that thiosemicarbazones block DNA synthesis in mammalian cells by inhibiting the enzyme, ribo-nucleoside-diphosphate reductase, presumably either *via* chelation with an iron ion required by the enzyme or because a preformed metal chelate of the inhibitor interacts with the target enzyme [27,28]. Reports also point out the capacity of thiosemicarbazones to sever the DNA strands [29]. A major clinical challenge in successful treatment of cancer with anticancer drugs is that certain tumour cells develop a particular phenotype, called multi drug resistance (MDR), which makes these cells resistant to other classes of anticancer agents to which the tumor cells have not been treated previously [30]. Synthesis and characterization of a palladium complex of phenathrenequinone thiosemicarbazone and evaluation of its antiproliferative properties in breast cancer cells and normal cells have been described [31]. The study suggests that the complex

is a potent antineoplastic agent that has selective activity against tumour cells and is effective against drug resistant breast cancer cells.

A number of authors have been interested in investigating the biological and medicinal properties of transition metal complexes of thiosemicarbazones in recent years. New square planar complexes of general formula, [M(NNS)Cl] (M = Pd(II), Pt(II); NNS = anionic forms of the 6-methyl-2-formylpyridine Schiff bases of *S*-methyl and *S*-benzyldithiocarbazates) have been prepared. Both the Schiff bases exhibit strong cytotoxicity against the human ovarian cancer (Caov-3) cell lines, the *S*-methyl derivative being two times more active than the *S*-benzyl derivative [32]. Palladium(II) and platinum(II) complexes of 5-chloro-1,3-dihydro-3-[2-(phenyl)-ethylidene]-2H-indol-2-one-hydrazine carbothioamide have been prepared and screened for their antimicrobial activity against the fungi *Macrophomina phaseolina* and *Fusarium oxysporum* by agar plate technique. The results prove that the compounds exhibit antimicrobial properties and it is important to note that the metal chelates show more inhibitory effects than the parent ligands. The increased lipophilic character of these complexes seems to be responsible for their enhanced biological potency [33].

The iron(II) complexes of 2-benzoylpyridine thiosemicarbazone as well as its N(4)-methyl and N(4)-phenyl analogues have been found to undergo oxidation giving the iron(III) analogues, which could be reduced back by cellular thiols such as thioredoxine, suggesting that this process could occur in biological media. The thoisemicarbazones have antifungal activity against *Candida albicans* that significantly decreases on coordination [34]. Cancer cells need more iron than normal body cells to sustain their abnormally rapid growth. Very recently, Prem Ponka from McGill University, Canada, and Des Richardson's group at the University of Sydney, Australia, have identified Dp44mT (di-2-pyridylketone-4,4,-dimethyl-3-thiosemicarbazone) as a particularly potent substance that can bind iron in a tight chelate complex and thus deplete tumors. Chelating behavior of di-2-pyridylketone thiosemicarbazones is an ongoing study in our laboratory also [7].

The antitumor activities of Mn^{2+}, Co^{2+}, Ni^{2+} and Cu^{2+} chelates of anthracene-9-carboxaldehyde thiosemicarbazone [35] and the cytotoxic activity of phenylglyoxal bis(thiosemicarbazone) against *Ehrlich ascites* carcinoma cells have been reported. These compounds were also screened for antimicrobial activity on *B.subtilis* and *E.coli* and it was found that they inhibited the bacterial growth considerably [36].

Platinum complexes of 2-acetylpyridine thiosemicarbazone has been synthesized in which intermolecular hydrogen bonds, π- π and weak Pt-Pt and Pt- π contacts lead to aggregation and to a two-dimensional supramolecular assembly. The complexes were found to have a completely lethal effect on Gram+ bacteria. Additionally, some of them showed effective antifungal activity towards yeast [37]. The effect of Pt(II) and Pd(II) complexes of 2-acetylpyridine thiosemicarbazone (HAcTsc) on sister chromatid exchange (SCE) rates, human lymphocyte proliferation kinetics, and leukemia P388 have been investigated. Among these compounds, $[Pt(AcTsc)_2]\cdot H_2O$ and $[Pd(AcTsc)_2]$were found to be the most effective in inducing antitumor and cytogenetic effects [38]. Antifungicidal, antibacterial and antifertility activities of biologically active heterocyclic thoisemicarbazones and their coordination complexes with the dimethylsilicon moiety have been described. Some ligands and their corresponding dimethylsilicon(IV) complexes have been tested for their effects on several pathogenic fungi and bacteria. Two representative complexes have also been found to act as sterilizing agents by reducing the production of sperm in male mice [39].

Adverse biological activities of thoisemicarbazones have been widely studied in rats and in other animal species using different doses, times and routes of administration. In this study, the rats were injected subcutaneously with a new thiosemicarbazone (HL) and its CuL_2 and ZnL_2 complexes. The aim of this study was to determine the effect of the new compounds on the serum antioxidant vitamins (A, E, C), selenium (Se), malondialdehyde (MDA) levels, erythrocyte GSH-Px enzyme activity and morphological changes in the liver, kidney and adrenal gland tissues. It was observed that erythrocyte GSH-Px activity, serum MDA and vitamins A, E concentrations were statistically changed, but serum levels of selenium, and vitamin C

were not changed. In conclusion, the parameters measured show that CuL_2 caused considerable oxidative stress and ZnL_2 behaved as an antioxidant [40].

1.3. Thiosemicarbazones in the analytical field

Thiosemicarbazones have applications in analytical field also. Some of the thiosemicarbazones produce highly colored complexes with metal ions. These complexes have been proposed as analytical reagents that can be used in selective and sensitive determinations of metal ions [41, 42]. Ferrocene derivatives containing thiosemicarbazone side chain have been investigated by cyclic voltammetry and positron annihilation lifetime (PAL) measurements. Positrons can form the positron-electron pair in molecular solids. Interest in the behaviour of the positron-electron pair is great because the probability of its formation and its lifetime depend upon the physical and chemical properties of the solid. It has been shown that the redox and the electron capture processes took place on the Fe atom [43]. Cu(II), Co(II) and Fe(II) in pharmaceutical preparations could be determined using pre-column derivatization and solvent extraction with 2-acetylpyridine-4-phenyl-3-thiosemicarbazone as complexing reagent [44].

The inhibition of corrosion of aluminium in HCl solution by some derivatives of thiosemicarbazones has been studied using weight loss and hydrogen evolution techniques. The thosemicarbazone dreivatives used are 2-acetylpyridine-4-phenyl thiosemicarbazone, 2-acetylpyridine-4-phenylisomethyl thiosemicarbazone and 2-acetylpyridine-4-phenylisoethyl thiosemicarbazone. The inhibition efficiency depended on the compound concentation [45].

1.4. Thiosemicarbazones – the coordinating agents

Thiosemicarbazones are thiourea derivatives obtained by condensation of thiosemicarbazide or N(4)-substituted thiosemicarbazide with a suitable aldehyde or ketone. Thiosemicarbazones are represented by the general formula (**I**), and when N(4) is substituted they can be represented by the general formula (**II**). The numbering

scheme shown in the figure is in accordance with the IUPAC system of numbering for thiosemicarbazones. However, it should be noted that the numbering schemes in the crystal structures are based on the types of different atoms present. In the formula (**II**), R^3 and R^4 can be alkyl or aryl groups or a part of a cyclic system. According to the IUPAC recommendations for the nomenclature of organic compounds, derivatives of thiourea represented by the general formula R^1R^2C=N-NH-CS-N R^3R^4, may be named by adding the class name thiosemicarbazone after the name of condensed aldehyde or ketone [46].

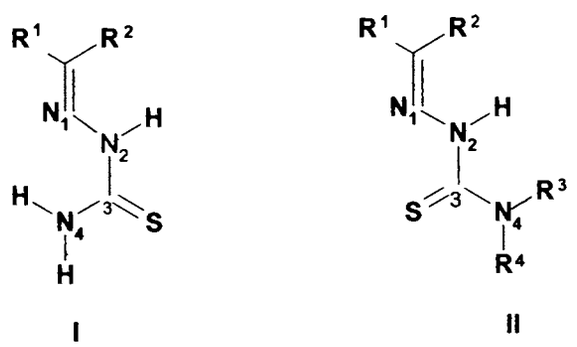

Fig. 1.1. General structures of thiosemicarbazones

Presence of C=N, make thiosemicarbazones exist as *E* and *Z* stereoisomers. Considering the thermodynamic stability, *E* isomer will predominate in the mixture [47]. The structure of the C=N-NH-CS-N backbone is usually almost planar with the S atom trans to azomethine N. Zhi Min Jin *et al.* have reported the crystal structure of pyridine-2-carbaldehyde thiosemicarbazone showing the *E* configuration [48].

Recently we have reported the crystal structure of pyridine-2-carbaldehyde N(4)-phenethylthiosemicarbazone in which the thiosemicarbazone group adopts an *EE* configuration, i.e., *trans* configurations are observed about both the azomethine and hydrazinic bonds [49]. Although there are several electronic and steric factors that may contribute to the adoption of this arrangement, the most important is probably that the trans arrangement places the amine and azomethine nitrogen atoms in relative positions more suitable for intramolecular hydrogen bonding [50]. In fact, the

complete substitution of amine hydrogens results in crystallization with S atom *cis* with azomethine nitrogen giving *Z* configuration.

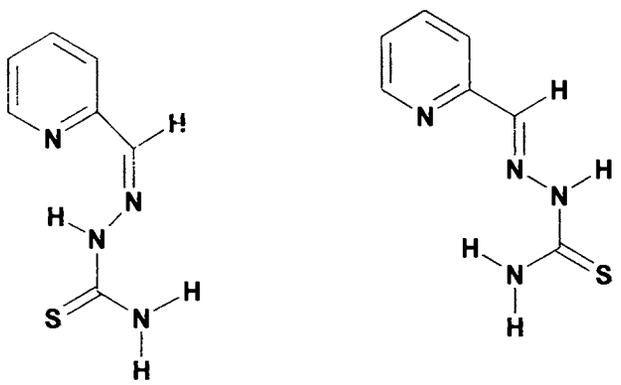

Z isomer *E* isomer

Fig. 1.2. *Z* and *E* isomers of pyridine-2-carbaldehyde thiosemicarbazone

Presence of NH-C=S group in thiosemicarbazones can bring about thione–thiol tautomerism. In solution thiosemicarbazones exist as an equilibrium mixture of thione (**III**) and thiol (**IV**) forms.

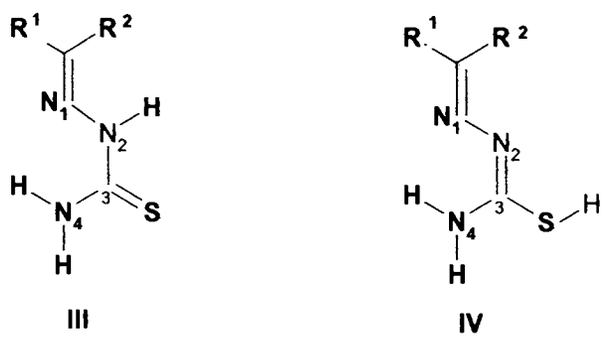

III **IV**

Fig. 1. 3. Thione and thiol forms of thiosemicarbazones

Enolization into the thiol form results in an effective conjugation along the thiosemicarbazone skeleton thus enhancing electron delocalization along the moiety. In the case of hetero aromatic thiosemicarbazones, delocalization of electron cloud is extended along with the generation of new potential sites for coordination. Upon coordination to a metal centre, the delocalization is further increased through the metal

chelate rings. This is one of the reasons for choosing pyridine-2-carbaldehyde as the carbonyl base of our ligands. Though thiosemicarbazones can coordinate to metals in the neutral thione form, usually chelation takes place through the anion formed by deprotonation of the hydrazinic NH group, *via* enolization to the thiol form. The stereochemistry adopted by the thiosemicarbazone ligand with transition metal ion depends essentially on the presence of additional coordination sites in the ligand moiety and the charge on the ligand which in turn is influenced by the thione-thiol equilibrium, and pH of the medium used for reaction. Studies have revealed that the steric effects of the various substituents in the thiosemicarbazone moiety considerably affect the stereochemistry.

Thiosemicarbazones can adopt a variety of different coordination modes. In most of the cases, thiosemicarbazones coordinate as bidentate ligands *via* azomethine nitrogen and thione/thiolato sulfur. When additional coordination functionality is present in the proximity of the donating centers, the ligands will coordinate in a tridentate manner. This can be accomplished either by the neutral molecule or by the monobasic anion upon loss of hydrogen. Although the thione form predominates in the solid state, solutions of thiosemicarbazone molecules show a mixture of both tautomers. As a result, depending upon the preparative conditions, the metal complex can be cationic neutral or anionic. There are cases where both the neutral and anionic forms of the ligand are involved in coordination [21]. The various coordination geometries encountered in this study will be discussed in the chapters following.

1.5. Scope and significance of the present work

The significance of thiosemicarbazones and their metal complexes, apart from their diverse chemical and structural characteristics, stems from not only their potential but also their proved application as biologically active molecules. The relationship between structure and biological activity has been covered in several papers [47,51]. Pyridine-2-carbaldehyde thiosemicarbazone was the first α-(N)-heterocyclic carboxyaldehyde thiosemicarbazone, reported to have carcinostatic effects [28,52]. Reports show that greatest activity occurs for 2-substituted pyridine

thiosemicarbazones with differences observed for 2-formylpyridine, 2-acetylpyridine and 2-benzoylpyridine derivatives and their metal complexes [53]. The highest biological activity for pyridine related thiosemicarbazones is achieved when N(4) position bears bulky groups [54-56]. Recently, the partial transformation of thioamide group into nitrile in pyridine-2-carbaldehyde thiosemicarbazonato copper(II) entities in aqueous basic medium was reported [57].

Thus, it is worthwhile to carry out the structural and spectral studies of heterocyclic thiosemicarbazones with different structural features as well as their metal complexes. Bearing in mind these findings and as part of our continuing studies on the synthetic utility and understanding of coordination geometry of thiosemicarbazones and their metal complexes we accepted the aims of this work as:

1. To synthesise and physico-chemically characterize the following new thiosemicarbazone ligands:

a) Pyridine-2-carbaldehyde-N(4)-*p*-methoxyphenyl thiosemicarbazone [HL^1]

b) Pyridine-2-carbaldehyde-N(4)-phenylethyl thiosemicarbazone [HL^2]

c) Pyridine-2-carbaldehyde N(4)-methyl, N(4)-phenyl thiosemicarbazone [HL^3]

d) Pyridine-2-carbaldehyde-N(4)-pyridyl thiosemicarbazone [HL^4]

e) Salicylaldehyde-N(4)-phenylethyl thiosemicarbazone [H_2L^5]

2. To find optimal conditions for synthesis of copper(II), manganese(II), cobalt(iii), nickel(II) and zinc(II) complexes of these ligands.
3. To find the compositions and probable structures of the complexes and study their spectral properties.
4. To confirm the structures of ligands and complexes by single crystal XRD studies.
5. To understand the intermolecular interactions in the ligands and complexes.

1.6. Introduction to the relevant analytical techniques

Several methods, conventional and modern are available for elucidating the structure of ligands and their coordination compounds. They include partial elemental

analysis, conductivity measurements, magnetic susceptibility studies, IR, UV-Vis, NMR and EPR spectral techniques and single crystal X-ray diffraction studies. Some of the physico chemical methods adopted during the present investigation are discussed below.

1.6.1. Elemental analysis

Elemental analyses were carried out using a Vario EL III CHNS analyzer at SAIF, STIC, Kochi, India and at Central Drug Research Institute, Lucknow, India using a Heraeus Elemental Analyser.

1.6.2. Magnetic susceptibility measurements

The magnetic susceptibility and the magnetic moment are often used to describe the magnetic behaviors of substances. A magnetic dipole is a macroscopic or microscopic magnetic system in which the north and south poles are separated by a short but definite distance. In the presence of a magnetic field, magnetic dipoles within a material experience a turning effect and become partially oriented. The magnetic moment refers to the turning effect produced when a magnetic dipole is placed in a magnetic field. The fundamental unit of magnetic moment is the Bohr magneton. For isotropic substances the magnetic susceptibility (χ) is defined by,

$$\chi = \mathbf{M/H}$$

where **M** is the magnetic moment per unit volume (magnetization) and **H** is the strength of magnetic field. The molar susceptibility χ_M is simply defined as the susceptibility per gram-mole. Hence,

$$\chi_M = \chi \times \textbf{molecular weight}$$

The magnetic susceptibility value calculated from magnetic measurements is the sum of paramagnetic and diamagnetic susceptibilities. To calculate the exact paramagnetic susceptibility (μ_{eff}), the value of diamagnetic susceptibility is subtracted from the susceptibility calculated from observed results. When the structural formula of the complexes is correctly known, diamagnetic correction can be calculated from Pascal's constants.

The magnetic susceptibility measurements were carried out in the polycrystalline state on a Vibrating Sample Magnetometer (VSM) at 5.0 kOe field strength at room temperature at the Indian Institute of Technology, Roorkee.

1.6.3. Infrared spectroscopy

The vibrational states of a molecule can be probed in a variety of ways. The most direct way is infrared spectroscopy because vibrational transitions typically require an amount of energy that corresponds to the infrared region of the spectrum between 4000 and 400 cm^{-1} (wavenumbers). Radiation in this region can be utilized in structure determination in coordination chemistry by making use of the fact that interatomic bonds in ligands absorb it.

Infrared spectra were recorded on a Thermo Nicolet AVATAR 370 DTGS model FT-IR Spectrophotometer with KBr pellets at SAIF, Kochi, India. The far IR spectra were recorded using polyethylene pellets in the 500-100 cm^{-1} region on a Nicolet Magna 550 FTIR instrument at Regional Sophisticated Instrument Facility, Indian Institute of Technology, Bombay.

1.6.4. Electronic spectroscopy

Electronic spectroscopy is the measurement of the wavelength and intensity of absorption of near-ultraviolet and visible light by a sample. UV-vis spectroscopy is usually applied to organic molecules and inorganic ions or complexes. The absorption of UV or visible radiation corresponds to the excitation of outer electrons.

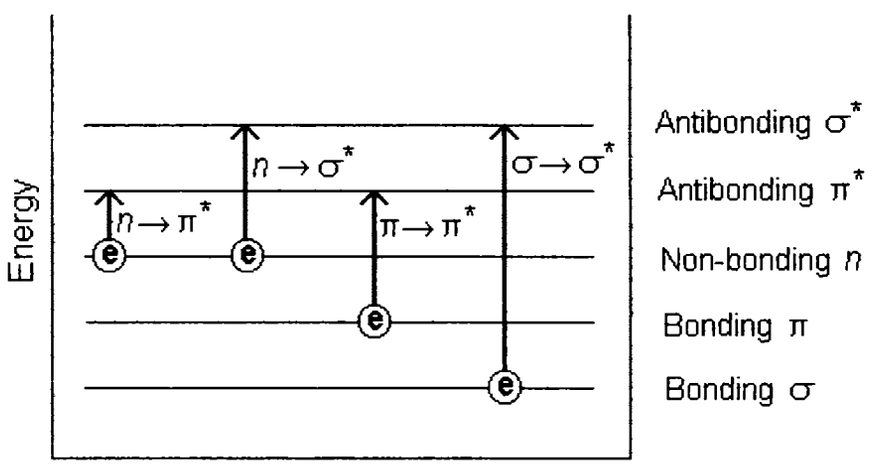

Fig. 1. 4. Possible transitions of π, σ, and n electrons

There are three types of electronic transitions that can be considered for coordination compounds. These are transitions involving a) π, σ, and *n* electrons of

ligands b) charge-transfer electrons and c) *d* and *f* electrons. Possible transitions of π, σ, and *n* electrons are shown in the Fig. 1.4. Most absorption spectroscopy of ligands is based on $n \rightarrow \pi^*$ and $\pi \rightarrow \pi^*$ transitions. Many inorganic species show Ligand-to-Metal Charge Transfer (LMCT) transitions and Metal-to-Ligand Charge Transfer (MLCT) transitions (not as common as LMCT). Transition probability in ligand field transitions (*d-d* transitions) is determined by the spin selection rule and the orbital (Laporte) selection rule.

Electronic spectra were recorded on a Cary 5000, version 1.09 UV-Vis-NIR Spectrophotometer from solutions of compounds in Chloroform/DMF at SAIF, Kochi.

1.6.5. NMR Spectroscopy

^{1}H NMR spectra were recorded using Bruker AMX 400 FT-NMR Spectrometer using TMS as the internal standard at Sophisticated Instrumentation Facility, Indian Institute of Science, Bangalore.

1.6.6. EPR spectroscopy

Electron paramagnetic resonance (EPR) is the process of resonant absorption of microwave radiation by paramagnetic ions or molecules, with at least one unpaired electron spin, in the presence of a static magnetic field. EPR was discovered by Zavoisky in 1944. For an electron with spin, s = ½, the spin angular momentum quantum number will have values $m_s = \pm ½$ which gives rise to a doubly degenerate spin energy state. In presence of an external magnetic field the degeneracy is lifted and these electron spin states are separated. The low energy state will have the spin magnetic moment aligned with the applied field ($m_s = - ½$). The high-energy state will have the spin magnetic moment opposed to the applied field ($m_s = + ½$). A transition is induced by microwave radiation of frequency *v* such that $\Delta E = h\nu = g\beta H$, where *h* is Planck's constant, β is the Bohr magneton, and *H* is the magnitude of the applied field. The proportionality factor *g* is a function of the electron's environment and it is called the spectroscopic splitting factor or Lande splitting factor (for the theoretical 'free'

electron, g = 2.0023). These electronic states are again split by their interaction with the spin of the nucleus (termed hyperfine coupling) into different energy states, each separated by the hyperfine coupling constant, A. Number of hyperfine lines is given by (2nI+1) where n is the number of equivalent nuclei with spin I. Further splitting of states by nearby nuclei, such as ^{14}N is referred to as superhyperfine coupling [58]. Symmetry can also have an effect on EPR spectra. If the spectra are obtained from frozen solutions or from a powder, where the anisotropy is not averaged away by motion of the molecule, a complex pattern can emerge. When $g_x = g_y = g_z$ in a perfectly cubic crystal, such a g value is the isotropic one. In axial environment the g factors are anisotropic ($g_z = g_{\parallel}$ and g_x, $g_y = g_{\perp}$). For a rhombic molecular environment, three g factors are observed.

EPR spectral measurements were carried out on a Varian E-112 X-band spectrometer using TCNE as standard at Regional Sophisticated Instrumentation Facility, Indian Institute of Technology, Bombay.

1.6.7. Conductivity measurements

The molar conductivities of the complexes in dimethylformamide (DMF) solutions (10^{-3} M) at room temperature were measured using a direct reading conductivity meter at DAC, CUSAT, Kochi.

1.6.8. X-Ray crystallography

The crystallographic data were collected using 1) a CrysAlis CCD, Oxford Diffraction Ltd. with graphite monochromated Mo Kα (λ = 0.71073 Å) radiation at the National Single Crystal X-Ray Diffraction Facility, IIT, Bombay, India, 2) a Bruker Smart Apex CCD diffractometer equipped with graphite monochromated Mo Kα (λ = 0.71073 Å) radiation at temperature 293 K, at Department of Chemistry, Punjab University, Chandigarh and at Analytical Sciences Division, Central Salt and Marine Chemicals Research Institute, Bhavnagar, Gujarat 3) a Bruker Smart Apex2 CCD area detector diffractometer equipped with graphite monochromated Mo Kα (λ = 0.71073 Å) radiation at temperature 283 K at X-ray Crystallography Unit, School of Physics, Universiti Sains Malaysia, Penang, Malaysia. The trial structure was solved using

SHELXS-97 [60] and refinement was carried out by full- matrix least squares on F^2 (SHELXL) [60]. Molecular graphics employed were ORTEP-III [61] and PLATON [62].

Conclusion

This chapter has dealt with an extensive literature study relating thiosemicarbazones and their transition metal complexes. Many authors have reported the anticancer, antitumor, antifungal, antibacterial, antimalarial, antifilarial, antiviral and anti-HIV activities of these compounds. They have been tested against leprosy, psoriasis, rheumatism and smallpox. A number of metal complexes of thiosemicarbazones have found application as analytical reagents. The nature of the aldehyde and ketone from which the thiosemicarbazone is obtained and the nature of the substituents attached at N(4) influence the biological activity. Based on preparative conditions and availability of additional bonding site in the ligand moiety, complexes of thiosemicarbazones assume various stereochemical forms. Thiosemicarbazones exist as *E* and *Z* isomers and they exhibit thione–thiol tautomerism. The analytical methods in thiosemicarbazone coordination chemistry include elemental analyses, conductivity measurements, magnetic susceptibility studies, various spectral studies and single crystal X-ray diffraction.

References

1. C. Orvig, M.J. Abrams, Chem. Rev. 99 (1999) 2201.
2. B. Rosenberg, L. Vancamp, J.E. Troska, V.H. Mansour, Nature (London) 222 (1969) 385.
3. B. Rosenberg, L. Vancamp, Cancer Res. 30 (1970)1977.
4. A.R. Cowley, J.R. Dilworth, P.S. Donnelly, E. Labisbal, A. Sousa, J. Am. Chem. Soc. 124 (2002) 5270.
5. G.V. Bahr, G. Schleizer, Z. Anorg. Chem. *280* (1955) 161.

6. D.L. Klayman, J.P. Scovill, J.F. Bartosevich, J.Bruce, J. Med.Chem. 26 (1983) 35. and references therein.
7. V. Philip, V. Suni, M.R.P. Kurup, M. Nethaji, Polyhedron 25 (2006) 1931.
8. F.A. French, E.J. Blanz Jr., J. Med. Chem. 9 (1996) 585.
9. M. Das, S.E. Livingstone, Br. J. Cancer 37 (1978) 466.
10. A.S. Dobek, D.L.Klayman, E.T. Dickson, J.P. Scovill, E.C.Tramont, Antimicrob. Agents Chemother. 18 (1980) 27.
11. A. Usman, I.A. Razak, S. Chantrapromma, H-K. Fun, A. Sreekanth, S. Sivakumar, M.R.P. Kurup, Acta Cryst. C (2002) 461.
12. D.L. Klayman., A.J. Lin, J.W. McCall, J. Med. Chem. 34 (1991) 1422.
13. C. Shipman Jr., H. Smith, J.C. Drach, D.L. Klayman, Antiviral Res. 6 (1986) 197.
14. A.K. El-Sawaf, D.X. West, R.M. El-Bahnasawy, F.A. El-Saied, Transition Met. Chem. 23 (1998) 227.
15. N.Takahashi, Y. Fujibayashi,Y. Yonekura, M.J. Welch, A.Waki, T. Tsuchida, N. Sadato, K. Sugimoto, H. Itoh, Ann. Nucl. Med.14 (2000) 323.
16. M.D. Yu, M.A. Green, B.H. Mock, S.M. Shaw, J. Nucl. Med. 30 (1989), 920.
17. C.J. Anderson, M. J. Welch, J. Chem. Rev. 99 (1999) 2219.
18. J.G. Tojal, A.G. Orad, J.L. Serra, J.L. Pizarro, L. Lezama, Arriortua, T. Rojo, J. Inorg. Biochem. 75 (1999) 45.
19. S. Padhye, G.B. Kauffman, Coord. Chem. Rev. 63 (1985) 127.
20. E. Lukevics, D. Jansone, K. Rubina, E.Abele, S. Germane, L.Leite, M. Shymaska, J. Popelis,. Eur. J. Med. Chem. 30 (1995) 983.
21. M. Joseph, M. Kuriakose, M.R. P. Kurup, E. Suresh, A. Kishore, S.G. Bhat, Polyhedron 25 (2006) 61.
22. S.K. Jain, B.S. Garg, Y.K. Bhoon, Spectrochim. Acta A 42 (1986) 959.
23. M.E. Hossain, M.N. Alam, J. Begum, M.A. Ali, M. Nazimudhin, F.E. Smith, R.C. Hynes, Inorg. Chim. Acta 249 (1996) 207.
24. W.-Hu, W. Zhou, C.-Xia, X. Wen, Bioorg. & Med. Chem. Lett. 16 (2006) 2213.
25. N. Farrel, Coord. Chem. Rev. 1 (2002) 232.

26. H. Beraldo, D. Gambino, Mini Rev. Med. Chem. 4 (2004) 159.
27. I. Antonini, F. Claudi, P. Franchetti, M. Grifantini, S. Martelli, J.Med. Chem. 20 (1977) 447.
28. A.C. Sarotelli, K.C. Agarwal, A.S. Tsiftsoglou, A.E.Moore, Advances in enzyme regulation, Pergamon, New York 15 (1997) 117.
29. P. Sonawane, A. Kumbhar, S.B. Padhye, R.J. Butcher, Transition Met. Chem. 19 (1994) 277.
30. J.S.K. Chen, N. Agarwal, K. Mehta, Breast Cancer Res. Treat. 71 (2002) 237.
31. S. Padhye, Z. Afrasiabi, E. Sinn, J. Fok, K. Mehta, N. Rath, Inorg.Chem. 44 (2005) 1154.
32. M.A. Al, A.H. Mirza, R.J. Butcher, K.A. Crouse, Transition Met.Chem. 31 (2006) 79.
33. R.V. Singh, N.Fahmi, M.K. Biyala, J. Iranian Chem. Soc. 2 (2005) 40.
34. R.F.F. Costa, A.P. Rebolledo, T. Matencio, H.D.R. Calado, J.D. Ardisson, M.E. Cortés, B. L. Rodrigues, H. Beraldo, J.Coord.Chem. 58 (2005) 1307.
35. J.Thomas, G. Parameswaran, Asian J. Chem.14 (2002) 1354.
36. N. Murthy, T.S. Dharmarajan, Asian J. Chem.14 (2002) 1325.
37. D.K-Demertzi, M.A. Demertzis, J.R. Miller, C. Papadopoulou, C. Dodorou, G. Filousis, J.Inorg.Biochem. 86 (2001) 555.
38. Z. Iakovidou, A. Papageorgiou, M.A. Demertzis, E. Mioglou, D. Mourelatos, A. Kotsis, P. N. Yadav, D.K-Demertzi, Anti-Cancer Drugs 12 (2001) 65.
39. D. Singh, R.V. Singh, R.B. Goyal, Appl. Organomet. Chem. 5 (2004) 45.
40. M. Karatepe, F. Karatas, Cell Biochem. Funct. Sept.(2005).
41. T. Atalay, E.G. Akgemci, Tr. J. Chem. 22 (1998) 123.
42. R. B. Singh, B. S. Garg, R.P. Singh, Talanta 25 (1978) 619.
43. J.E.J.C. Graúdo, C. A. L. Filgueiras, A. M-Netto, A. A. Batista, J. Braz. Chem. Soc. 11 (2000) 237.
44. Y. Khuhawar, Z.P. Memon, S.N. Lanjwani, Chromatographia 41 (1995) 236.
45. P.C. Okafor, E.E. Ebenso, U.J. Ekpe, Bull. Chem.Soc. Ethiopia, 18(2004) 181.
46. R. Panico, W.H. Powell, J.C. Richer (Eds), IUPAC Nomenclature of Organic Compounds, Blackwell, London, (1993) 105.

47. D.X. West, A.E Liberta, S.B. Padhye, R C. Chikate, P.B Sonawane, A.S. Kumbhar, R.G. Yerande, Coord. Chem. Rev. 123 (1993) 49.
48. Z.M. Jin, L.S.L. He, H. Guo, H.T. Wang, Acta Cryst. E59 (2003) o1909.
49. H.K. Fun, S.Chantrapromma, P. F.Rapheal, V. Suni, M. R.P. Kurup. Acta Cryst. E62 (2006) o125.
50. D. Chattopadhyay, S. K. Mazumdar, T. Banerjee, W. S. Sheldrick, Acta Cryst. C45 (1989) 314.
51. D. X. West, S. B. Padhye, P. B.Sonawane, Struct. Bond. 76 (1991) 1.
52. F.A. French, E. Blanz Jr. J Med. Chem 13 (1970) 1117.
53. A.E. Liberta, D.X. West, Biometals 5 (1992) 121.
54. G.M. de Lima, J.L. Neto, H. Beraldo, H.G.L. Siebald, D.J. Duncalf, J. Mol. Str. 604 (2002) 287.
55. D.L. Klayman, J.P. Scovill, J.F. Bartosevich, C.J. Mason, J. Med.Chem. 22 (1979) 1367.
56. D.L. Klayman, J.P. Scovill, J.F. Bartosevich, T.S. Griffin, C.J. Mason, J. Med.Chem. 22 (1979) 855.
57. P. G-Saiz , R. G-García , M.A. Maestro, J. L. Pizarro , M.I. Arriortua, L. Lezama, T .Rojo, J.G-Tojal, Eur. J. Inorg. Chem. 17 (2005) 3409.
58. T.S. Smith, R.L. Brutto, V.L. Pecoraro, Coord. Chem. Rev. 228 (2002) 1.
59. W.J. Geary, Coord. Chem. Rev. 7 (1971) 81.
60. G. M. Sheldrick (1997) SHELXS97 and SHELXL97. Bruker AXS Inc., Madison, Wisconsin, USA.
61. G. M. Sheldrick (1997) SHELXS97 and SHELXL97. Bruker AXS Inc., Madison, Wisconsin, USA.
62. A. L. Spek, J. Appl. Cryst. 36 (2003) 7.

Syntheses and characterization of the new thiosemicarbazone ligands

2.1. Introduction

The need for novel antimicrobial compounds is of absolute importance, as many of the antimicrobial agents currently in use are showing decreased effectiveness due to increased microbial resistance towards them. Current biological and chemical research, therefore, has focused much attention on this ever-present and increasingly dangerous problem. Among the many types of compounds being investigated for antimicrobial properties, the thiosemicarbazones have a very important position. Many of these compounds have shown significant biological activity (antibacterial, antiviral, antifungal, antitumoural etc.), especially those containing heterocyclic and/or aromatic rings. Earlier works have also shown that transition metal complexes of thiosemicarbazones often show an even greater amount of bioactivity. In keeping with past research, we present in this chapter the preliminary results of a study of the following five thiosemicarbazones.

a) Pyridine-2-carbaldehyde-N(4)-*p*-methoxyphenyl thiosemicarbazone [HL^1]

b) Pyridine-2-carbaldehyde-N(4)-phenylethyl thiosemicarbazone [HL^2]

c) Pyridine-2-carbaldehyde [N(4)-methyl, N(4)-phenyl thiosemicarbazone [HL^3]

d) Pyridine-2-carbaldehyde-N(4)-pyridyl thiosemicarbazone [HL^4]

e) Salicylaldehyde-N(4)-phenylethyl thiosemicarbazone [H_2L^5]

2.2. Experimental

The thiosemicarbazone ligands (Fig. 2.1) were synthesized by adopting and modifying a reported procedure of Scovill *et al.* [1].

2.2.1. Materials

Pyridine-2-carabaldehyde (2-formylpyridine), salicylaldehyde, 2-amino-pyridine, paraanisidine, 2-phenylethylamine (Fluka), carbondisulphide, N-methylaniline (Merck), hydrazine hydrate (98%, Glaxo fine Chemicals) were used as received. Acetonitrile (S.D.fine) was dried overnight and distilled over activated

alumina. Methanol and ethanol were dried over fused $CaCl_2$ and distilled. Other solvents were purified and dried by using standard procedures.

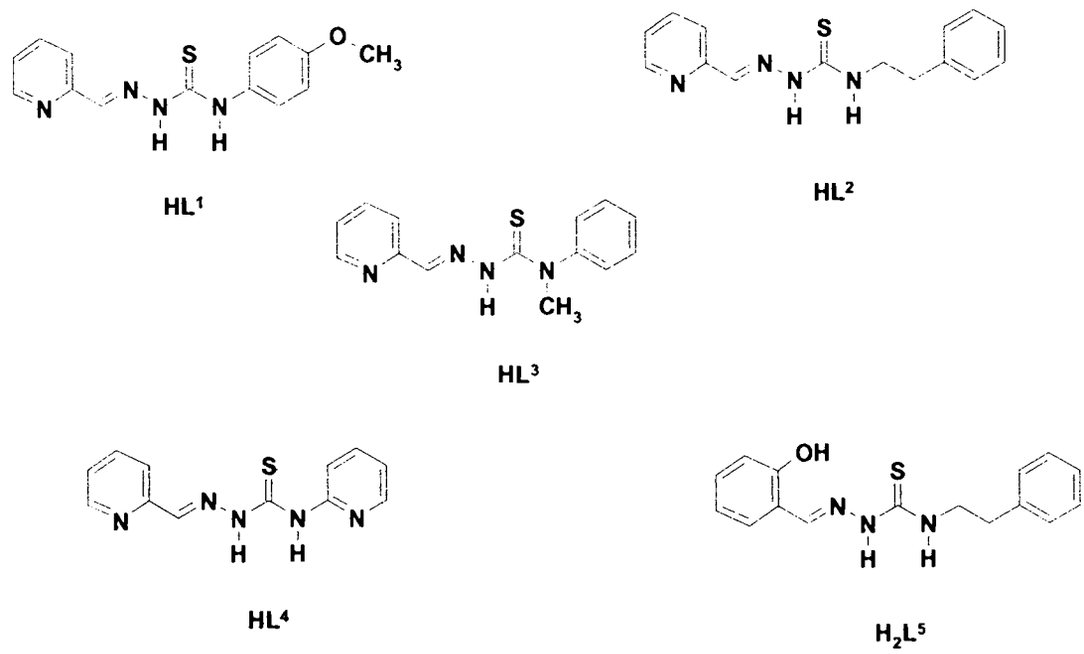

Fig. 2. 1. Structures of the thiosemicarbazones

2.2.2. Preparation of ligand precursors

2.2.2.1.. Carboxymethyl-N-methyl-N-phenyl dithiocarbamate

A mixture consisting of 12 ml CS_2 (15.2 g, 0.2 mol) and 21.6 ml (21.2 g, 0.2 mol) of N-methylaniline was stirred with a solution of 8.4 g (0.21mol) of NaOH in 250 ml water for 4 hours. When the organic layer had disappeared, the straw-coloured solution was treated with 23.2 g of sodium chloroacetate and allowed to stand over night (17 hrs). The solution was acidified with concentrated HCl (25 ml) and the solid that formed was filtered, washed well with water and dried. This afforded 39.7 g (82%) of the pale buff colored carboxymethyl-N-methyl-N-phenyl dithiocarbamate (m.p.197-198 °C). (Scheme 2.1).

2.2.2.2. N-methyl-N-phenyl-3-thiosemicarbazide

A mixture containing carboxymethyl-N-methyl-N-phenyl dithiocarbamate (17.8 g, 0.073 mol), hydrazine hydrate (98%, 20 ml) and water (10 ml) was heated on the rings of the water bath for 22 minutes. The compound formed was filtered, washed with water, dried and recrystallised from 2:1 alcohol. Yield 78%. m.p. 124-125 °C. (Scheme 2.2).

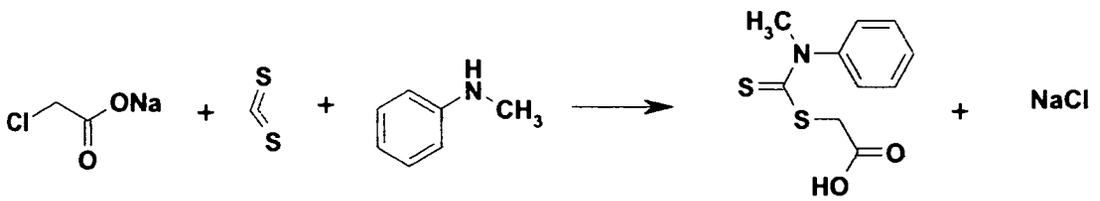

Scheme 2.1

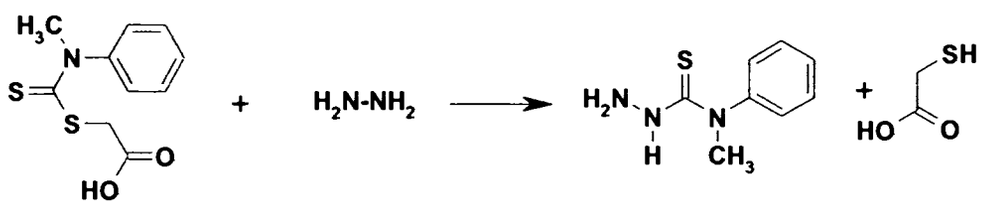

Scheme 2.2

2.2.3. Syntheses of ligands

2.2.3.1. Pyridine-2-carbaldehyde-N(4)-p-methoxyphenyl thiosemicarbazone [HL^1]

A solution containing 1.00 g (5.52 mmol) of 4-methyl-4-phenyl-3-thiosemicarbazide, 0.679 g (5.52 mmol) of 4-methoxyaniline (*p*-anisidine) and 0.591 g (5.52 mmol) of pyridine-2-carbaldehyde in 5 ml of MeCN was heated at reflux for 1½ hours. The solution was chilled (overnight) and the compound that formed was filtered and washed well with MeCN. The compound was recrystallised from ethanol and dried *in vacuo* over P_4O_{10} Yield 58%. m.p. 175-177 °C (Scheme 2.3).

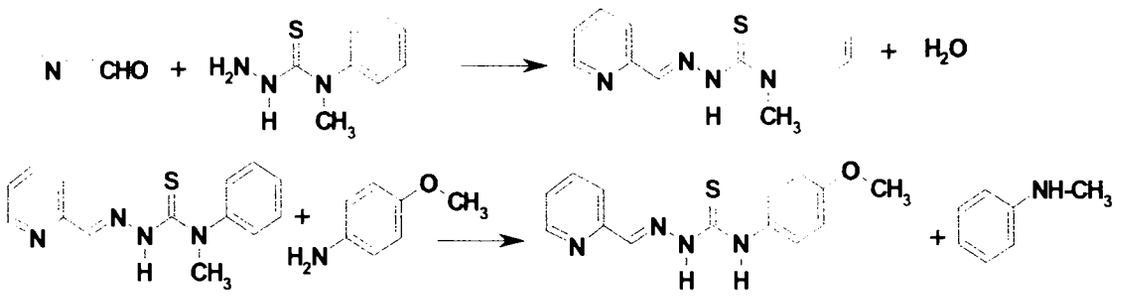

HL^1

Scheme 2.3

2.2.3.2. Pyridine-2-carbaldehyde-N(4)-phenylethyl thiosemicarbazone [HL^2]

A solution containing 1 g (5.52 mmol) of 4-methyl-4-phenyl-3-thiosemicarbazide, 0.725 ml (5.52 mmol) 2-phenylethylamine and 0.591 g (5.52 mmol) pyridine-2-carbaldehyde in 5 ml MeCN was heated at reflux for 1 hr. The solution was chilled (overnight) and the compound that formed was filtered and washed well with MeCN. The compound was recrystallised from ethanol and dried *in vacuo* over P_4O_{10}. Yield 73%. m.p. 153-155 °C. Single crystals of XRD quality were obtained by the slow evaporation of ethanol solution of the compound. (Scheme 2.4).

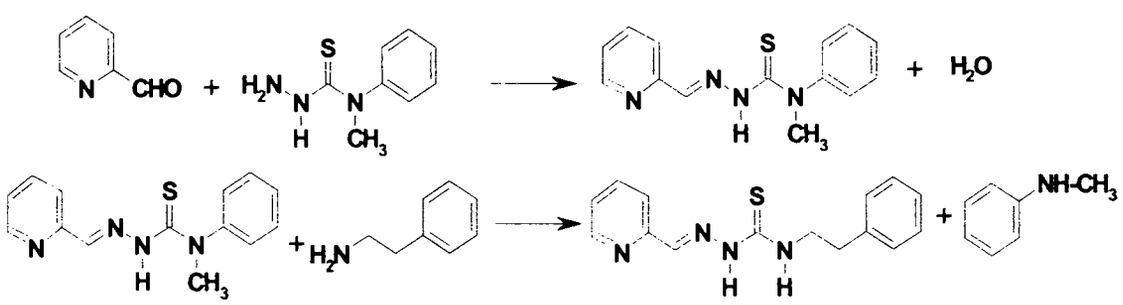

HL^2

Scheme 2. 4

2.2.3.3. Pyridine-2-carbaldehyde[N(4)-methyl, N(4)-phenyl thiosemicarbazone [HL^3]

A solution containing 1.00 g (5.52 mmol) of 4-methyl-4-phenyl-3-thiosemicarbazide and 0.591 g (5.52 mmol) of pyridine-2-carbaldehyde in 5 ml of MeCN was heated at reflux for 1 hour. The solution was chilled (overnight) and the compound that formed was filtered and washed well with MeCN. The compound was

recrystallised from ethanol and dried *in vacuo* over P_4O_{10}. Yield 63%. m.p. 193-195 °C. Single crystals of XRD quality were obtained by the slow evaporation of ethanol solution of the compound. (Scheme 2.5).

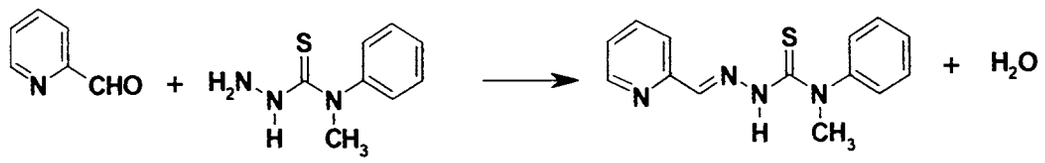

Scheme 2.5 HL^3

2.2.3.4. Pyridine-2-carbaldehyde-N(4)-pyridyl thiosemicarbazone [HL^4]

A solution containing 1.00 g (5.52 mmol) of 4-methyl-4-phenyl-3-thiosemicarbazide, 0.520 g (5.52 mmol) of 2-aminopyridine and 0.591 g of pyridine-2-carbaldehyde in 5 ml of MeCN was heated at reflux for 15 minutes. The solution was chilled (overnight) and the compound that formed was filtered and washed well with MeCN. The compound was recrystallised from ethanol. Yield 52%. m.p. 175-177 °C (Scheme 2.6).

2.2.3.5. Salicylaldehyde-N(4)-phenylethyl thiosemicarbazone [H_2L^5]

A solution containing 1.00 g (5.52 mmol) of 4-methyl-4-phenyl-3-thiosemicarbazide, 0.725 ml (5.52 mmol) of 2-phenylethylamine and 0.675 g (5.52 mmol) of salicylaldehyde in 5 ml of MeCN was heated at reflux for 15 minutes. The solution was chilled (overnight) and the compound that formed was filtered and washed well with MeCN. The compound was recrystallised from ethanol. Yield 82%. m.p. 186-188 °C (Scheme 2.7).

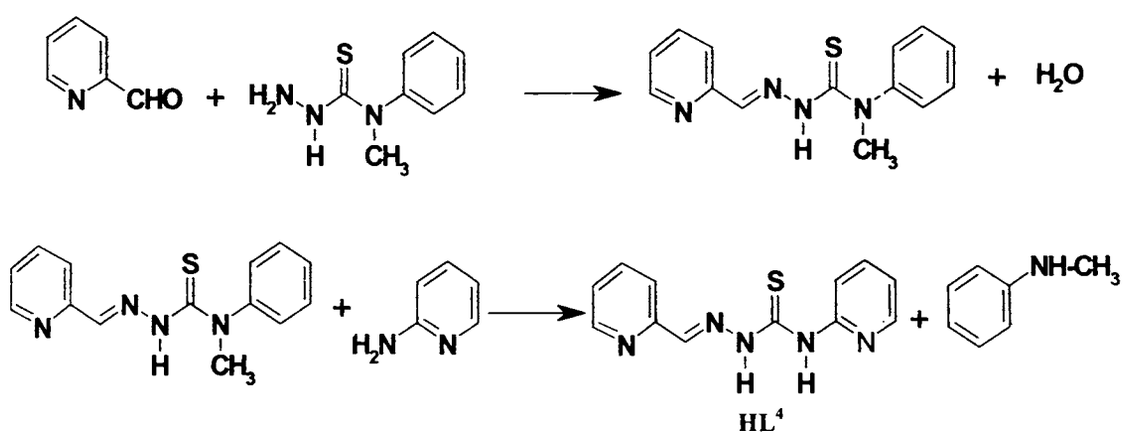

Scheme 2. 6

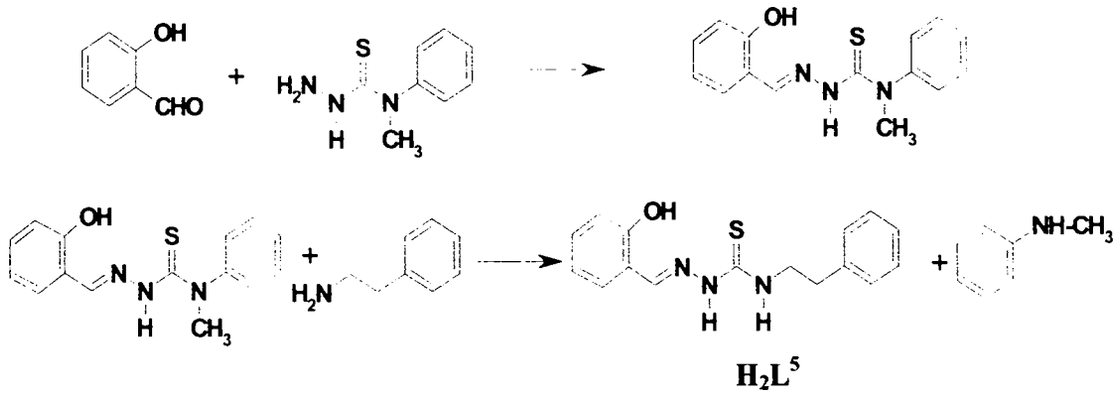

Scheme 2.7

Interestingly, during the synthesis of HL^4, we could isolate single crystals of an unusual intermediate product, *N-(pyridin-2-yl)hydrazinecarbothioamide (HL^4A)*, from the reaction mixture. The structure of this compound was also resolved by X-ray diffraction.

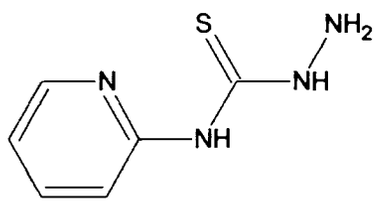

Fig. 2.2. Structure of HL^4A

2.3. Physical Measurements

Elemental analyses were carried out using a Vario EL III CHNS analyzer at SAIF, Kochi, India. Infrared spectra were recorded on a Thermo Nicolet AVATAR 370 DTGS model FT-IR spectrophotometer with KBr pellets at SAIF, Kochi, India. Electronic spectra were recorded on a Cary 5000, version 1.09 UV-Vis-NIR spectrophotometer from a solution in chloroform. ^1H NMR spectra were recorded using Bruker AMX 400 FT-NMR Spectrometer using TMS as the internal standard at Sophisticated Instrumentation Facility, Indian Institute of Science, Bangalore.

2.4. X-Ray crystallography

The crystallographic data and structure refinement parameters for HL^2, HL^3 and HL^4A are given in Tables 2.5, 2.7 and 2.13 respectively. The data of HL^3 and

HL^4A were collected using a Bruker Smart Apex CCD area detector diffractometer equipped with graphite monochromated Mo Kα (λ = 0.71073 Å) radiation, at Central Salt and Marine Chemicals Research Institute, Bhavnagar, Gujarat, India. The compound HL^2 was diffracted by a Bruker Smart Apex2 CCD area detector diffractometer equipped with graphite monochromated Mo Kα (λ = 0.71073 Å) radiation, at School of Physics, Universiti Sains Malaysia, Penang, Malaysia. The trial structures were solved using SHELXS-97 [2] and refinement was carried out by full-matrix least squares on F^2 using the SHELXL [2] and SHELXTL [3] software packages. The collected data were reduced using SAINT program [4]. Molecular graphics employed were ORTEP-III [5] and PLATON [6].

2.5. Results and discussion

The synthesis of thiosemicarbazones from 4-methyl-4-phenyl-3-thiosemicarbazide comprises two processes namely condensation and transamination. The former involves condensation of 4-methyl-4-phenyl-3-thiosemicarbazide with an appropriate carbonyl compound and latter involves removal of N-methylaniline from the condensation product by the reaction with a primary or secondary amine. It has been found that amine used for transamination also functions as a catalyst and the stronger the basicity of amine, the better will be its transamination ability. The compound HL^4A mentioned above might have formed by the transamination between 4-methyl-4-phenyl-3-thiosemicarbazide and 2-aminopyridine. The solvent also plays a very important role in shaping the product and in the control of rate of reaction. In the synthesis of N-N-S donor ligands, acetonitrile was found to be very efficient but for O-N-S donor ligands, methanol is a better solvent.

Table 2. 1. Stoichiometries and partial elemental analyses of the thiosemicarbazones

Compound	Stoichiometry	Found (Calc.)%			
		C	H	N	S
HL^1	$C_{14}H_{14}N_4OS \cdot H_2O$	55.08(55.25)	5.16(5.30)	18.31(18.41)	10.12(10.54)
HL^2	$C_{15}H_{16}N_4S$	63.66(63.35)	5.93(5.67)	19.63(19.70)	11.44(11.28)
HL^3	$C_{14}H_{14}N_4S$	61.51(62.20)	4.98(5.22)	20.46(20.72)	11.92(11.86)
HL^4	$C_{12}H_{11}N_5S$	55.72(56.01)	4.40(4.31)	27.75(27.22)	12.18(12.46)
H_2L^5	$C_{16}H_{17}N_3OS \cdot 1/3EtOH$	63.42(63.60)	5.93(6.08)	13.86(13.35)	10.70 (10.19)

Table 2.1 lists the stoichiometries and partial elemental analyses of the thiosemicarbazones. All of them are yellow in colour.

2.5.1. Infrared spectra

Table 2. 2. Infrared spectral assignments (cm^{-1}) of the thiosemicarbazones

Compound	ν(C=N)	ν(N-N)	ν/δ(C-S)	py(ip)	py(op)	ν(^{2}N-H)	ν(^{4}N-H)	ν(O-H)
HL^1	1584	1024	1334,837	613	401	3134	3310	----
HL^2	1586	1079	1324,897	622	406	3129	3374	----
HL^3	1590	1035	1307,779	614	421	3158	----	----
HL^4	1593	1078	1298,929	614	412	3117	3313	----
H_2L^5	1619	1003	1383,840	----	----	3250	3346	3455

The assignments of IR spectral bands most useful in establishing the structural identity of the ligands are listed in Table 2.2. The ν(S-H) band expected at 2570 cm^{-1} is absent in the IR spectra of these ligands but ν(^{2}N-H) bands are present at 3134, 3129, 3158, 3117, and 3250 cm^{-1} respectively for HL^1, HL^2, HL^3, HL^4 and H_2L^5, indicating that the ligands remain in the thione form in the solid state [7,8]. The bands corresponding to ν(^{4}N-H) appear in the range 3310 - 3374 cm^{-1} [9]. The ν(O-H) stretching band of H_2L^5 is observed at 3455 cm^{-1}. The azomethine bands ν(C=N) appear at 1584 - 1619 cm^{-1}, in agreement with earlier reports of N(4)-substituted thiosemicarbazones [10,11].

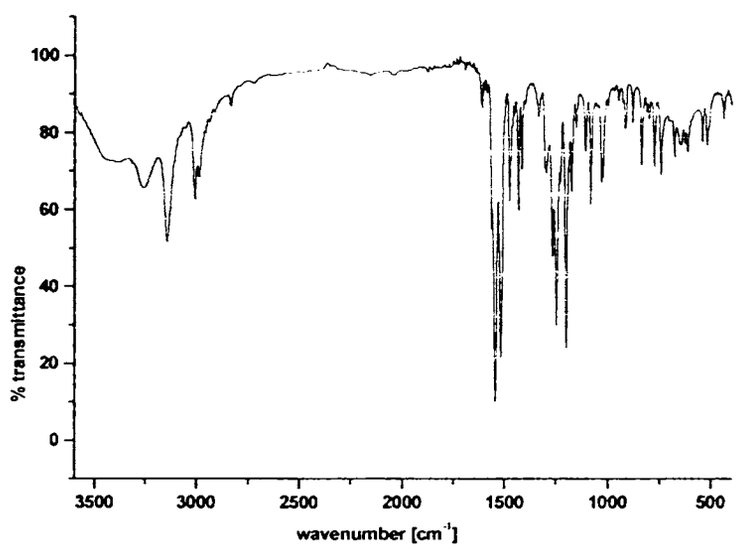

Fig. 2. 3. IR spectrum of HL^1

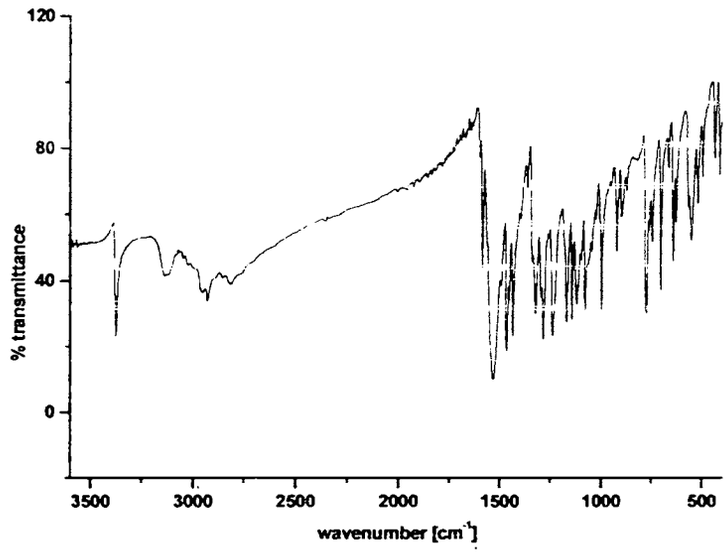

Fig. 2. 4. IR spectrum of HL^2

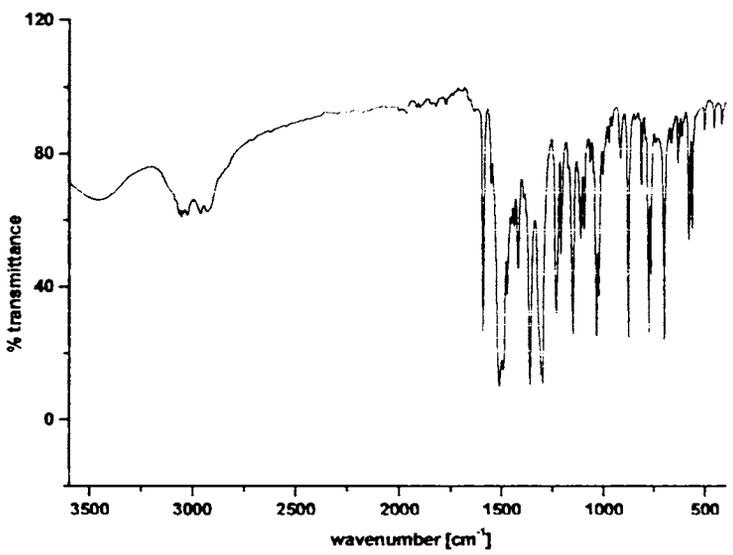

Fig. 2. 5. IR spectrum of HL^3

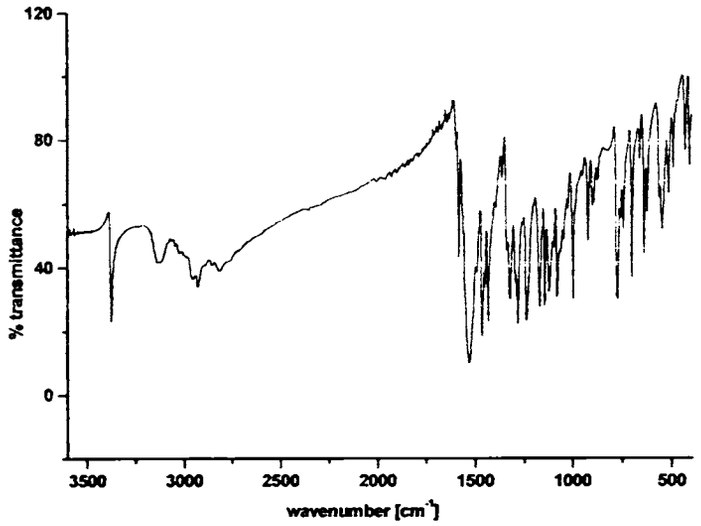

Fig. 2. 6. IR spectrum of HL[4]

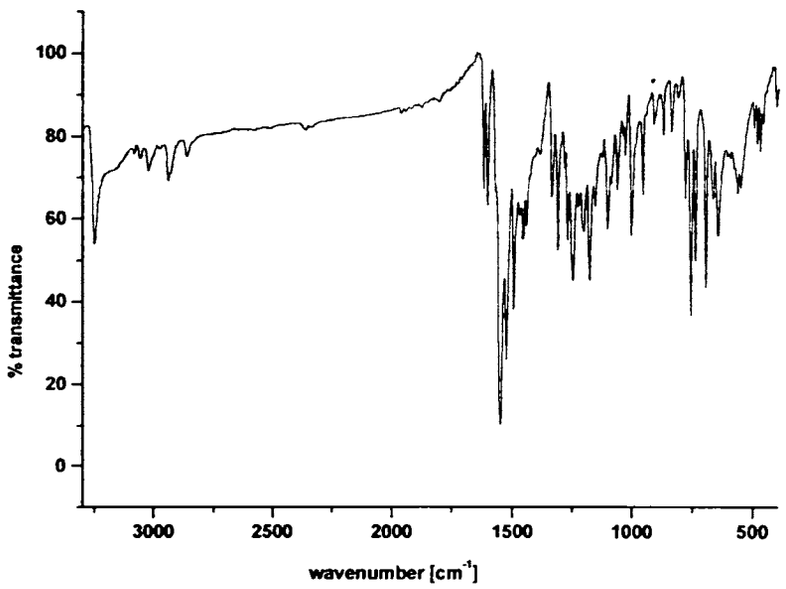

Fig. 2. 7. IR spectrum of H_2L[5]

IR spectra of compounds in which C=S group is attached to nitrogen atom contain several bands in the region 1560-700 cm^{-1} due to vibrations involving interactions between C=S and C-N stretching. The bands observed in the range 1298-1383 cm^{-1} are assigned to ν(C=S) and those in the range 837-929 cm^{-1} are assigned to δ(C=S) [12]. Medium bands are observed in the range 1003-1079 cm^{-1}, for the hydrazinic (N-N) bonds [13]. The 1600-1400 cm^{-1} region of the spectra is complicated by the presence of thioamide bands and ring breathing vibrations of the pyridyl and phenyl rings. However, in-plane and out-of-plane deformation vibrations characteristic of pyridyl ring are observed respectively in the range 613-622 and 401-421cm^{-1} [14].

2.5.2. Electronic spectra

The tentative assignments of the significant electronic spectral bands of ligands are presented in Table 2.3. The electronic spectra of HL^1, HL^2, HL^3, HL^4 and H_2L^5 in DMF solution show the following intraligand absorption maxima: Two bands corresponding to $\pi\rightarrow\pi^*$ transitions of the pyridyl ring, benzene ring and imine function of the thiosemicarbazone moiety are observed in the range 41840-43290 and 33560-38760 cm^{-1}; the $n\rightarrow\pi^*$ transitions of the pyridyl ring and imine function of the thiosemicarbazone moiety are observed in the range 29500-30960 cm^{-1} [15]. A second $n\rightarrow\pi^*$ band is found for HL^4 and H_2L^5 at 25120 and 28820 cm^{-1} respectively [16].

Table 2. 3. Electronic spectral assignments of the thiosemicarbazones

Compound	$\pi\rightarrow\pi^*$	$n\rightarrow\pi^*$
HL^1	42730,38760	30770
HL^2	42190,36630	30960
HL^3	43290,38610	30840
HL^4	41840,35840	29500,25120
H_2L^5	42020,33560	29670,28820

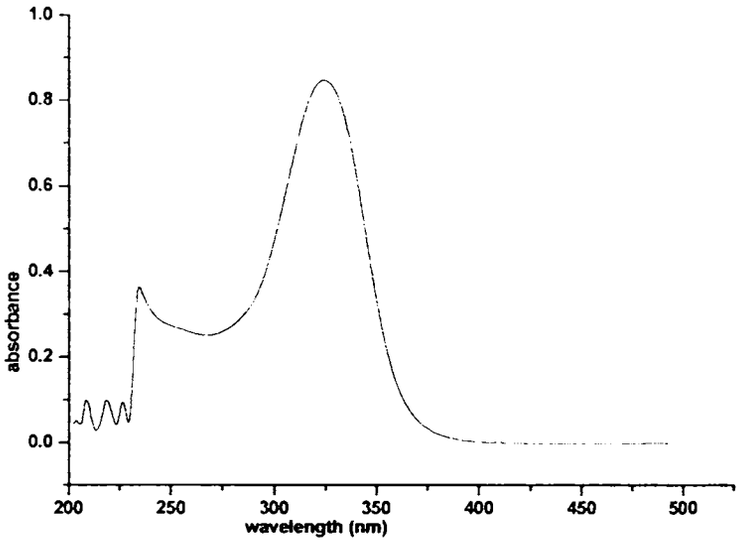

Fig. 2. 8. Electronic spectrum of HL^1

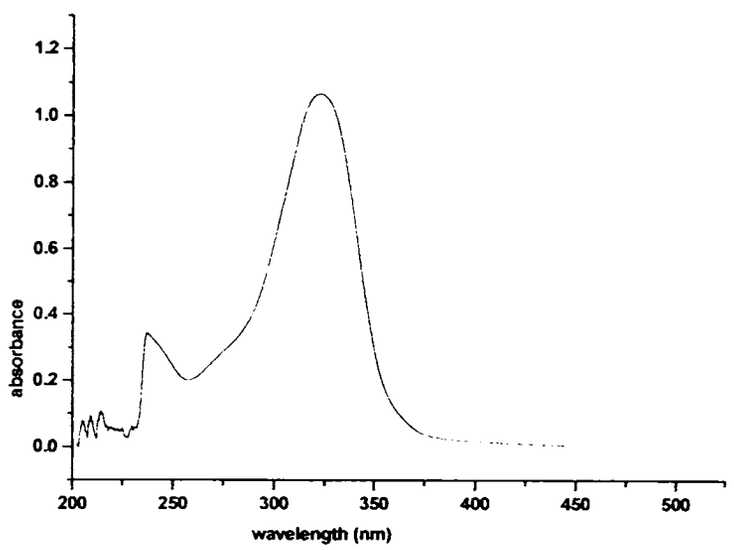

Fig. 2. 9. Electronic spectrum of HL^2

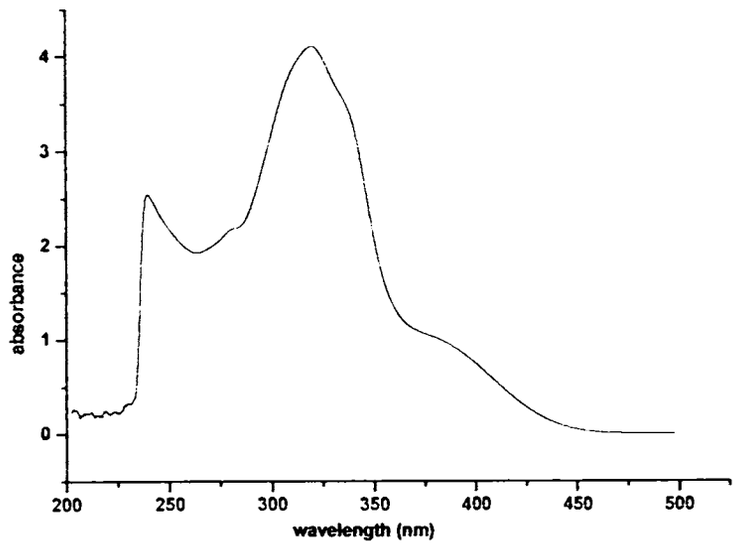

Fig. 2. 10. Electronic spectrum of HL[4]

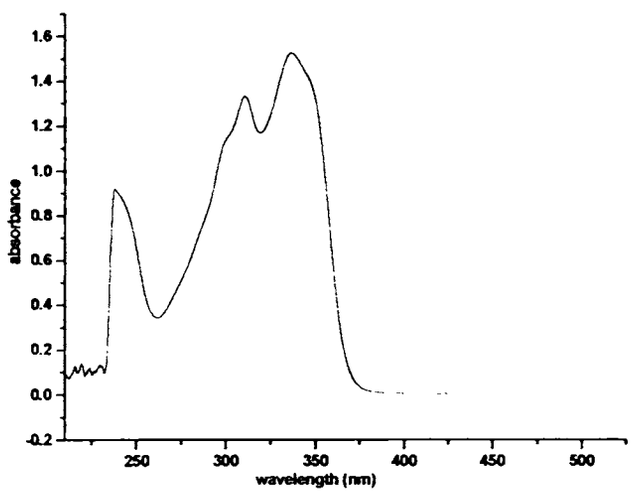

Fig. 2. 11. Electronic spectrum of H_2L^5

2.5.3. ^{1}H *NMR spectra*

The numbering scheme used in the assignment of NMR signals is given in the Fig.2.13. In the spectrum of HL^3, the N(3)H resonance, at a downfield value of δ =14.49 ppm, is consistent with the intramolecular hydrogen bonding between N(3)–H and pyridyl nitrogen. The crystal structure of HL^3 furnishes additional evidence for this assignment.

In the spectrum of HL^4, the N(3)H resonance, occurs at δ = 14.71 ppm [17]. On D_2O exchange the intensity of N(3)–H signal of HL^3 decreases and signals for N(3)H and N(4)H (δ =10.23 ppm) of HL^4 disappear proving the exchangeability of these hydrogens. In the spectra of HL^1 and HL^2, signals at δ =11.93 and 11.72 ppm, are assigned to the N(3)H protons [12,18]. For these compounds the N(4)H signals appear at δ = 10.13 and 8.72 ppm respectively. These signals also disappear on D_2O exchange. The pyridine C(1)H in all these four ligands is very sensitive to the changes in electron density of the pyridyl nitrogen that occur because of interactions such as hydrogen bonding and coordination. It is observed to be deshielded as it is close to the pyridyl nitrogen and this proton is assigned δ =8.57, 8.56, 8.45 and 9.05 ppm respectively in HL^1, HL^2, HL^3 and HL^4, in accordance with earlier reports [19].

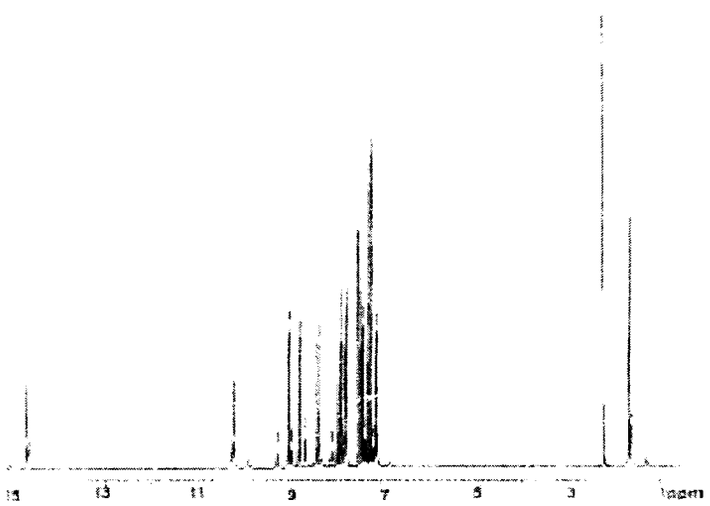

Fig. 2. 12. ^{1}H NMR spectrum of HL^3

The formyl hydrogen C(6)H signal is observed at 8.17, 8.09, 7.91, and 8.39 ppm, the values being in agreement with other studies of thiosemicarbazones derived from pyridine-2-carbaldehyde [9]. Multiplets for other pyridyl hydrogens are observed at about 8.44, 8.19, 7.93 and 7.90 ppm respectively for HL^1, HL^2, HL^3 and HL^4. Similarly, the multiplets for phenyl protons appear at about 6.94, 7.32 and 7.69 ppm respectively for HL^1, HL^2 and HL^3. The methyl protons in HL^1 and HL^3 appear at about 3.32 ppm and multiplet of methylene protons in HL^2 appear at 2.07-3.79 ppm.

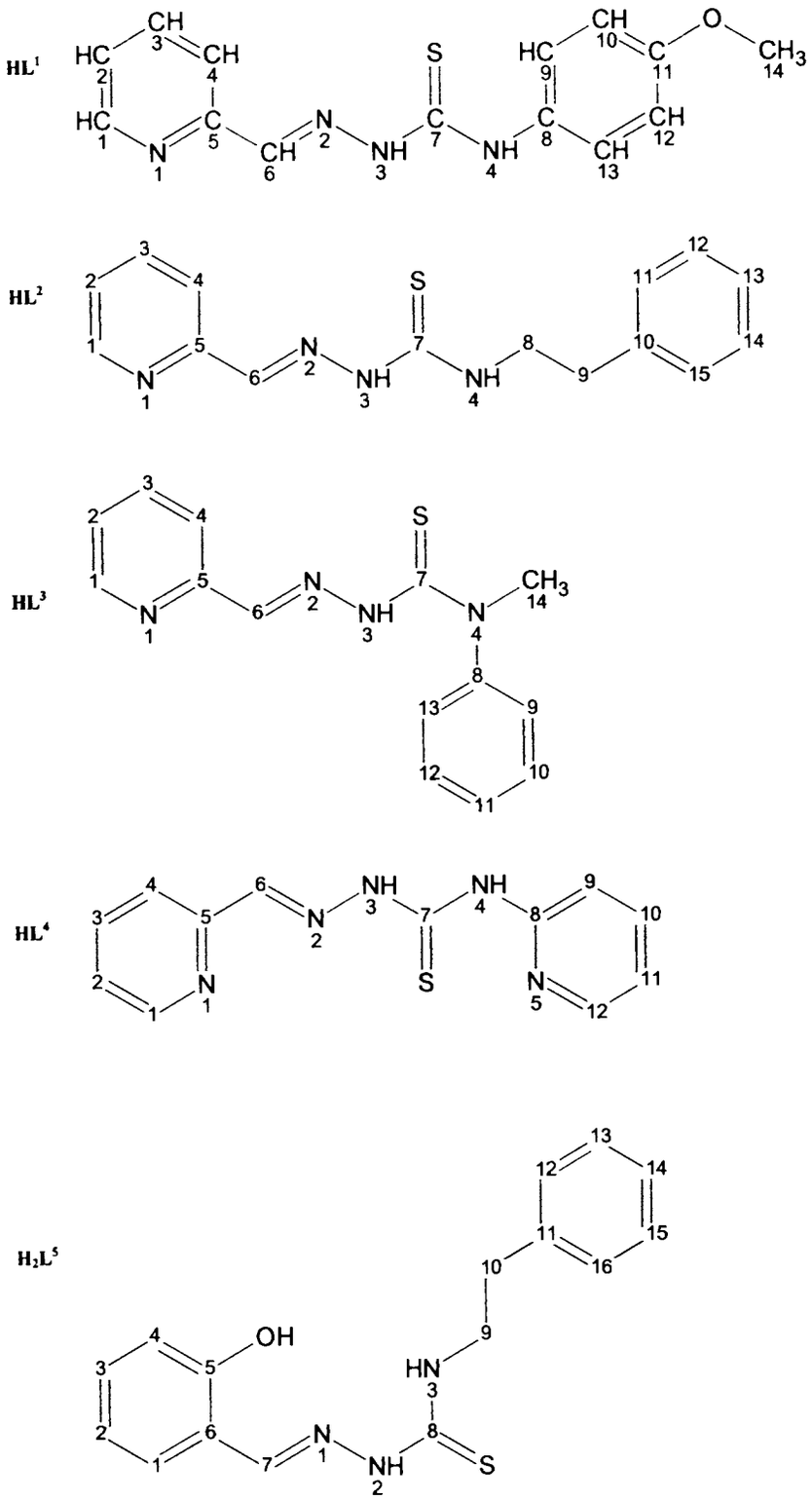

Fig. 2.13. Numbering scheme of the ligands for NMR spectral assignment

The ^{1}H NMR spectrum of H_2L^5 shows signals at 11.44, 9.89, 8.36 and 7.27 ppm corresponding to OH, N(2)H, C(7)H and N(3)H protons respectively. Aromatic protons appear as a multiplet at 6.81-7.85 ppm and multiplet of methylene protons at 2.09-3.77 ppm. The assignments are in agreement with the values already reported [11].

2.5.4. Crystal structure of HL^2

The compound HL^2 is shown in Fig. 2.14, and selected bond lengths and angles are given in Table 2.4.

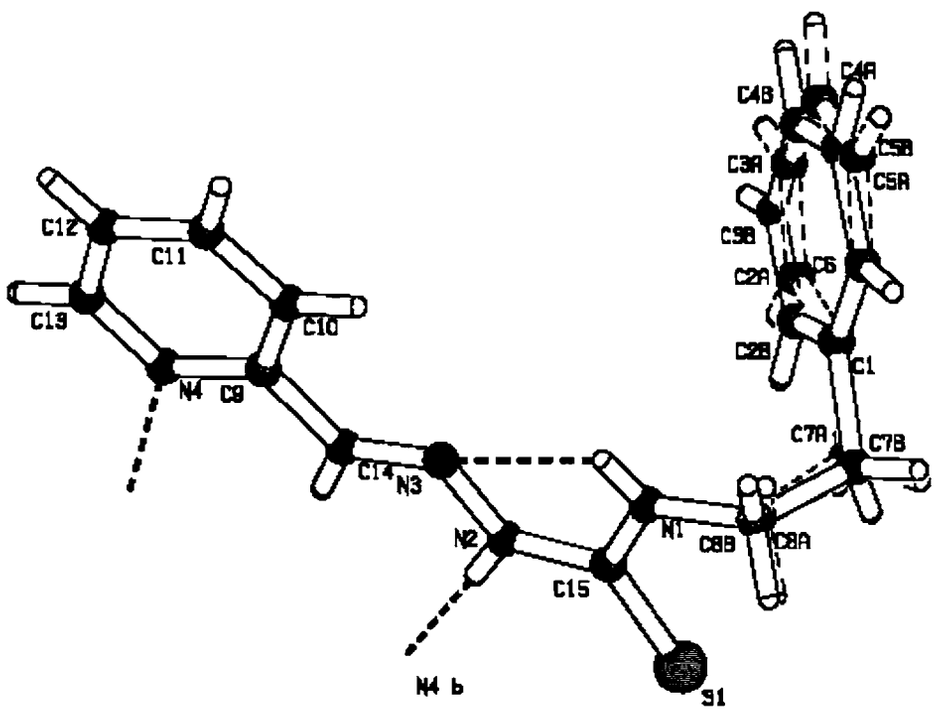

Fig. 2. 14. The molecular structure of HL^2, with ellipsoids drawn at the 60% probability level. Dashed lines denote hydrogen bonds.

The C15 = S1 and C15—N2 bond distances are typical for these types of bonds, as are the remaining bond lengths and angles [20], and are similar to those in the structures of previously reported thiosemicarbazones [17,19]. The thiosemicarbazone reveals an *EE* configuration, since *trans* configurations are observed about both the C14 — N3 and C15—N2 bonds. The phenylethyl group (atoms C1–C8) is disordered over two sites, with relative occupancies 0.433 (11) and 0.567 (11) for the A and B components; the H atom attached to N1 is also disordered,

with these same occupancies. The pyridyl ring is coplanar with the thiosemicarbazone group (S1/N2/N3/C14/C15), with an r.m.s. deviation of 0.025 Å and a maximum deviation of 0.173 (1) Å for atom S1. The dihedral angles between the thiosemicarbazone group and the phenyl ring disorder components are 52.3 (2) and 50.78 (16)° for the A and B disorder components, respectively.

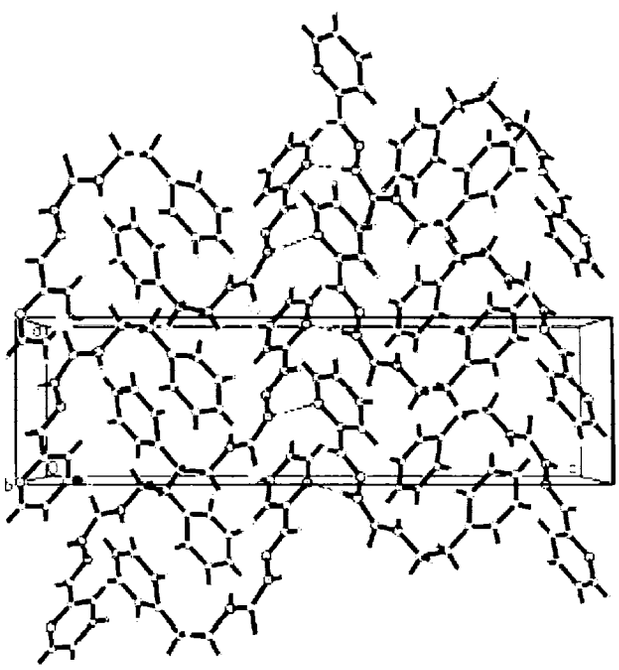

Fig. 2. 15. The crystal packing of HL^2, viewed along the b axis. Hydrogen bonds are shown as dashed lines

Table 2. 4. Selected geometric parameters (Å, °) for HL^2

S1-C15	1.6849 (13)	C14-N3-N2	114.37(10)	C2A-C1-C7A-C8A	-111.5 (7)
N3-C14	1.2837 (15)	C15-N2-N3	120.47(10)	C15-N1-C8A-C7A	73.6 (10)
N3-N2	1.3783 (14)	C15-N1-C8A	119.9 (5)	C15-N1-C8B-C7B	81.3 (7)
N2-C15	1.3587 (16)	C15-N1-C8B	126.7 (4)	N3-N2C15-S1	175.08 (8)
N1-C15	1.3401 (16)	N3-C14-C9	121.90(11)		
N1-C8A	1.407 (13)				
N1-C8B	1.506 (8)				
N4-C13	1.3416 (16)				
N4-C9	1.3488 (16)				

In addition to an intramolecular N—H...N hydrogen-bonded ring, the molecules are linked by intermolecular N—H...N hydrogen bonds to form one-

dimensional chains in the *a*-axis direction (Fig. 2.15 and Table 2.6). In the crystal structure, further stabilization is provided by weak C—H...π (arene) interactions (Table 2.6).

Table 2. 5. Crystal data of HL^2

Parameters	
Empirical formula	$C_{15}H_{16}N_4S$
Formula weight	284.39
Temperature	100.0 (1) K
Diffractometer used	Bruker SMARTAPEX2 CCDareadetector diffractometer
Radiation used, Wavelength	Mo Kα radiation, 0.71073 Å
Crystal system, Space group	Orthorhombic, P212121
Unit cell dimensions	a = 6.7341 (9) Å b = 8.9533 (12) Å c = 24.003 (3) Å
Volume	1447.2 (3) $Å^3$
Z, Calculated Density	4, 1.305 Mg m^{-3}
Absorption coefficient	0.22 mm^{-1}
Crystal size	0.43 × 0.19 × 0.13 mm
Color, Nature	Colourless, Rod
Theta range for data collection	1.7–30.0°
Max. and min. transmission	T_{min} = 0.951, T_{max} = 0.972
Index ranges	h = -9 → 9 k =-12 → 12 l =-33→ 33
Reflections collected	4232 reflections
Independent reflections	4232 independent reflections R_{int} = 0.041
Refinement method	Refinement on F^2
Weighting scheme	$w = 1/ [\sigma^2(F_o^2) + (0.0358P)^2 + 0.2742P]$ where $P = (F_o^2 + 2F_c^2)/3$
Final R indices, 4232 reflections	$R[F^2 > 2\sigma(F^2)] = 0.032$
R indices (all data)	$wR(F^2) = 0.077$
Largest diff. peak and hole	$\Delta\rho_{max}$ = 0.29 e $Å^{-3}$ $\Delta\rho_{min}$ = 0.19 e $Å^{-3}$

Table 2. 6. Hydrogen bond geometry (Å, °) of HL^2

D-H...A	D-H	H...A	D...A	D-H...A
N1-H1B...N3	0.90	2.23	2.6481 (15)	108
N1-H1A...N3	0.90	2.29	2.6481 (15)	104
N2-H1N2...N4[a]	0.90 (2)	2.06 (2)	2.9597 (14)	176
C10-H10A..Cg2[b]	0.93	2.85	3.625 (3)	142
C12-H12A...Cg1[c]	0.93	2.87	3.6495 (15)	142

Symmetry codes: (a) x + ½ , -y + ½, -z; (b) -x + 1, y -½ ,-z + ½; (c) x - ½, -y - ½,-z.
Cg1 and Cg2 are the centroids of rings N1/C9–C13 and C1/C2A–C4A/C6, respectively

2.5.5. Crystal structure of HL^3

The molecular structure of the compound with the atom-numbering scheme is given in the Fig. 2.16. HL^3 exists in the thione form as confirmed by the C=S bond length of 1.6750(14) Å [21]. The molecule exists in the *E* conformation about the N2-N3 bond. The intramolecular hydrogen bond N3-H1N3...N1 and the intermolecular hydrogen bond C6-H6...N2 facilitate this geometry.

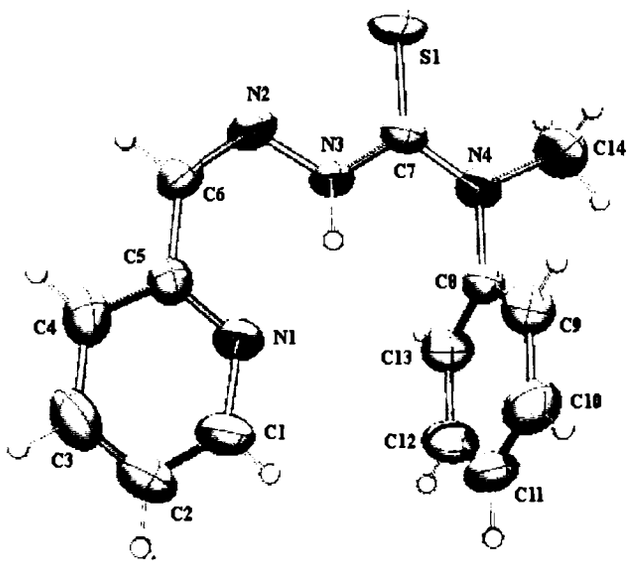

Fig. 2. 16. ORTEP diagram of HL^3 in 50% probability ellipsoids

The core thiosemicarbazone moiety C6, N2, N3, C7, S1, N4 is in a plane with a maximum deviation of –0.0576(15) Å for N2 atom and makes an angle of 16.79(8)°

with the pyridyl ring. But the phenyl ring plane is almost perpendicular [85.38(8)°] to this thiosemicarbazone plane. Relevant C-H… π and Cg…Cg interactions are given in Table 2.10.

Table 2. 7. Crystal refinement parameters of compound HL[3]

Parameters	
Empirical Formula	$C_{14}H_{14}N_4S$
Formula weight (M)	270.35
Temperature (T) K	293(2)
Wavelength (Mo *Kα*) (Å)	0.71073
Crystal system	Triclinic
Space group	$P\bar{1}$
Lattice constants	
a (Å)	9.2038(10)
b (Å)	9.6372(11)
c (Å)	9.6497(12)
α (°)	63.773(2)
β (°)	65.060(2)
γ (°)	75.410(2)
Volume V (Å^3)	693.94(14)
Z	2
Calculated density (*ρ*) (Mg m^{-3})	1.294
Absorption coefficient, *μ*(mm^{-1})	0.225
F(000)	284
Crystal size (mm)	0.33 x 0.24x 0.18
Color, Nature	Yellow, Block
θ Range for data collection	2.36–28.34
Limiting Indices	$-7 \le h \le 11, -12 \le k \le 12, -12 \le l \le 12$
Reflections collected	4140
Independent Reflections	3024 [R(int) = 0.0112]
Refinement method	Full-matrix least-squares on F^2
Data / restraints / parameters	3024/ 0 / 177
Goodness-of-fit on F^2	1.050
Final *R* indices [I > 2σ (I)]	$R_1 = 0.0440$, $wR_2 = 0.1214$
R indices (all data)	$R_1 = 0.0516$, $wR_2 = 0.1274$
Largest difference peak and hole (e Å^{-3})	0.251 and -0.197

Table 2. 8. H-bonding interactions in HL[3]

Residue	D-H...A	D-H	H...A	D...A	D-H...A
1	N3-H1N3…N1[a]	0.88	1.98	2.6768	135
1	C6-H6…N2[b]	0.93	2.61	3.3540	137

D=donor, A=acceptor, Eqivalent position codes : a= x,y,z; b=-x,-y,1-z;

Table 2. 9. Selected bond lengths (Å) and bond angles (°)HL[3]

S(1)–C(7)	1.6750(14)
N(2)–C(6)	1.285(2)
N(2)– N(3)	1.3613(17)
N(3)–C(7)	1.3644(18)
N(4)–C(7)	1.345(2)
C(6)–N(2)–N(3)	117.75(13)
N(2)–N(3)–C(7)	120.25(12)
N(4)–C(7)–N(3)	113.87(12)
N(3)–C(7)–S(1)	122.89(12)
N(4)–C(7)–S(1)	123.22(11)

Table 2.10. Interaction parameters of the compound HL[3]

π----π interactions

Cg(I)-Res(I)----Cg(J)	Cg-Cg(Å)	α °	β °
Cg(1) [1] ----Cg(1)[a]	3.6040	0.02	13.54

Eqivalent position codes : a= -X,1-Y,1-Z; Cg(1)= N1,C1,C2,C3,C4,C5

CH----π interactions

X-H(I)Res(1)----Cg(J)	H..Cg(Å)	X..Cg(Å)	X-H..Cg (°)
C(14)-H(14B)[1]...Cg(2)[a]	2.95	3.7088	137

Equivalent position code; a= 1-X,-Y,2-Z; Cg(2)= C(8),C(9),C(10),C(11),C(12),C(13)

2.5.6. Crystal structure of HL[4]A

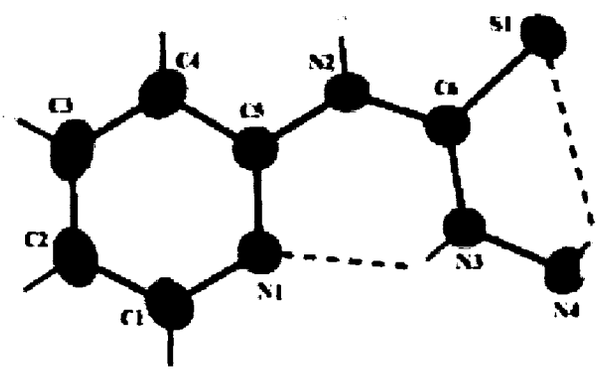

Fig. 2. 17. A view of HL[4]A, showing the atom-numbering scheme. Displacement ellipsoids are drawn at the 50% probability level and H atoms are shown as spheres of fixed radii. Dashed lines denote the intramolecular N---H—N and S---H—N interactions.

The molecular structure of the compound with the atom-numbering scheme is given in the Fig 2.17. The C—S bond distance of 1.6897(13) Å in HL[4]A is

intermediate between the values of 1.82 Å for a C—S single bond and 1.56 Å for a C=S bond [22]. Similarly, the C6—N2 and C6—N3 bond distances (Table 2.11) indicate some double-bond character and the existence of extensive delocalization in the thiosemicarbazide moiety. The thiosemicarbazide moiety is planar, with a maximum deviation of 0.0127 (1) Å for atom C6. The N4—N3—C6—N2 torsion angle of 177.77 (16)° indicates that the hydrazinic N4 atom is positioned trans to the thioamide N2 atom, while the S1—C6—N3—N4 torsion angle of -0.42 (24)° indicates that atom N4 is *cis* to the thionyl S1 atom about the C6—N3 bond. These are in agreement with values in thiosemicarbazones [23]. This is due to the presence of the pyridine ring N atom, which forms an intramolecular hydrogen bond and facilitates the geometry. This observation was confirmed by the geometry of 4-phenyl-1-(propan-2-ylidene) thiosemicarbazide[24], where the hydrazinic N atom is *cis* to the thioamide N atom and *trans* to the thionyl S atom.

The intramolecular hydrogen bonds in HL^4A (Fig. 2.18 and Table 2.12) facilitate almost planar geometry in the compound, with a maximum deviation of 0.1440 (1) Å for N4. The N3—H6---N1 hydrogen bond forms a six-membered ring and the N4—H7---S1 hydrogen bond forms a five membered ring. In the packing, molecules are stacked along the b axis and an intermolecular N2—H5---N4* hydrogen bond (Fig. 2.18) produces independent polymeric chains (Fig. 2.19). The π-π interactions between the planar pyridine rings may be stabilizing the packing.

Table 2. 11. Selected geometric parameters (Å, °) for HL^4A

S1-C6	1.6897 (13)	N3-C6-N2	118.85(10)
N4-N3	1.4104 (16)	N3-C6-S1	122.79(12)
N2-C6	1.3639 (16)		
N2-C5	1.3947 (16)		
C6-N3	1.3283 (17)		

Table 2.12. Hydrogen bond geometry (Å, °) of HL^4A

D-H...A	D-H	H...A	D...A	D-H...A
N2-H5...N4[a]	0.86	2.21	3.058 (2)	169
N4-H7...S1	0.75 (3)	2.72 (3)	3.025 (2)	107 (2)
N3-H6...N1	0.79 (2)	2.06 (2)	2.6698(16)	134 (2)

Table 2. 13. Crystal refinement parameters of compound HL^4A

Parameters	
Empirical formula	$C_6H_8N_4S$
Formula weight	168.22
Temperature	293 (2) K
Diffractometer used	Bruker SMART APEX2 CCD area detector diffractometer
Radiation used, Wavelength	Mo Kα radiation, 0.71073 Å
Crystal system, Space group	Monoclinic, C2/c
Unit cell dimensions	a = 15.5846 (17) Å β = 121.118 (2) b = 10.1592 (11) Å c = 11.1622 (12) Å
Volume	1513.0 (3) $Å^3$
Z, Calculated Density	8, 1.477 mg m^{-3}
Absorption coefficient	0.36 mm^{-1}
Crystal size	0.32 × 0.28 × 0.22 mm
Color, Nature	Light yellow, Block
Theta range for data collection	2.7–28.2°
Index ranges	h = -20 → 16 k =-13 → 12 l =-11→ 14
Reflections collected	4378 reflections
Independent reflections	1748 independent reflections R_{int} = 0.015
Refinement method	Refinement on F^2
Weighting scheme	$w = 1/ [\sigma^2(F_o^2) + (0.0614P)^2 + 0.54762P]$ where $P = (F_o^2 + 2F_c^2)/3$
Final R indices, 4232 reflections	$R[F^2 > 2\sigma(F^2)] = 0.035$
R indices (all data)	$wR(F^2) = 0.107$
Largest diff. peak and hole	$\Delta\rho_{max}$ = 0.24 e $Å^{-3}$ $\Delta\rho_{min}$ = -0.22 e $Å^{-3}$

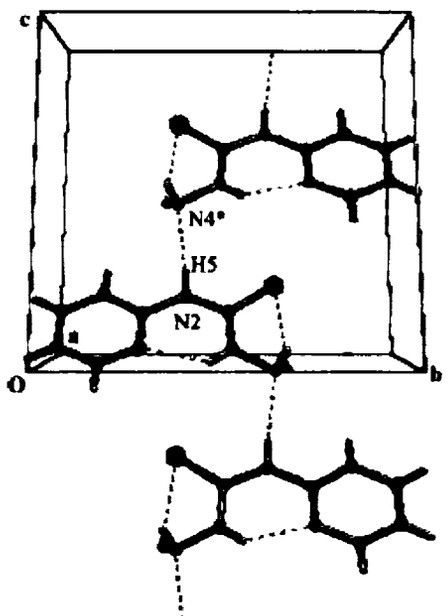

Fig. 2.18. A view of HL^4A along the a axis. Dashed lines indicate inter and intramolecular hydrogen bonds. The molecules are stacked along the b direction. [Symmetry code: (*) -x +½, y + 3/2, -z + ½.]

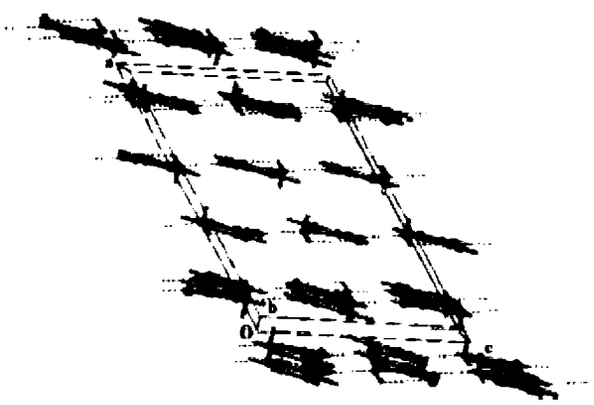

Fig. 2.19. The packing of HL^4A viewed along the b axis, showing the independent polymeric sheets stacked as layers along the c axis.

Conclusion

This chapter presents the details regarding the syntheses of four (HL^1, HL^2, HL^3, HL^4) N-N-S and one (H_2L^5) O-N-S donor ligands. They were characterized by partial elemental analyses, IR, electronic and ^1H NMR spectral techniques. X-Ray diffraction studies of the ligands HL^2 and HL^3 corroborate the spectral characterization. Single crystals of an interesting intermediate product (HL^4A) could be isolated during the synthesis of HL^4 and its structure was solved by X-ray diffraction.

References

1. J.P. Scovill, D.L. Klayman, C.F. Franchino, J. Med. Chem. 25 (1982) 1261.
2. G.M. Sheldrick (1997) SHELXS97 and SHELXL97. Bruker AXS Inc., Madison, Wisconsin, USA.
3. G.M. Sheldrick, (1998). SHELXTL. Version 5.10. Bruker AXS Inc., Madison, Wisconsin, USA.
4. Bruker (2005) APEX2 (Version 1.27), SAINT and SADABS. Bruker AXSInc., Madison, Wisconsin, USA.
5. L.J. Farrugia, J. Appl. Cryst. 30 (1997) 565.
6. A.L. Spek, J. Appl. Cryst. 36 (2003) 7.
7. Y-P. Tian, W-T. Yu, C-Y.Zhao, M-H. Jiang, Z-G. Cai, H- K. Fun, Polyhedron 21 (2002) 1219.
8. R.P. John, A. Sreekanth, M.R.P. Kurup, H. -K. Fun, Polyhedron 24 (2005) 601.
9. A.K. El-Sawaf, D.X. West, F.A. El-Saied, R.M. El-Bahnasawy, Transition Met. Chem. 23 (1998) 649.
10. V. Philip, V. Suni, M.R.P. Kurup, M. Nethaji, Polyhedron 25 (2006) 1931.
11. P. Bindu, M.R.P. Kurup, T.R. Satyakeerty, Polyhedron 18 (1999) 321.
12. D.X. West, A.M. Stark, G.A. Bain, A.E. Liberta, Transition Met. Chem. 21(1996) 289.
13. M. Joseph, M. Kuriakose, M.R.P. Kurup, E. Suresh, A. Kishore, S.G. Bhat, Polyhedron 25 (2006) 61.

14. E. Bermejo, A.Casteneiras, R. Dominguez, R. Carballo, C.M-Mossmer, J. Strahle, D.X. West, Z. Anorg. Allg.Chem. 625 (1999) 961.
15. A. Castineiras, E. Bermejo, D.X. West, L.J. Ackerman, J.V. Martinez, S.H-Ortega, Polyhedron 18(1999) 1469.
16. I.C. Mendes, L.R. Teixeira, R. Lima, H. Beraldo, N.L. Speziali, D.X. West, J. Mol. Struct. 559 (2001) 355.
17. V. Philip, V. Suni, M.R.P. Kurup, Acta Crystallogr. C60 (2004) o856.
18. R.L. de Lima, L.R. de Souza Teixeira, T.M.G .Carneiro, H. Beraldo, J. Braz. Chem. Soc.10 (1999) 184.
19. M. Joseph, V. Suni, C.R. Nair, M.R.P. Kurup,H.-K. Fun, J. Mol. Struct. 705 (2004) 63.
20. F.H. Allen, O. Kennard, D. G. Watson, L. Brammer, A.G. Orpen, R. Taylor, J. Chem. Soc. Perkin Trans. 2 (1987) S1.
21. L. Latheef, E. Manoj, M.R.P. Kurup, Acta.Cryst, C Cryst. Struc. Commun. C62 (2006) o16.
22. C.He, C.Y. Duan, C.J. Fang, Y.J. Liu, Q. J. Meng, J. Chem. Soc. Dalton Trans. (2000) 1207.
23. H.-K .Fun, S. Chantrapromma, V. Suni, A. Sreekanth, S. Sivakumar, M.R.P. Kurup, Acta. Cryst. E61 (2005) o1337
24. F. Jian, Z. Bai, H. Xiao, K. Li, Acta Cryst. E61 (2005) o653.

Syntheses of copper(II) complexes and studies on their structural and spectral characteristics

3.1. Introduction

The coordination chemistry involving heterocyclic thiosemicarbazones has been interesting research area in the last 30 years because of their well-documented biological activities. Thiosemicarbazone derivatives have considerable antibacterial, antimalarial, antiviral and antitumor activities [1]. Complexation of such thiosemicarbazone ligands with metal ions has been found to produce synergistic effects on the antiproliferative activities of the parent ligands [2]. It has been reported that copper(II) complexes of heterocyclic N(4)-substituted thiosemicarbazones exercise bio-activity through a mechanism involving either inhibition of the enzyme ribonucleotide reductase, or creation of lesions in DNA strands. Studies have also shown that, for these ligands, nature of substitution on the terminal N(4) atom is crucial for the antifungal activity [3].

Pyridine-2-carbaldehyde thiosemicarbazone was the first α-(N)-heterocyclic carboxaldehyde thiosemicarbazone, reported to have carcinostatic effects [4]. This thiosemicarbazone ligand coordinates to the metal ions in both the anionic (L^-) and neutral (HL) forms. The anionic L^- form is usually present in $[CuLX]_2$ dimers in which, the metal centres can either be bridged through the thiolate sulfur or the non-thiosemicarbazone co-ligand X (X= Cl, N_3, NCS etc.) [5]. It is reported that the formation of complexes with S-bridge or X-bridge, depends on the nature of the non-thiosemicarbazone ligands. However, the actual underlying reasons for the formation of S- over X-bridged systems are not clear to date [6]. On the basis of these findings, this chapter presents the optimal conditions for synthesis of fourteen copper(II) complexes with the five ligands, viz., pyridine-2-carbaldehyde N(4)-paramethoxyphenyl thiosemicarbazone (HL^1), pyridine-2-carbaldehyde N(4)-phenylethyl thiosemicarbazone (HL^2), pyridine-2-carbaldehyde N(4)-methyl, N(4)-phenyl thiosemicarbazone (HL^3), pyridine-2-carbaldehyde N(4)-pyridyl thiosemicarbazone [HL^4], salicylaldehyde-N(4)-phenylethyl thiosemicarbazone [H_2L^5]

and their characterization by physicochemical methods, together with X-ray crystal structure of one of the binuclear complexes, *viz.* $[CuL^3Cl]_2$.

3.2. Experimental

3.2.1 Materials

The details of materials used for the syntheses of ligands have been given in Chapter 2. The metal salts copper(II) nitrate trihydrate, copper(II) chloride dihydrate, copper(II) acetate monohydrate, copper(II) perchlorate hexahydrate, copper(II) sulphate pentahydrate, sodium azide and potassium thiocyanate (Merck) were used as supplied. The solvents were purified by standard procedures before use. **Caution!** Azide and perchlorate metal complexes with organic ligands are potentially explosive and should be handled with care.

3.2.2. Syntheses of ligands

The syntheses of thiosemicarbazone ligands have been discussed in detail in Chapter 2.

3.2.3. Syntheses of complexes

3.2.3.1. Syntheses of $[CuL^1Cl]$ (1), $[CuL^2Cl]_2$ (5), $[CuL^3Cl]_2$ (9), $[Cu(HL^4)Cl_2]$ (11) and $[Cu(HL^5)Cl]_2$ (13)

To a solution of the respective ligand (1.5 mmol) dissolved in hot ethanol (30 ml), was added $CuCl_2{\cdot}2H_2O$ (1.5 mmol). The mixture was refluxed for 1 hour and kept overnight at room temperature. The complex formed was filtered washed with water, ethanol and ether and dried *in vacuo* over P_4O_{10}.

3.2.3.2. Syntheses of $[CuL^1NO_3]_2$ (2), $[Cu(HL^4)(NO_3)_2]{\cdot}H_2O$ (12) and $[Cu(HL^5)NO_3]{\cdot}1/2H_2O$ (14)

To a solution of the respective ligand (1.5 mmol) dissolved in hot ethanol (25 ml), was added $Cu(NO_3)_2{\cdot}3H_2O$ (1.5 mmol) and stirred for 4 hours The complex formed was filtered washed with water, ethanol and ether and dried *in vacuo* over P_4O_{10}.

3.2.3.3. Syntheses of $[CuL^1N_3]_2{\cdot}2/3\ H_2O$ (3), and $[CuL^2N_3]$ (6)

To a solution of the respective ligand (1.5 mmol) dissolved in hot ethanol (30 ml), was added $Cu(Ac)_2{\cdot}H_2O$ (1.5 mmol). The mixture was refluxed for 1 hour, cooled to room temperature and a solution of NaN_3 (2 mmol) in water (10 ml) was added and

heated again at reflux for 30 minutes and kept overnight at room temperature. The complex formed was filtered, washed with water, ethanol and ether and dried *in vacuo* over P_4O_{10}.

3.2.3.4. Syntheses of $[CuL^1]_2(ClO_4)_2 \cdot 2H_2O$ *(4) and* $[Cu(HL^2)_2](ClO_4)_2 \cdot 1/2EtOH$ *(8)*

To a solution of the respective ligand (1.5 mmol) dissolved in hot ethanol (30 ml), was added $Cu(ClO_4)_2 \cdot 6H_2O$ (1.5 mmol). The mixture was refluxed for 1 hour and kept overnight at room temperature. The complex formed was filtered washed with water, ethanol and ether and dried *in vacuo* over P_4O_{10}.

3.2.3.5. Synthesis of $[Cu(HL^2)\ SO_4]_2 \cdot 4H_2O$ *(7)*

To a solution of HL^2 (1.5 mmol) dissolved in hot ethanol (30 ml), was added a solution of $CuSO_4 \cdot 5H_2O$ (1.5 mmol) dissolved in water (10 ml). The mixture was refluxed for four hours and kept overnight at room temperature. The complex formed was filtered, washed with water, ethanol and ether and dried *in vacuo* over P_4O_{10}.

3.2.3.6. Synthesis of compound $[CuL^3NCS] \cdot 1/2H_2O$ ***(10)***

To a solution of HL^3 (1.5 mmol) dissolved in hot methanol (30 ml), was added $Cu(Ac)_2 \cdot H_2O$ (1.5 mmol). The mixture was refluxed for 1 hour, cooled to room temperature and a solution of KCNS (2 mmol) in water (10 ml) was added and heated again at reflux for 30 minutes and kept overnight at room temperature. The complex formed was filtered, washed with water, methanol and ether and dried *in vacuo* over P_4O_{10}.

3.3. Physical Measurements

Elemental analyses of the ligand and the complexes were done on a Heracus elemental analyzer at CDRI, Lucknow, India and on a Vario EL III CHNS analyzer at SAIF, Kochi, India. The IR spectra were recorded on a Thermo Nicolet AVATAR 370 DTGS model FT-IR Spectrophotometer with KBr pellets at SAIF, Kochi. The far IR spectra were recorded using polyethylene pellets in the 500-100 cm^{-1} region on a Nicolet Magna 550 FTIR instrument at Regional Sophisticated Instrument Facility, Indian Institute of Technology, Bombay. Electronic spectra were recorded on a Cary 5000, version 1.09 UV-Vis-NIR Spectrophotometer from solutions in chloroform. The EPR spectra of the complexes were recorded in a Varian E-112 Spectrometer using TCNE as the standard at SAIF, IIT, Bombay, India. The magnetic susceptibility

measurements were carried out at the Indian Institute of Technology, Roorkee, at room temperature in the polycrystalline state on a PAR model 155 Vibrating sample magnetometer at 5 kOe. field strength. The molar conductivities of the complexes in dimethylformamide solutions (10^{-3} M) at room temperature were measured using a direct reading conductivity meter. The details regarding the various analytical methods have been discussed in Chapter 1.

3.4. X-Ray crystal structure study

Single crystals of compound **9** of X-ray diffraction quality were grown from its methanol solution by slow evaporation at room temperature in air

Table 3.1. Crystal refinement parameters of $[CuL^3Cl]_2$ (9)

Parameters	
Empirical Formula	$C_{28}H_{26}Cl_2Cu_2N_8S_2$
Formula weight (M)	736.71
Temperature (T) K	293(2)
Wavelength (Mo Kα) (Å)	0.71073
Crystal system	Triclinic
Space group	*P*-1
Lattice constants	
a (Å)	9.2246(18)
b (Å)	9.468(3)
c (Å)	10.714(3)
α (°)	69.41(2)
β (°)	83.157(17)
γ (°)	59.45(2)
Volume V ($Å^3$)	752.3(3)
Z	1
Calculated density (ρ) (mg m^{-3})	1.626
Absorption coefficient, μ (mm^{-1})	1.765
F(000)	374
Color, Nature	Green, Block
Crystal size (mm)	0.25 x 0.20x 0.20
Limiting Indices	-13≤h≤13, -13≤k≤13, -15≤l≤15
Reflections collected	10909
Independent Reflections	4439 [R(int) = 0.0185]
Refinement method	Full-matrix least-squares on F^2
Data / restraints / parameters	4439/ 0 / 190
Goodness-of-fit on F^2	0.987
Final *R* indices [I > 2σ (I)]	R_1 = 0.0274, wR_2 = 0.0708
R indices (all data)	R_1 = 0.0428, wR_2 =0.0743
Largest difference peak and hole (e $Å^{-3}$)	0.410 and -0.215

The crystallographic data and structure refinement parameters are given in Table 3.1. The data were collected using a CrysAlis CCD, Oxford Diffraction Ltd., version 1.171.29.2 with graphite monochromated Mo Kα (λ = 0.71073 Å) radiation on a single crystal of dimension 0.25×0.20×0.20 mm at the National Single Crystal X-Ray Diffraction Facility, IIT, Bombay, India. The unit cell dimensions and intensity data were measured at 293 K. Empirical absorption corrections were done using spherical harmonics, implemented in SCALE3 ABSPACK scaling algorithm. The trial structure was solved using SHELXS-97 [7] and refinement was carried out by full-matrix least squares on F^2 (SHELXL) [7]. Molecular graphics employed were ORTEP-III [8] and PLATON [9].

3.5. Results and discussion

In the compounds **1**, **2**, **3**, **4**, **5**, **6**, **9** and **10**, the thiosemicarbazones deprotonate and chelate in thiolate form as evidenced by the IR spectra. In **7**, **8**, **11**, **12**, **13** and **14**, the thiosemicarbazones are in the thione form. The absence of the band corresponding to ν(O-H) in **13** and **14** shows that the phenolic -OH group in H_2L^5 deprotonates and the oxygen atom coordinates with the metal. The complexes present themselves in a variety of empirical formulae which are in agreement with the partial elemental analyses data. The complexes of the HL ligands have the empirical formulae CuLX (**1**, **6**, **9**, **10**), $Cu(HL)X_2$ (**11**, **12**) and $Cu(HL)_2X_2$ (**8**) whereas the complexes **13** and **14** of the ligand H_2L^5 have the empirical formula Cu(HL)X where, X = Cl, NO_3, N_3, ClO_4 and NCS. The complex **7** of the ligand HL^2 turned out to be $Cu(HL)SO_4$. The complexes are appreciably soluble in methanol, ethanol, DMF and DMSO.

The colors, partial elemental analyses, molar conductivities and magnetic susceptibilities of the metal complexes are shown in Table 3.2. The green and brown colors are common to complexes involving thiosemicarbazone coordination due to the sulfur-to-metal charge-transfer bands, which dominate their visible spectra [10]. The molar conductivity values of the compounds except **4** and **8** in 10^{-3} M solution in DMF show that they are non-conductors [11] indicating that the anion and the ligand are coordinated to the central copper(II). However, the molar conductivity values of compounds **4** and **8** suggest that they are 2:1 electrolytes. The magnetic

Table 3. 2. Colors, partial elemental analyses, magnetic susceptibilities and molar conductivities of the complexes.

Compound	Color	Found (Calc.)%				μ (B.M.)	Λ_M*
		C	H	N	S		
$[CuL^1Cl]$ (**1**)	Brown	43.65(43.75)	3.48(3.41)	14.32(14.58)	8.20(8.34)	1.54	5
$[CuL^1NO_3]_2$ (**2**)	Green	41.12(40.92)	3.17(3.19)	16.97(17.04)	16.97(17.04)	1.14	51
$[CuL^1N_3]_2 \cdot 2/3H_2O$ (**3**)	Brown	42.36(42.36)	3.18(3.47)	24.83(24.70)	8.10(8.08)	1.39	18
$[CuL^1]_2(ClO_4)_2 \cdot 2H_2O$ (**4**)	Brown	35.85(36.06)	3.31(3.24)	11.84(12.01)	6.76(6.88)	0.86	160
$[CuL^2Cl]_2$ (**5**)	Green	47.54(47.12)	4.01(3.95)	14.88(14.65)	8.35(8.39)	0.99	6
$[CuL^2N_3]$ (**6**)	Brown	46.43(46.32)	3.63(3.89)	25.08(25.21)	8.14(8.24)	2.14	51
$[Cu(HL^2)SO_4]_2 \cdot 4H_2O$ (**7**)	Green	37.78(37.53)	4.06(4.20)	11.42(11.67)	13.01(13.36)	1.41	48
$[Cu(HL^2)_2](ClO_4)_2 \cdot 1/2EtOH$ (**8**)	Green	43.73(43.81)	4.17(4.37)	13.17(12.77)	7.00(7.31)	1.74	132
$[CuL^3Cl]_2$ (**9**)	Green	45.17(45.65)	3.48(3.56)	15.26(15.21)	8.75(8.71)	1.52	7
$[CuL^3NCS] \cdot 1/2H_2O$ (**10**)	Green	44.94(45.04)	3.13(3.53)	17.47(17.51)	15.50(16.03)	1.74	11
$[Cu(HL^4)Cl_2]$ (**11**)	Green	36.50(36.79)	2.97(2.83)	17.39(17.88)	8.47(8.18)	1.62	18
$[Cu(HL^4)(NO_3)_2] \cdot H_2O$ (**12**)	Green	31.73(31.14)	3.12(2.83)	21.03(21.18)	6.57(6.93)	1.70	42
$[Cu(HL^5)Cl]_2$ (**13**)	Green	48.07(48.36)	3.88(4.06)	10.46(10.57)	8.10(8.07)	1.12	19
$[Cu(HL^5)NO_3] \cdot 1/2H_2O$ (**14**)	Green	44.26(44.39)	4.35(3.96)	12.54(12.94)	7.51(7.41)	1.90	54

*Molar conductivity of 10^{-3} M DMF solution, in $ohm^{-1}cm^2\ mol^{-1}$

susceptibilities at room temperature per copper atom of the complexes except **6**, **8**, **10**, **11**, **12** and **14** suggest interaction between metal centres [12].

3.5.1. Infrared spectra

The IR bands most useful for the determination of the mode of coordination are presented in Table 3.3. The far IR assignments are shown in Table 3.4. The strong bands in the range 3310 - 3374 cm^{-1} in the spectra of HL^1, HL^2, HL^4 and H_2L^5 have been assigned to $\nu(^4N\text{-}H)$. In the spectra of complexes these bands shift to both higher and lower energies, suggesting differences in hydrogen bonding of N(4)H between the uncomplexed and complexed thiosemicarbazone [13]. A medium band in the range 3129-3250 cm^{-1} in the free ligands due to $\nu(^2N\text{-}H)$ vibration disappears in the spectra of complexes **1**, **2**, **3**, **4**, **5**, **6**, **9** and **10**, providing a strong evidence for the ligand coordination around copper(II) ion in the deprotonated thiol form. In the spectra of **7**, **8**, **11**, **12**, **13** and **14**, $\nu(^2N\text{-}H)$ bands appear in the range 3069 - 3291 cm^{-1} respectively, but ν(S-H) band at 2570 cm^{-1} is absent showing that the ligands are in the thione form in these complexes [14]. The intense bands at 1584, 1586, 1590, 1593 and 1619 cm^{-1} in the spectra of HL^1, HL^2, HL^3, HL^4 and H_2L^5 respectively have been assigned to ν(C=N) of the thiosemicarbazone moiety. These bands are shifted to lower energies in the spectra of the complexes indicating azomethine nitrogen coordination [15].

The bands in the 402-425 cm^{-1} range are assigned to $\nu(Cu\text{-}N_{azomethine})$ in agreement with previous studies of metal complexes of 2-formylpyridine N(4)-substituted thiosemicarbazones [16]. Strong bands found at 1024-1079 cm^{-1} in the ligands are assigned to the ν(N–N) band of the thiosemicarbazone. The increase in the frequency of this band in the spectra of complexes is due to the increase in the bond strength, again confirming the coordination *via* the azomethine nitrogen [17]. For the complexes containing the anionic ligands, a second band due to ν(N=C) is often resolved, but a number of complexes show only a single, broad band for both ν(C=N) and ν(N=C) modes [18]. The complexes **1**, **2**, **3**, **4**, **5**, **6**, **9** and **10** show bands corresponding to ν(N=C) in the range 1588-1615 cm^{-1} whereas these bands are not present in the spectra of the complexes **7**, **8**, **11**, **12**, **13** and **14**.

Table 3. 3. Infrared spectral data (cm^{-1}) of thiosemicarbazones and the complexes

Compounds	ν(C=N)	ν(N=C)	ν(N-N)	ν/δ(C-S)	py(ip)	py(op)	ν(^{2}N-H)	ν(^{4}N-H)
HL^1	1584	---	1024	1334,837	613	401	3134	3310
$[CuL^1Cl]$ (**1**)	1558	1596	1133	1307,826	646	409	---	3340
$[CuL^1NO_3]_2$ (**2**)	1564	1597	1135	1308,830	617	417	---	3321
$[CuL^1N_3]_2 \cdot 2/3\ H_2O$ (**3**)	1561	1606	1135	1301,829	617	413	---	3251
$[CuL^1]_2(ClO_4)_2 \cdot 2H_2O$ (**4**)	1560	1609	1121	1300,837	636	409	---	3286
HL^2	1586	---	1079	1324,897	622	406	3129	3374
$[CuL^2Cl]_2$ (**5**)	1560	1588	1138	1335,889	628	414	---	3443
$[CuL^2N_3]$ (**6**)	1573	1592	1083	1313,867	626	412	---	3446
$[Cu(HL^2)\ SO_4]_2 \cdot 4H_2O$ (**7**)	1560	---	1165	1361,890	618	412	3219	3403
$[Cu(HL^2)_2]\ (ClO_4)_2 \cdot 1/2$ EtOH (**8**)	1565	---	1139	1367,886	635	419	3206	3330
HL^3	1590	---	1035	1307,779	614	421	3158	---
$[CuL^3Cl]_2$ (**9**)	1553	1615	1138	1289,775	636	449	---	---
$[CuL^3NCS] \cdot 1/2H_2O$ (**10**)	1558	1607	1140	1291,773	631	453	---	---
HL^4	1593	---	1078	1298,929	614	412	3057	3310
$[Cu(HL^4)Cl_2]$ (**11**)	1573	1605	1130	1253,920	642	456	3075	3434
$[Cu(HL^4)(NO_3)_2] \cdot H_2O$ (**12**)	1565	1608	1131	1255,899	640	438	3069	3385
H_2L^5	1619	---	1003	1383,840	---	---	3250	3346
$[Cu(HL^5)Cl]_2$ (**13**)	1595	1605	1042	1356,818	---	---	3291	3430
$[Cu(HL^5)NO_3] \cdot 1/2H_2O$ (**14**)	1600	1617	1032	1338,820	---	---	3239	3402

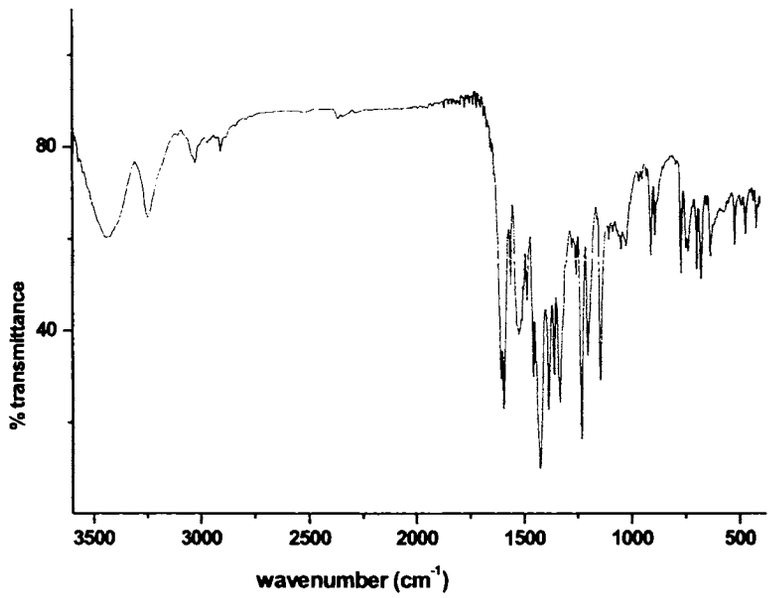

Fig. 3. 1. Infrared spectrum of $[CuL^2Cl]_2$ (5)

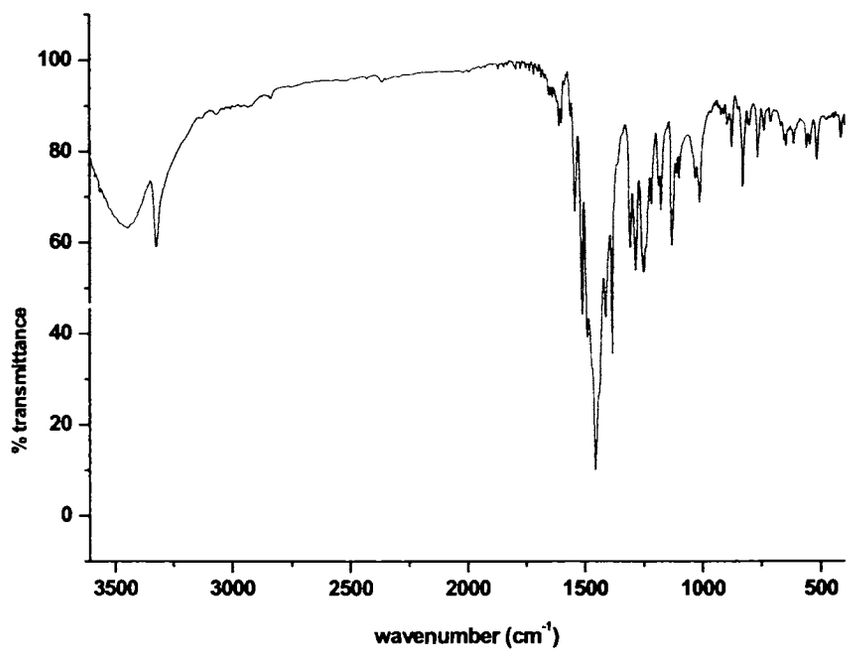

Fig. 3. 2. Infrared spectrum of $[CuL^1NO_3]_2$ (2)

The two bands appearing in the ranges 1298 - 1383 cm^{-1} [ν(CS)+ν(CN)] and 779 - 929 cm^{-1} (thioamide IV band) in the spectra of ligands have been shifted to lower frequencies indicating coordination of the thione/thiolato sulfur [19]. The presence of new bands in the range 323 to 350 cm^{-1} which is assignable to ν(Cu-S) is another indication of sulfur coordination which is found to be consistent with earlier reports [20]. Coordination of the pyridine nitrogen in the complexes except **13** and **14** is indicated by a positive shift of the in-plane and out-of-plane ring deformation bands [21]. Pyridine nitrogen coordination is further proved by strong bands observed in the region 262–313 cm^{-1} assignable to $\nu(Cu–N_{py})$ as suggested by Clark and Williams [22]. Based on the above spectral evidences, it is confirmed that the ligands HL^1, HL^2, HL^3 and HL^4 are tridentate, coordinating *via* the azomethine nitrogen, the pyridyl nitrogen and thione/thiolate sulfur. The ligand H_2L^5 is also tridentate, coordinating *via* phenolic oxygen, the azomethine nitrogen and thione sulfur.

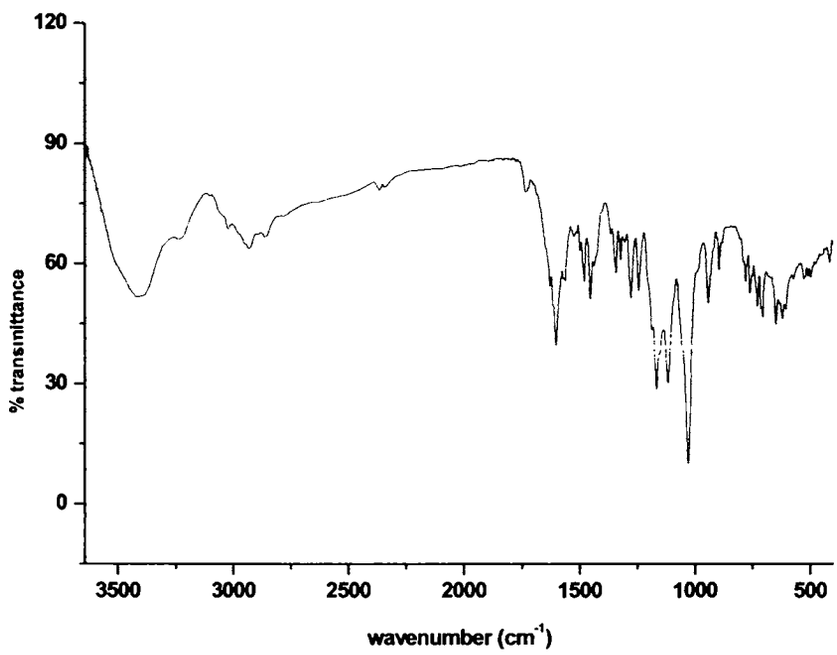

Fig. 3. 3. Infrared spectrum of $[Cu(HL^2)SO_4]_2{\cdot}4H_2O$ (7)

The chloro complexes **1** and **11** show ν(Cu-Cl) band at 304 and 318 cm^{-1}, respectively which is similar to its assignment for terminal chloro ligands in other thiosemicarbazone complexes [23]. In the chloro complexes **5, 9** and **13**, the strong

bands observed at 329, 315 and 325 cm^{-1} together with bands at 162, 164 and 165 cm^{-1} respectively has been assigned to the ν(Cu-Cl) in a bridging mode [24]. The crystal structure of **9** confirms the presence of two bridging chlorine atoms.

The nitrato complex **2** has two strong bands at 1287 and 1412 cm^{-1} with a separation of 125 cm^{-1} corresponding to ν_1 and ν_4 and a medium band at 1016 cm^{-1} corresponding to ν_2 of the nitrato group indicating the presence of a terminal monodentate nitrato group [25]. The $\nu_1+\nu_4$ combination bands considered as diagnostic for the monodentate nitrato group are observed at 1734 and 1749 cm^{-1}. The ν_3, ν_5 and ν_6 bands are observed at 743, 712 and 803 cm^{-1} respectively [26]. Besides, in the far IR spectrum of the complex, the band observed at 255 cm^{-1} can be assigned to ν(Cu–ONO_2) consistent with the bands at 253-280 cm^{-1} range reported earlier for ν(Cu–ONO_2) in metal complexes [27]. The spectrum of **12** exhibits strong bands at 1385 and 1256 cm^{-1} with a separation of 129 cm^{-1}, together with a weak band at 1016 cm^{-1} indicatng the monodentate nitrate ion. Presence of monodentate nitrate in **14** is evidenced from the bands at 1385 and 1279 cm^{-1} along with the combination bands at 1753 and 1735 cm^{-1}.

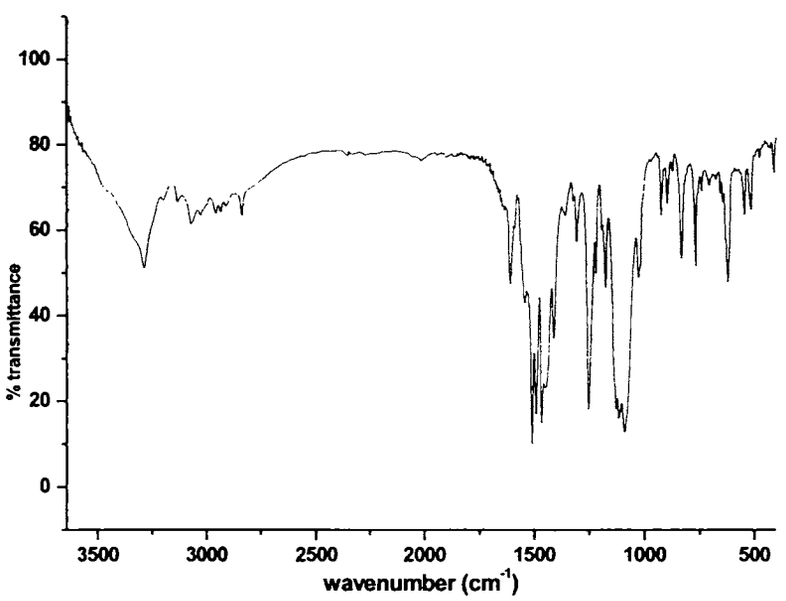

Fig. 3. 4. Infrared spectrum of $[CuL^1]_2(ClO_4)_2 \cdot 2H_2O$ (4)

The azido complexes **3** and **6** show sharp bands 2056 and 2038 cm^{-1} and strong bands at 1243 and 1356 cm^{-1} respectively. These are assigned to ν_a and ν_s of the coordinated azido group. The broad bands observed at 647 cm^{-1} for both complexes are assigned to δ(N-N-N). In the far IR spectra, the $\nu(Cu\text{-}N_{azido})$ bands are observed at 446 and 435 cm^{-1} respectively for **3** and **6**.

The perchlorate complexes **4** and **8** show single broad bands at 1121 cm^{-1} and strong bands at 626 cm^{-1}, indicating the presence of ionic perchlorate. The bands at 1121 cm^{-1} are assignable to $\nu_3(ClO_4)$ and the unsplit bands at 626 cm^{-1} are assignable to $\nu_4(ClO_4)$. In the spectrum of the compound **4**, a medium band at 926 cm^{-1} may be due to $\nu_1(ClO_4)$ suggesting that ionic perchlorate is distorted from tetrahedral symmetry due to lattice effects or hydrogen bonding by the NH functions of the coordinated ligand [28]. However, no band assignable to $\nu_1(ClO_4)$ is observable in the spectrum of compound **8**.

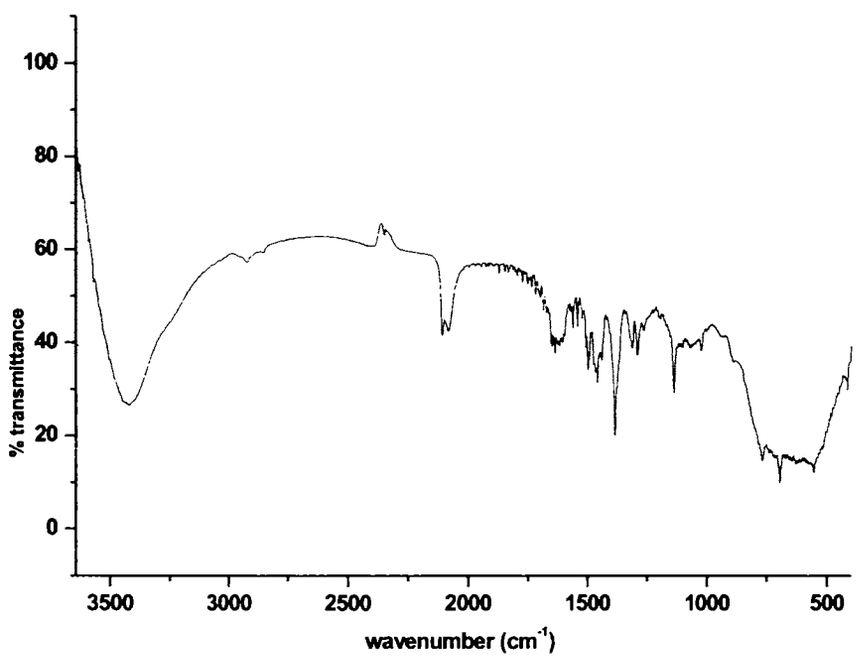

Fig. 3. 5. Infrared spectrum of $[CuL^3NCS]\cdot 1/2H_2O$ (10)

For the sulfato complex **7**, strong bands at 1116 and 1028 cm^{-1} are assignable to ν_3 of the mono coordinated sulfato group. Medium bands at 939 cm^{-1} (ν_1) and 644 cm^{-1} (ν_4) further confirm the unidentate behaviour of sulfato group [25].

Thiocyanato complex **10** exhibits a strong and sharp band at 2079 cm^{-1}, a weak band at 773 cm^{-1} and another weak band at 484 cm^{-1} which can be attributed to ν(CN), ν(CS) and δ(NCS) respectively. These values are typical for N-bonded thiocyanato complexes. A medium band at 325 cm^{-1} corresponds to $\nu(Cu\text{-}N_{thiocyanato})$ vibrations is in agreement with the earlier reported values [29].

Table 3. 4. Metal-ligand stretching frequencies (cm^{-1}) of the copper(II) complexes

Compound	$\nu Cu\text{-}N_{azo.}$	$\nu Cu\text{-}N_{py}$	νCu-S	νCu-Cl
$[CuL^1Cl]$ (**1**)	415	250	325	304
$[CuL^1NO_3]_2$ (**2**)	415	313	323	---
$[CuL^1N_3]_2 \cdot 2/3\ H_2O$ (**3**)	407	272	332	---
$[CuL^1]_2(ClO_4)_2 \cdot 2H_2O$ (**4**)	412	271	325	---
$[CuL^2Cl]_2$ (**5**)	415	275	344	329,162
$[CuL^2N_3]$ (**6**)	402	262	338	---
$[Cu(HL^2)SO_4]_2 \cdot 4H_2O$ (**7**)	415	280	324	---
$[Cu(HL^2)_2]\ (ClO_4)_2 \cdot 1/2$ EtOH (**8**)	414	276	325	---
$[CuL^3Cl]_2$ (**9**)	413	297	325	315,164
$[CuL^3NCS] \cdot 1/2H_2O$ (**10**)	413	297	325	---
$[Cu(HL^4)Cl_2]$ (**11**)	421	254	338	318
$[Cu(HL^4)(NO_3)_2] \cdot H_2O$ (**12**)	417	312	350	---
$[Cu(HL^5)Cl]_2$ (**13**)	425	---	336	325,165
$[Cu(HL^5)NO_3] \cdot 1/2H_2O$ (**14**)	415	---	325	---

3.5.2. Electronic spectra

The electronic absorption spectra are often very helpful in the evaluation of results furnished by other methods of structural investigation. The tentative assignments of the significant electronic spectral bands of ligands and their copper(II) complexes are presented in Table 3.5. The electronic spectra in $CHCl_3$ solution of the complexes show the following intraligand absorption maxima (Fig.3.6 & Table 3.5). The $\pi \rightarrow \pi^*$ transitions are not significantly altered on complex formation, but the $n \rightarrow \pi^*$ transitions associated with the pyridine ring observed above 30000 cm^{-1} in the spectra of the thiosemicarbazones are shifted to higher energies, the blue shift indicating coordination *via* the pyridyl nitrogen [30].

Strong bands in the range 22880–25770 cm^{-1} observed in the spectra of all Cu(II) complexes are assigned to S → Cu and py →Cu charge-transfer bands [19]. For the chloro complexes **1**, **5** and **13**, the Cl→Cu(II) charge transfer bands are found at 27700, 29150 and 27620 cm^{-1} respectively and band at 27850 cm^{-1} in the spectrum of nitrato complex (**2**) is attributable to nitrato O →Cu(II) ligand to metal charge transfer transition [31].

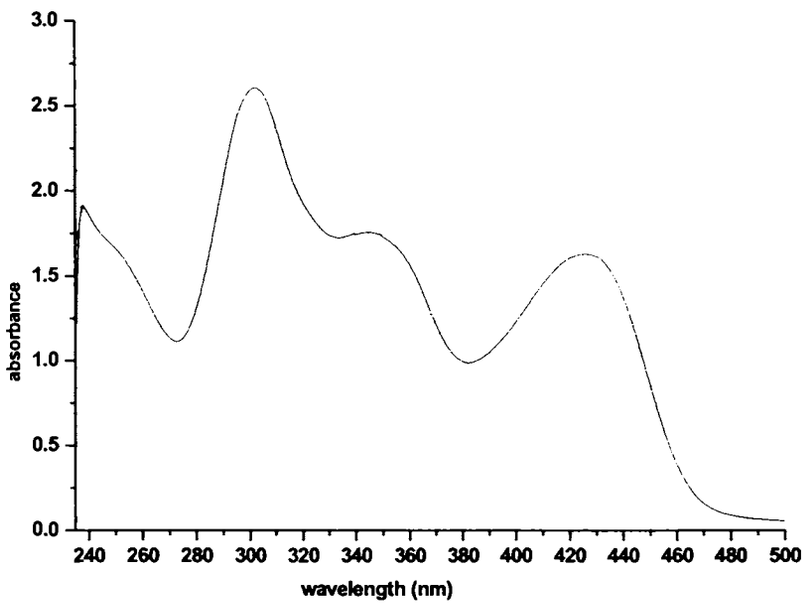

Fig. 3.6. Electronic spectrum of $[CuL^2Cl]_2$ (5) –Intraligand bands

Table 3. 5. Electronic spectral data (cm^{-1}) of thiosemicarbazones and their copper(II) complexes

Compound	π→π*	n→π*	C T	d -d
HL^1	42730,38760	30770	---	---
$[CuL^1Cl]$ (**1**)	41840,36230	31150	22990,27700	16420
$[CuL^1NO_3]_2$ (**2**)	42190,37490	35460	23150,27850	14880
$[CuL^1N_3]_2 \cdot 2/3\ H_2O$ (**3**)	42020,37050	34280	23510	16190
$[CuL^1]_2(ClO_4)_2 \cdot 2H_2O$ (**4**)	41670,37880	----	24040	15290
HL^2	42190,36630	30960	---	---
$[CuL^2Cl]_2$ (**5**)	42190,38610	33000	23420,29150	16230
$[CuL^2N_3]$ (**6**)	42120,38790	33210	23310	16270
$[Cu(HL^2)\ SO_4]_2 \cdot 4H_2O$ (**7**)	41840	33110	23870,28980	16080
$[Cu(HL^2)_2]\ (ClO_4)_2 \cdot 1/2$ EtOH (**8**)	42190,38760	32570	22880	16780
HL^3	43290,38610	30840	---	---
$[CuL^3Cl]_2$ (**9**)	42190,38760	32470	23200	16370
$[CuL^3NCS] \cdot 1/2H_2O$ (**10**)	42270,38620	31440	23760	16150
HL^4	41840,35840	29500	---	---
$[Cu(HL^4)Cl_2]$ (**11**)	41840	29240	24040	15080
$[Cu(HL^4)(NO_3)_2] \cdot H_2O$ (**12**)	42190	32570	24750	15060
H_2L^5	42020,33560	29670	---	---
$[Cu(HL^5)Cl]_2$ (**13**)	42370	34720	27620	15900
$[Cu(HL^5)NO_3] \cdot 1/2H_2O$ (**14**)	44840	---	25770	14770

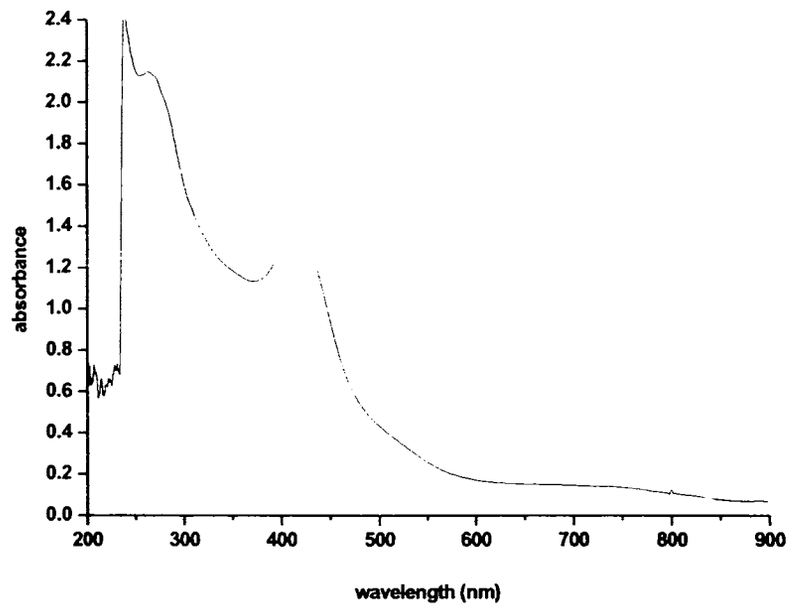

Fig. 3. 7. Electronic spectrum of $[CuL^1]_2(ClO_4)_2 \cdot 2H_2O$ (4)

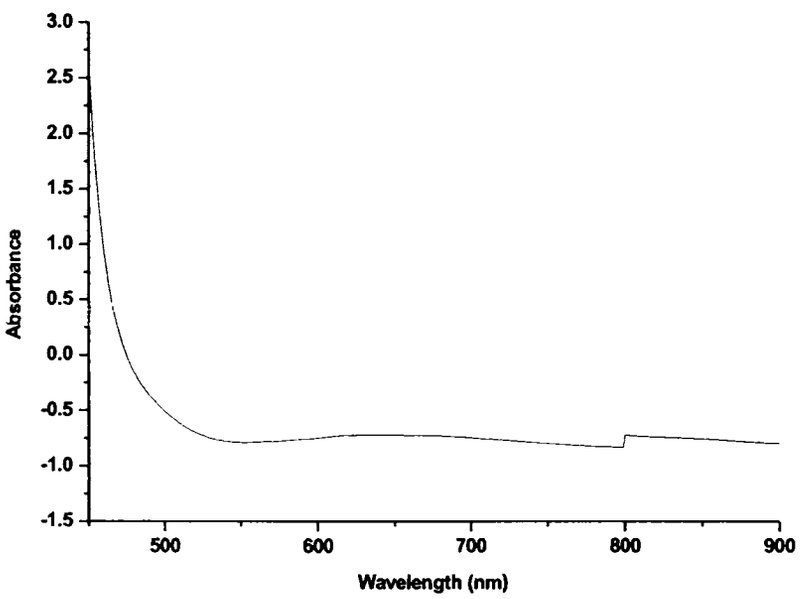

Fig. 3. 8. Electronic spectrum of $[CuL^3Cl]_2$ (9)

The spectra of the complexes **1**, **3**, **5**, **6**, **7**, **9**, **10** and **13**, exhibit weak d-d bands at *ca.* 16000 cm^{-1}, and that of **2**, **4**, **11**, **12** and **14** appear at *ca.*15000 cm^{-1}. For a square planar complex with $d_{x^2-y^2}$ ground state, three transitions are possible *viz*, $d_{x^2-y^2} \rightarrow d_{z^2}$,

$d_{x^2-y^2} \rightarrow d_{xy}$ and $d_{x^2-y^2} \rightarrow d_{xz}$, d_{yz} ($^2A_{1g} \leftarrow {}^2B_{1g}$, $^2B_{2g} \leftarrow {}^2B_{1g}$ and $^2E_g \leftarrow {}^2B_{1g}$) and square pyramidal complexes have the $d_{x^2-y^2} \rightarrow d_{xz}, d_{yz}$ and $d_{x^2-y^2} \rightarrow d_{z^2}$ transitions [32-34]. Since the four *d* orbitals lie very close together, each transition cannot be distinguished by their energy and hence it is very difficult to resolve the bands into separate components. The broad band observed at 16780 cm^{-1} in the electronic spectrum of the complex **8** is assigned to $^2E_g \leftarrow {}^2T_{2g}$ transition [35,36].

3.5.3. EPR spectra

The magnetic parameters measured in EPR study are related to the structure of the paramagnetic complex, the number of ligands, nature of bonding and spatial arrangements of the ligands around the central metal ion. The copper(II) ion, with a d^9 configuration, has an effective spin of S = 1/2 and is associated with a spin angular momentum, $m_s = \pm 1/2$, leading to a doubly degenerate spin state in the absence of a magnetic field. In a magnetic field the degeneracy is lifted between these states and the energy difference between them is given by $E = h\nu = g\beta H$, where h is Planck's constant, ν is the microwave frequency for transition from $m_s = +½$ to $m_s = -½$, g is the Lande splitting factor (equal to 2.0023 for a free electron), β is the Bohr magneton and H is the magnetic field. For the case of a $3d^9$ copper(II) ion, the appropriate spin Hamiltonian assuming a B_{1g} ground state is given by:

$$\hat{H} = \beta[g_{\parallel} H_z S_z + g_{\perp} (H_x S_x + H_y S_y)] + A_{\parallel} I_z S_z + A_{\perp} (I_x S_x + I_y S_y)$$

The EPR spectra of the complexes in the polycrystalline state at 298 K, in solution at 298 and 77 K were recorded in the X band, using 100 kHz field modulation and the g factors were quoted relative to the standard marker TCNE (g = 2.00277). EPR spectral assignments of the copper(II) complexes along with the spin Hamiltonian and orbital reduction parameters are given in the Table 3.6. The EPR spectra of compounds **8**, **10**, **13** and **14** in the polycrystalline state (298 K) show only one broad signal at 2.076, 2.077, 2.094 and 2.031 respectively, due to dipolar broadening and enhanced spin lattice relaxation. The spectra of the compounds **2**, **3**, **4**, **5**, **6**, **7**, **9** and

Table 3. 6. EPR spectral parameters of the copper(II) complexes

	1	2	3	4	5	6	7	8	9	10	11	12	13	14
Polycrystalline (298 K)														
$g_{\parallel}$	2.1167(g_3)	2.1769	2.1349	2.1931	2.1661	2.1635	2.1806	---	2.1842	---	2.1733(g_3)	2.2121	---	---
$g_{\perp}$	2.0341(g_1) 2.0746(g_2)	2.0585	2.0471	2.0501	2.0388	2.0423	2.0879	---	2.0533	---	2.0533(g_1) 2.0812(g_2)	2.0598	---	---
g_{iso} or g_{av}	---	2.0979	2.0764	2.0978	2.0812	2.0827	2.1188	2.0762	2.0969	2.0765	---	2.1039	2.0936	2.0309
DMF (298 K)														
g_{iso}	2.081	2.0955	2.0809	2.0955	2.081	2.0809	2.0955	2.0955	2.081	2.0955	2.0810	2.0810	2.0667	2.0667
A_{iso}	95.53	88.05	92.29	88.05	95.53	92.29	88.05	88.86	95.53	88.86	93.92	93.92	64.33	64.33
DMF (77 K)														
$g_{\parallel}$	2.1607	2.1787	2.1544	2.1787	2.1625	2.1563	2.1824	2.1697	2.1609	2.1679	2.2046	2.1888	2.1848	2.1904
$g_{\perp}$	2.0566	2.0585	2.0487	2.0533	2.0533	2.0504	2.0664	2.0469	2.0518	2.0549	2.0696	2.0614	2.0735	2.0551
$A_{\parallel}$(Cu)	186.6	195	187.75	194.9	188.5	187.92	191.9	192.5	186.63	193.99	152.66	194.90	194.64	199.41
G	2.19	3.11	2.96	3.99	4.49	4.03	2.08	3.75	3.57	3.15	2.63	3.65	2.56	3.56
α^2	0.7400	0.7822	0.7335	0.7797	0.7457	0.7366	0.7785	0.7611	0.7382	0.7670	0.6952	0.7932	0.7937	0.8046
β^2	0.8468	0.8048	0.8311	0.8184	0.8392	0.8351	0.8493	0.8556	0.8481	0.8283	0.9761	0.8209	0.8339	0.8049
γ^2	0.9916	0.9085	0.9182	0.8801	0.9479	0.9363	0.9730	0.8833	0.9476	0.9336	0.9784	0.9242	0.9648	0.8528
K	0.4184	0.4053	0.4067	0.4122	0.4203	0.4069	0.4089	0.3884	0.4141	0.4070	0.3823	0.4416	0.3441	0.3436
$K_{\parallel}$	0.6266	0.6295	0.6096	0.6381	0.6258	0.6151	0.6612	0.6512	0.6261	0.6353	0.6786	0.6512	0.6619	0.6476
$K_{\perp}$	0.7338	0.7106	0.6735	0.6862	0.7069	0.6897	0.7575	0.6723	0.6995	0.7161	0.7828	0.7331	0.8268	0.6862
P	0.0231	0.0251	0.0229	0.0242	0.0233	0.0207	0.0237	0.0241	0.0229	0.0239	0.0194	0.025	0.0241	0.0253

12 show typical axial behavior with slightly different $g_{\|}$ and $g_{\perp}$ values. The spectra of compounds **1** and **11** give three g values *viz.* g_1, g_2 and g_3 indicating rhombic distortion in geometry (Fig. 3.9 & 3.10).

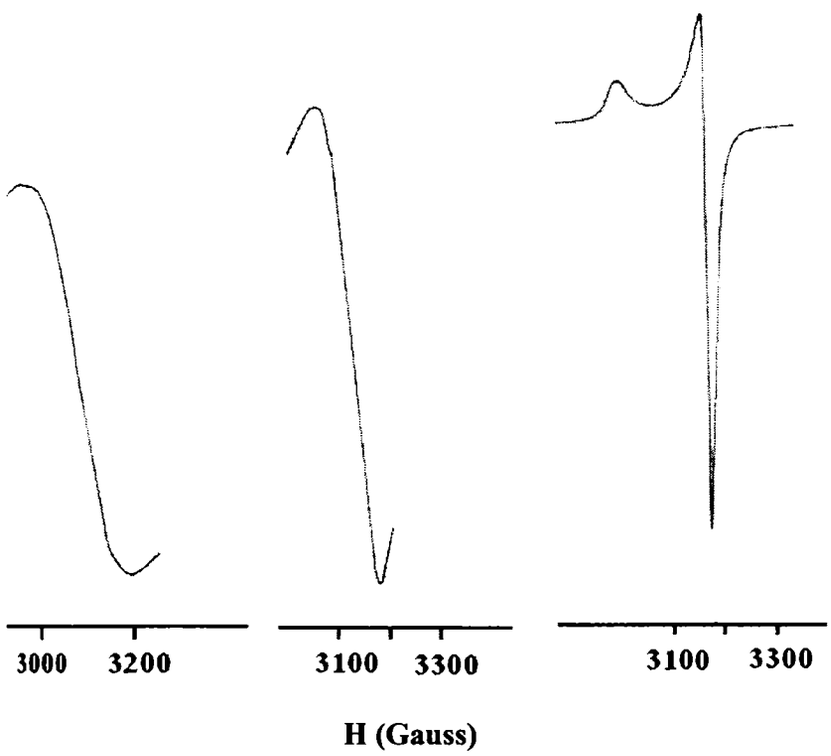

Fig. 3. 9. EPR spectra of 8 (left), 10 (middle), and 6 (right) in polycrystalline state at 298 K

The geometric parameter G, which is a measure of the exchange interaction between the copper centres in the polycrystalline compound, is calculated using the equation: $G = (g_{\|}-2.0023)/(g_{\perp}-2.0023)$ for axial spectra and for rhombic spectra, $G = (g_3-2)/(g_{\perp}-2)$ and $g_{\perp} = (g_1+g_2)/2$. If G>4, exchange interaction is negligible and if it is less than 4, considerable exchange interaction is indicated in the solid complex [37]. In all the copper(II) complexes $g_{\|} > g_{\perp} > 2.0023$ and G value within the range 2.08–4.49 are consistent with a $d_{x^2-y^2}$ ground state [38].

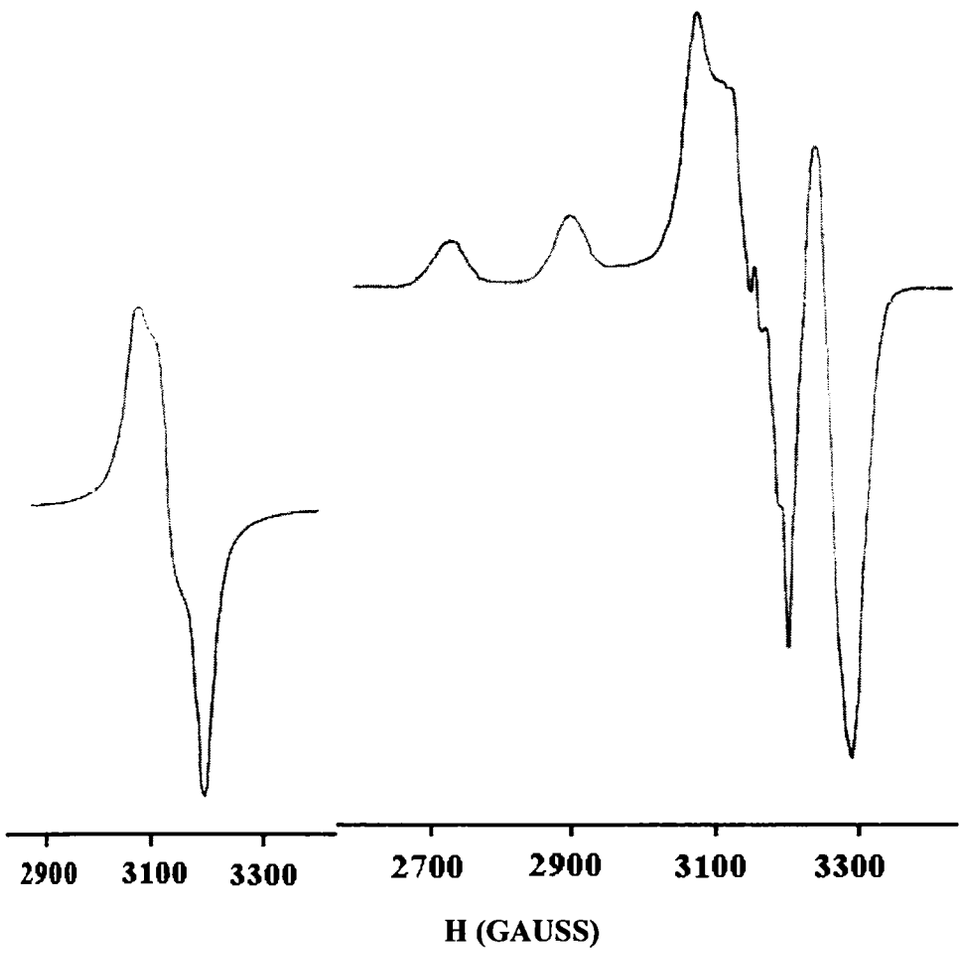

Fig. 3. 10. EPR spectra of compound 1 in polycrystalline state at 298 K (left) and in DMF solution at 77 K (right)

The solution spectra of complexes were recorded in DMF at 298 K. They are isotropic in nature with well-resolved four hyperfine lines (Fig. 3.11). The hyperfine splitting is due to the interaction of the electron spin with the copper nuclear spin (^{63,65}Cu, I = 3/2). The parameters A_{iso} and g_{iso} were determined from this spectra and A_{iso} varies from 64.33×10^{-4} to 95.53×10^{-4} cm^{-1}. In **7**, **8** and **13**, five lines corresponding to the isotropic nitrogen superhyperfine splitting are observed on the high field peaks with splitting constant values 9.78×10^{-4}, 10.37×10^{-4} and 14.47×10^{-4} cm^{-1} respectively.

The spectra of all the complexes in DMF at 77 K are axial with four copper hyperfine lines in both the parallel and perpendicular regions (Fig. 3.10, 3.12, 3.13 and

3.14). For the spectra of all the complexes in frozen DMF, the $g_{\parallel} > g_{\perp}$ values rules out the possibility of trigonal bipyramidal structures for which $g_{\perp} > g_{\parallel}$ is expected.

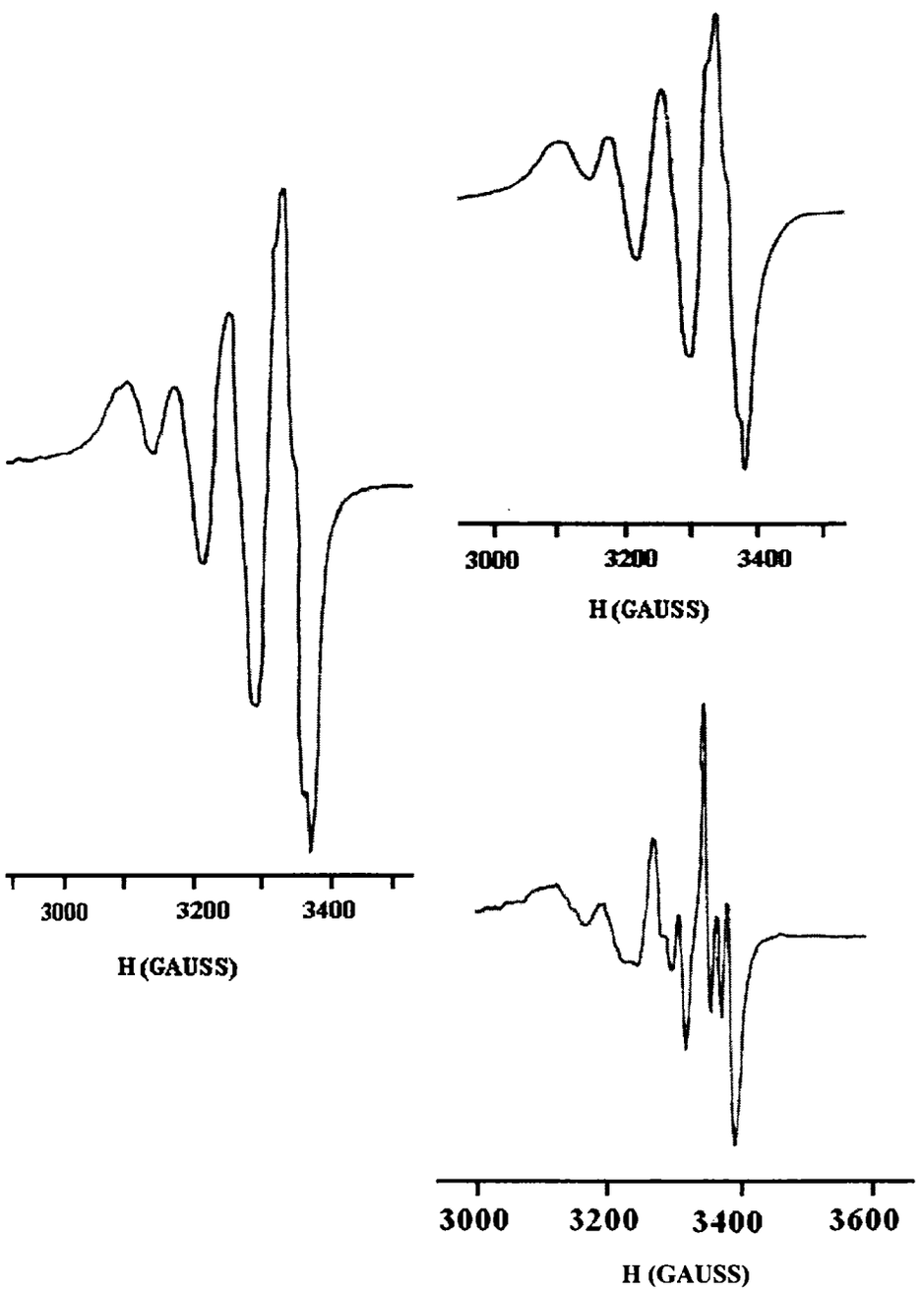

Fig. 3.11. EPR spectra of 7 (left), 8 (top)and 13 (bottom) in DMF solution at 298 K

The binuclear nature of **2**, **3**, **4**, **7**, **9** and **13** was confirmed by the presence of half-field signals ($\Delta M_s = \pm 2$) at *ca.*1600 G (Fig 3.12, 3.13 and 3.14) with g values

4.017, 4.254, 4.043, 4.254, 4.068 and 4.167 respectively. The half-field resonances were obtained in the solution spectra in DMF at 77 K for all dimeric complexes except **9** for which the signal was observed in the powder spectrum at 298 K. Probably the dissolution of **9** in DMF results in the breaking of the binuclear complex into a mononuclear one. Interaction of Cu^{2+} - Cu^{2+} pairs (S = 1) in frozen DMF solutions is evidenced from the appearance of half-field signals [39]. However, for **5**, the half-field signal was not well resolved.

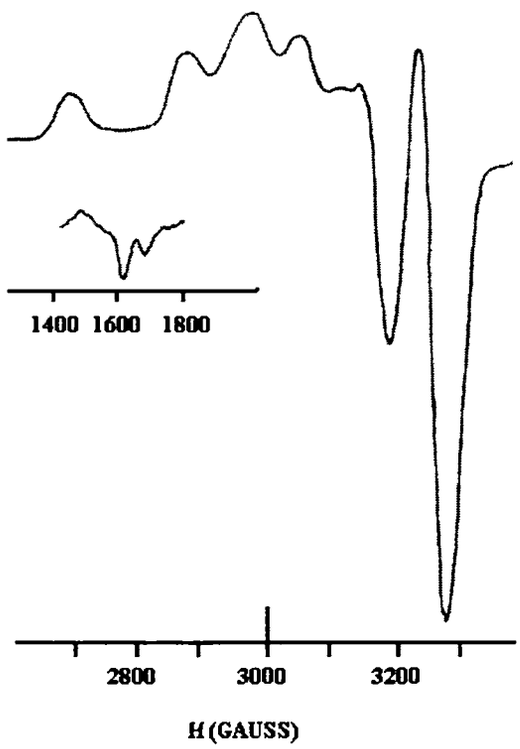

Fig. 3. 12. EPR spectrum of 2 in DMF solution at 77 K

The EPR parameters $g_{\|}$, $g_{\perp}$, g_{av}, $A_{\|}$(Cu) and $A_{\perp}$(Cu) and the energies of *d–d* transitions were used to evaluate the bonding parameters α^2, β^2 and γ^2, which may be regarded as measures of the covalency of the in-plane σ bonds, in-plane π bonds, and out-of-plane π bonds respectively. The value of in-plane σ bonding parameter α^2 was estimated from the expression of Kivelson and Neiman [40].

$$\alpha^2 = -A_{\|}/0.036 + (g_{\|} - 2.0023) + 3/7(g_{\perp} - 2.0023) + 0.04$$

The orbital reduction factors $K_{\|} = \alpha^2\beta^2$ and $K_{\perp} = \alpha^2\gamma^2$ were calculated using the following expressions [41,42].

$$K_{\parallel}^{2} = (g_{\parallel} - 2.0023)\ \Delta E(d_{xy}\text{-}d_{x^2-y^2})/8\lambda_0$$

$K_{\perp}^{2} = (g_{\perp} - 2.0023)\ \Delta E(_{dxz,yz}\text{-}d_{x^2-y^2})/2\lambda_0$ where λ_0 is the spin orbit coupling constant and has the value $-828\ cm^{-1}$ for a copper(II) d^9 system.

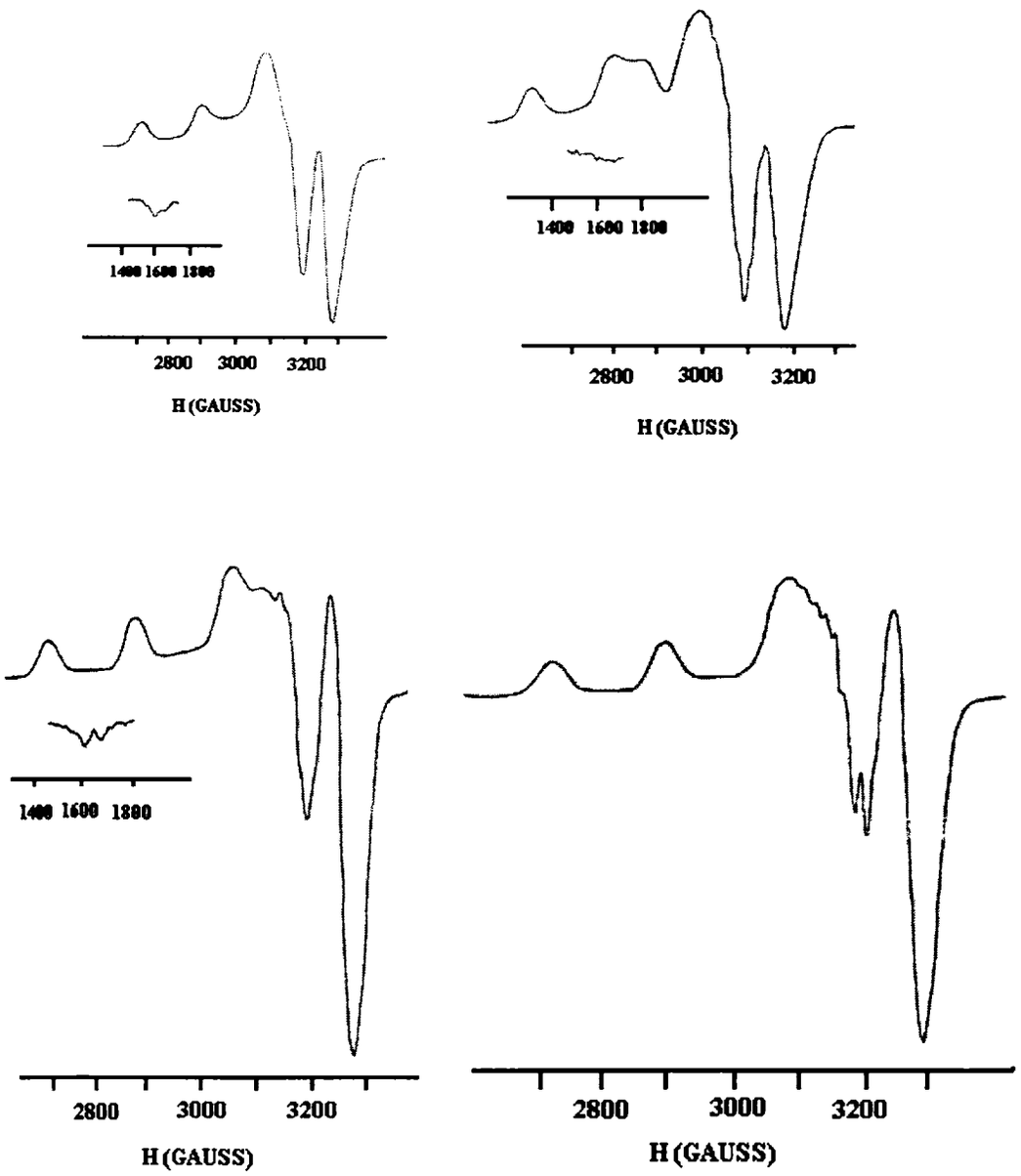

Fig. 3.13. EPR spectra of 3 (top left), 9 (top right), 4 (bottom left) and 5 (bottom right) in DMF solution at 77 K

According to Hathaway [43], $K_{\|} = K_{\perp} = 0.77$ for pure σ bonding and $K_{\|} < K_{\perp}$ for in-plane π bonding, while for out-of-plane π bonding $K_{\|} > K_{\perp}$. In all the copper(II) complexes, it is observed that $K_{\|} < K_{\perp}$ which indicates the presence of significant in-plane π bonding. Furthermore, α^2, β^2 and γ^2 have values less than 1 which are expected for 100% ionic character of the bonds and become smaller with increasing covalent bonding. The evaluated values of α^2, β^2 and γ^2 of the complexes are consistent with both strong in-plane σ and in-plane π bonding. The $g_{\|}$ values are nearly the same for all the complexes indicating that the bonding is dominated by the thiosemicarbazone moiety. The fact that the $g_3/g_{\|}$ values are less than 2.3 is an indication of significant covalent bonding in the complexes [44].

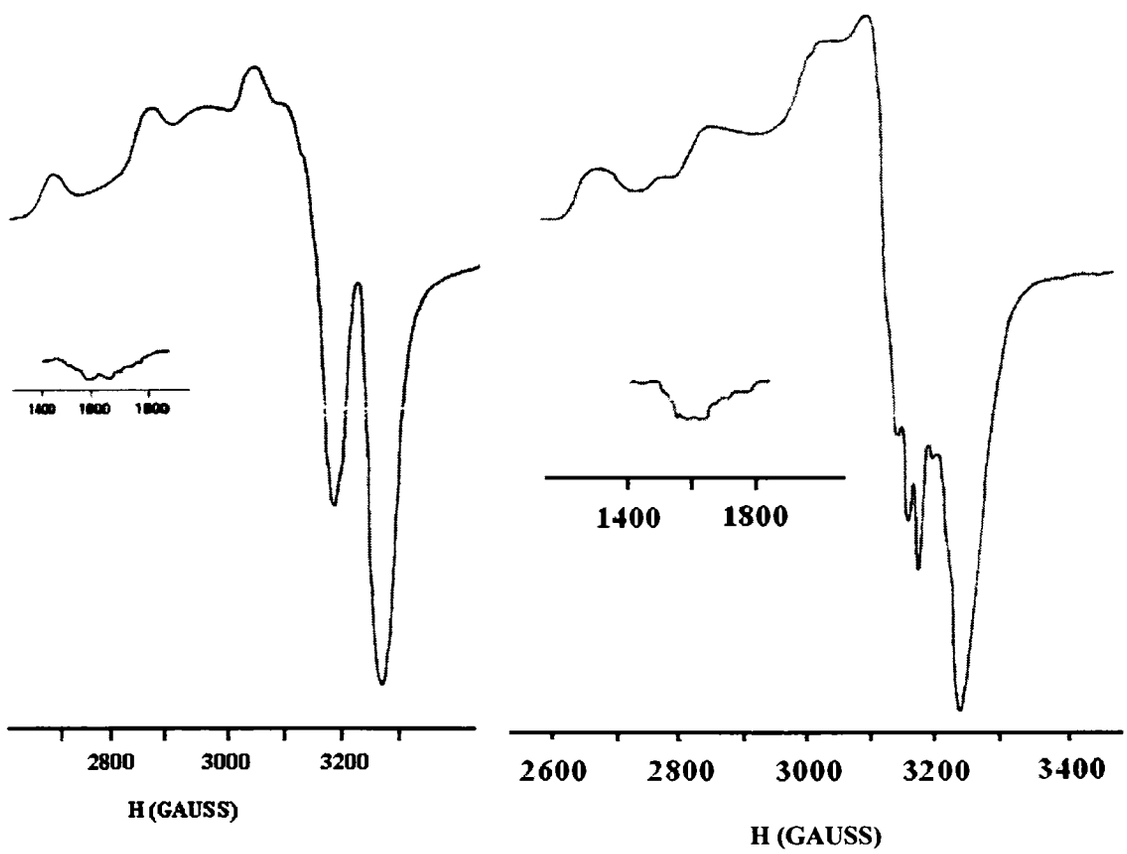

Fig. 3.14. EPR spectra of 7 (left) and 13 (right) in DMF solution at 77 K

The Fermi contact hyperfine interaction term K may be obtained from [45]

$$K = A_{iso}/P\beta^2+(g_{av}-2.0023)/\beta^2$$

where P is the free ion dipolar term and its value is 0.036. K is a dimensionless quantity, which is a measure of the contribution of *s* electrons to the hyperfine interaction. The K values obtained for all the complexes are in agreement with those estimated by Assour [46] and Abragam and Pryce [47].

3.5.4. Crystal structure of $[CuL^3Cl]_2$ *(9)*

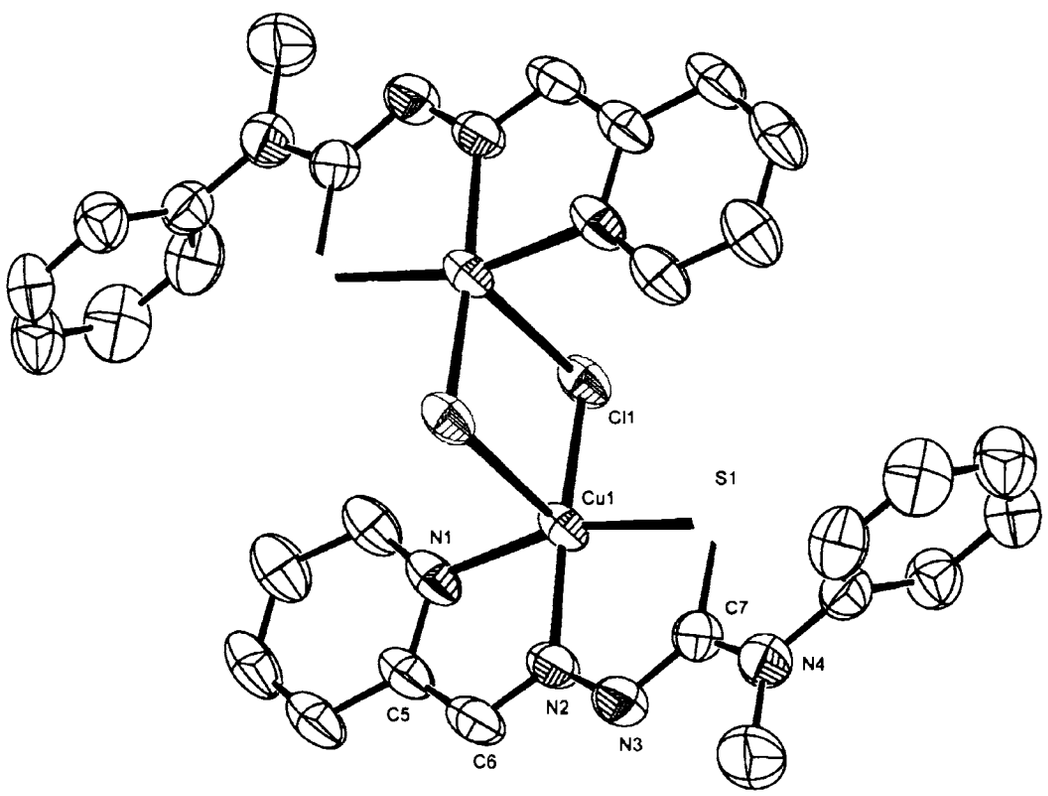

Fig. 3.15. ORTEP diagram of $[CuL^3Cl]_2$ (9) in 50% probability ellipsoids

The molecular structure of the compound **9** along with atom numbering scheme are given in Fig. 3.15. The asymmetric unit is formed by one half of the molecule and the other half is related by a center of inversion in the Cu(1)Cl(1)-Cu(1a)-Cl(1a) ring. The coordination geometry at each Cu(II) is square pyramidal. The ligand HL^3 coordinates to the metal in a tridentate manner through its pyridyl nitrogen, azomethine

nitrogen and thiolate sulfur, after enolization and deprotonation, to form the basal plane along with one chlorine atom. The basal chlorine atom takes the axial position of the adjacent monomer like its counterpart does to form two distorted square pyramids. The Cu-Cu separation is found to be 3.5330(11) Å. The τ value [48] of 0.139 at metal centres indicates slight distortion from perfect square pyramidal geometry. Thus, the two metal centres are bridged *via* chlorine atoms resulting in the formation of four five membered rings in which one copper atom is shared by two fused rings. A four membered ring involving the copper atoms and the chlorine atoms is also formed. The five membered ring Cu(1), N(1), C(5), C(6), N(2) is approximately planar with a maximum deviation of 0.0135(18) Å for C5, but Cu(1), N(2), N(3), C(7), S(1) ring is slightly distorted as evidenced by the maximum deviation of 0.1349(18) Å for C7; likewise for their counterpart rings. The four membered ring Cl(1), Cu(1), Cl(1a), Cu(1a) makes an angle of 83.62(3)° with the mean plane of bicyclic chelate system N(1), C(5), C(6), N(2), N(3), C(7), S(1), Cu(1) which is slightly distorted from planarity with a maximum deviation of –0.1979(18) Å for C5.

Relevant bond lengths and angles are featured in Table 3.7. The bridging chlorine atoms are positioned at distances of 2.2587(7) Å for Cl(1) and 2.7245(12) Å for Cl(1a) and make an angle of 90.20(3)° at each metal centers and are in agreement with previous reports [24,30]. The Cu-$N_{azomethine}$ bond length [1.9784(14) Å] is lesser by 0.0541(19) Å compared to Cu-$N_{pyridine}$, indicates the strength of former bond than the latter [12,24].

The ligand HL^3 suffers a structural reorientation upon complexation. The N3 and C5 atoms were in *Z* configuration about the azomethine bond in its metal free form of ligand, is now in *E* form to coordinate the metal in a NNS manner. Coordination lengthens the thiosemicarbazone moiety's C(7)-S(1) bond length by 0.0645(22) Å and shortens N(3)-C(7) by 0.0384(18) Å, suggesting deprotonation after enolization. A comparison of the changes in bond lengths and angles are given in Table 3.7.

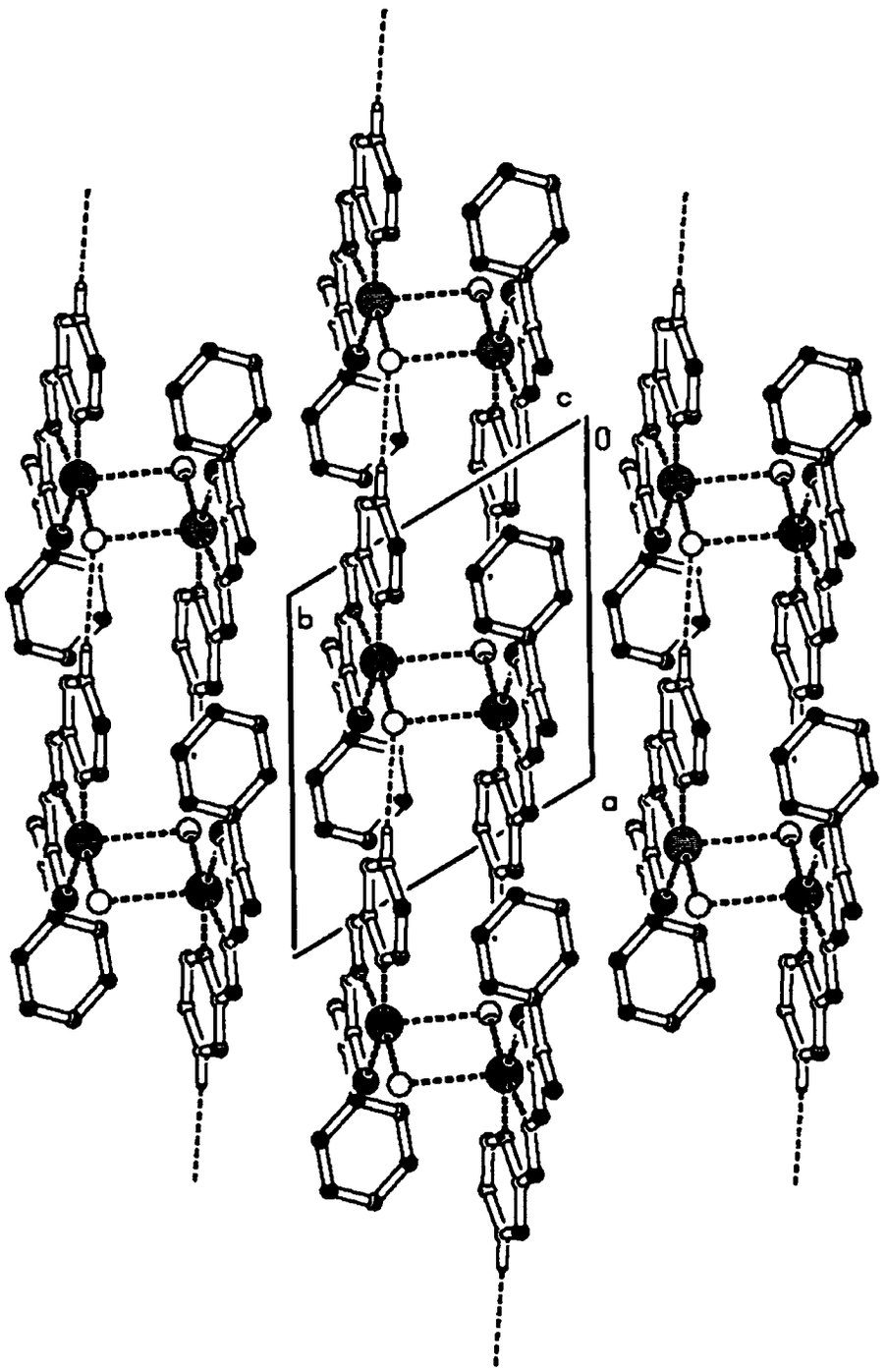

Fig. 3.16. A view of the unit cell packing of the molecule (9) showing hydrogen bonding interactions producing polymeric chains

Table 3. 7. Selected bond lengths (Å) and bond angles (°) of HL^3 and $[CuL^3Cl]_2$ (9).

	HL^3	$[CuL^3Cl]_2$ (9)
S(1)–C(7)	1.6750(14)	1.7395(18)
N(2)–C(6)	1.285(2)	1.287(2)
N(2)– N(3)	1.3613(17)	1.352(2)
N(3)–C(7)	1.3644(18)	1.326(2)
N(4)–C(7)	1.345(2)	1.352(2)
Cu(1)–S(1)		2.2481(6)
Cu(1)–N(1)		2.0325(14)
Cu(1)–N(2)		1.9784(14)
Cu(1)–Cl(1)		2.2587(7)
Cu(1)–Cl(1a)		2.7245(12)
C(6)–N(2)–N(3)	117.75(13)	121.34(14)
N(2)–N(3)–C(7)	120.25(12)	111.73(13)
N(4)–C(7)–N(3)	113.87(12)	116.42(15)
N(3)–C(7)–S(1)	122.89(12)	124.89(14)
N(4)–C(7)–S(1)	123.22(11)	118.69(13)
S(1)–Cu(1)–N(1)		162.41(5)
N(1)–Cu(1)–N(2)		80.52(6)
S(1)–Cu(1)–N(2)		83.78(5)
N(1)–Cu(1)–Cl(1)		96.93(5)
N(2)–Cu(1)–Cl(1)		170.75(4)
S(1)–Cu(1)–Cl(1)		97.32(2)
N(1)–Cu(1)–Cl(1a)		90.46(5)
N(2)–Cu(1)–Cl(1a)		98.68(5)
S(1)–Cu(1)–Cl(1a)		99.74(3)
Cl(1)–Cu(1)–Cl(1a)		90.20(3)

The molecules are packed along the *a* axis directed by the C3-H3...Cl1 intermolecular hydrogen bonding interaction (Table 3.8). This intermolecular hydrogen bonds link the molecules to form one-dimensional polymeric chains (Fig. 3.16). The aromatic π...π stacking interactions between pyridyl rings (symmetry code: 2-x, 1-y, 1-z and a Cg-Cg distance of 3.8896 Å) reinforces crystal structure cohesion in molecular packing in the crystal lattice

Table 3. 8. H-bonding interactions in compound 9

D-H...A	D-H (°)	H...A (°)	D...A (°)	D-H...A (Å)
C(1)-H(1)...Cl(1)[a]	0.93	2.81	3.3611	119
C(3)-H(3)...Cl(1)[b]	0.93	2.76	3.5754	148

D=donor, A=acceptor, Equivalent position codes: a= x, y, z; b=1+x, y, z

Conclusion

This chapter describes the syntheses and characterization of fourteen copper(II) complexes of five ligands *viz.*, pyridine-2-carbaldehyde N(4)-*p*-methoxyphenyl thiosemicarbazone (HL^1), pyridine-2-carbaldehyde N(4)-phenylethyl thiosemicarbazone (HL^2), pyridine-2-carbaldehyde N(4)-methyl, N(4)-phenyl thiosemicarbazone (HL^3), pyridine-2-carbaldehyde N(4)-pyridyl thiosemicarbazone [HL^4] and salicylaldehyde-N(4)-phenylethyl thiosemicarbazone [H_2L^5]. The physico-chemical methods of characterization include partial elemental analyses, conductivity and room temperature magnetic susceptibility measurements and IR, electronic and EPR spectral studies. The crystal structure of the compound $[CuL^3Cl]_2$ has been determined by X-ray diffraction studies and is found that the dimer consists of two square pyramidal Cu(II) centres linked by two chlorine atoms.

References

1. A.E. Liberta, D.X. West, Biometals 5 (1992) 121.
2. Z. Afrasiabi, E. Sinn, J. Chen, Y. Ma, A.L. Rheingold, L.N. Zakharov. N. Rath, S. Padhye, Inorg. Chim. Acta 357 (2004) 271.
3. D.X. West, A.E. Liberta, S.B. Padhye, R.C Chikate, P.B. Sonawane, A.S. Kumbhar, R.G. Yerande, Coord. Chem. Rev. 123 (1993) 49.
4. A.C. Sartorelli, K.C. Agrawal, A.S. Tsiftsoglou, A.C. Moore, Adv. Enz. Reg. 15 (1977) 117.
5. J.G- Tojal, L. Lezama, J.L. Pizarro, M. Insausti, M.I. Arriortua, T. Rojo, Polyhedron 18 (1999) 3703.
6. P.G- Saiz, J.G- Tojal, A. Mendia, B. Donnadieu, L. Lezama, J.L. Pizarro, M.I. Arriortua, T. Rojo, Eur. J. Inorg. Chem. 518 (2003) 527.
7. G.M. Sheldrick (1997) SHELXS 97 and SHELXL 97, Bruker AXS Inc., Madison, Wisconsin, USA.
8. L.J. Farrugia, J. Appl. Cryst. 30 (1997) 565.
9. A.L. Spek, J. Appl. Cryst. 36 (2003) 7.
10. D.X. West, J.S. Ives, G.A. Bain, A.E. Liberta, J. Valdes-Martinez, K.H. Ebert, S. H-Ortega, Polyhedron 16 (1997) 1895.

11. W.J. Geary, Coord. Chem. Rev. 7 (1971) 81.
12. V. Philip, V. Suni, M.R.P. Kurup, M. Nethaji, Polyhedron 25 (2006) 1931.
13. N.S. Youssef, K.H. Hegab, Synth. React. Inorg. Met-Org. Nano-Met.Chem. 35 (2005) 391.
14. Y.-P. Tian, W.-T. Yu, C.-Y.Zhao, M.-H. Jiang, Z.-G. Cai, H.-K. Fun, Polyhedron 21 (2002) 1219.
15. R.P. John, A. Sreekanth, M.R.P. Kurup, A. Usman, I.A. Razak, H. -K. Fun, Spectrochim. Acta 59A (2003) 1349.
16. D.X. West, N.M. Kozub, Transition Met. Chem. 21 (1996) 52.
17. M. Joseph, V. Suni, M.R.P. Kurup, M. Nethaji, A. Kishore, S.G. Bhat, Polyhedron 23 (2004) 3069.
18. A. Sreekanth, H.-K. Fun, M.R.P. Kurup, J. Mol. Struct. 737 (2005) 61.
19. R. P. John, A. Sreekanth, M. R. P. Kurup, S. M. Mobin, Polyhedron 21 (2002) 2515.
20. K.H. Reddy, M.R. Reddy, K.M. Raju. Ind. J. Chem. 38A (1999) 299.
21. B.S. Garg, M.R.P. Kurup, S.K. Jain, Y.K. Bhoon, Transition Met. Chem. 16 (1991) 111.
22. R.J. Clark, C.S. Williams, Inorg. Chem. 4 (1965) 350.
23. M. B. Ferrari, G. G. Fara, M. Lafranchi, C. Pelizzi, and M. Tarasconi, Inorg. Chim. Acta 181 (1991) 253.
24. M. Joseph, M. Kuriakose, M.R.P. Kurup, E. Suresh, A. Kishore, S.G. Bhat, Polyhedron 25 (2006) 61.
25. K. Nakamoto, Infrared and Raman Spectra of Inorganic and Coordination Compounds, 5th ed., Wiley-Interscience, New York, (1997) 86.
26. D.N. Sathyanarayana, Vibrational Spectroscopy, New Age International, New Delhi (2004) 400.
27. S .K. Jain, B. S.Garg, Y. K. Bhoon, Spectrochim. Acta 42A (1986) 701.
28. A.M. Bond, R.L. Martin, Coord. Chem. Rev. 54 (1984) 23.
29. E. W. Ainscough, A. M. Brodie, J. D. Ranford, J. M. Waters, Dalton Trans. 23 (1991) 2125.
30. A. Sreekanth, M.R.P. Kurup, Polyhedron 22 (2003) 3321.

31. P. Bindu, M.R.P. Kurup, T.R.Satyakeerty, Polyhedron 18 (1999) 321.
32. R.P. John, A.Sreekanth, V. Rajakannan, T.A. Ajith, M.R.P. Kurup, Polyhedron 23 (2004) 2549.
33. A.B.P. Lever, Inorganic Electronic Spectroscopy, 2nd ed., Elsevier, Amsterdam, 1984.
34. B.J. Hathaway, A.A.G. Tomlinson, Coord. Chem. Rev. 5 (1970) 24.
35. N. Raman, S. Ravichandran, C. Thangaraja, J. Chem. Sci. 116 (2004) 215.
36. S. E. Livingstone, J. E. Oluka, Transition Met. Chem. 2 (1977) 190.
37. B.J. Hathaway, D.E. Billing, Coord. Chem. Rev. 5 (1970) 1949.
38. M.J. Bew, B.J. Hathaway, R.R. Faraday, J. Chem. Soc. Dalton Trans. (1972) 1229.
39. O.I. Singh, M. Damayanti, N.R. Singh, R.K.H. Singh, M. Mohapatra, R.M. Kadam, Polyhedron 24 (2005) 909.
40. D. Kivelson, R. Neiman, J. Chem. Soc., Dalton Trans. 35 (1961) 149.
41. B.N. Figgis, Introduction to Ligand Fields, Interscience, New York, 1966, p.295.
42. D.X. West, J. Inorg. Nucl. Chem. 43 (1984) 3169.
43. B.J. Hathaway, in: G. Wilkinson, R.D. Gillard, J.A. McCleverty (Eds.), Comprehensive Coordination Chemistry, Pergamon Press, 1987 (Chapter 53 ,ref-903).
44. J.R. Wasson, C. Trapp, J. Phys. Chem. 73 (1969) 3763.
45. L.S. Lund, J.B. Raynor, J. Chem. Soc. Dalton Trans. (1975) 1389.
46. M. Assour, J. Chem. Phys. 43 (1965) 2477.
47. A. Abragam, M.H.L. Pryce, Proc. R. Soc. London, Sect. A 206 (1961) 164.
48. C.R. Cornman, K.M. Geiser-Bush, S.P. Rowley, P.D. Boyle, Inorg. Chem. 36 (1997) 6401.

Syntheses of manganese(II) complexes and studies on their structural and spectral characteristics

4.1. Introduction

Manganese (Mn) is a gray-white, hard and very brittle metal, with atomic number, 25 and atomic mass, 54.938045(5) g/mol. It can be very easily oxidized, the common oxidation states being +2, +3, +4, +6 and +7. The name originates from *magnes*, (Latin) meaning "magnet". The Swedish chemist Scheele was the first to recognize that manganese was an element. Manganese(II) complexes are well known for their excellent catalytic activity towards the disproportionation of hydrogen peroxide and a number of them have been shown to catalyze the low temperature peroxide bleaching of fabrics [1]. They are also interesting due to their catalytic antioxidant activity [2]. Potential importance of manganese complexes is evidenced by the realization that the active site in photosystem II (PSII) is a tetranuclear manganese complex [3]. Manganese has a vital role in many enzymatic systems such as superoxide dismutase, peroxidase, dioxygenase and catalase in which mononuclear Mn active centers are present [4]. In this chapter the syntheses and structural and spectral characteristics of five manganese(II) complexes of the three thiosemicarbazone ligands, viz., pyridine-2-carbaldehyde N(4)-*p*-methoxyphenyl thiosemicarbazone (HL^1), pyridine-2-carbaldehyde N(4)-phenylethyl thiosemicarbazone (HL^2), pyridine-2-carbaldehyde N(4)-methyl N(4)-phenyl thiosemicarbazone (HL^3) have been dealt with.

4.2. Experimental

4.2.1. Materials

Manganese(II) chloride tetrahydrate, manganese(II) acetate tetrahydrate, manganese(II) perchlorate hexahydrate and potassium thiocyanate (Merck) were used as supplied and solvents were purified by standard procedures before use. **Caution!** Perchlorate complexes of metals with organic ligands are potentially explosive and should be handled with care.

4.2.2. Syntheses and characterization of ligands

The syntheses and characterization of the thiosemicarbazone ligands HL^1, HL^2, and HL^3 have been described in Chapter 2.

4.2.3. Syntheses of complexes

4.2.3.1. Syntheses of $[MnL^1_2]\cdot H_2O\cdot EtOH$ (15) and $[MnL^2_2]\cdot 3H_2O$ (17)

To a solution of the respective ligand (2 mmol) in hot ethanol (25 ml) was added $MnCl_2\cdot 4H_2O$ (1 mmol) and heated under reflux for two hours and kept at room temperature (overnight). The complexes formed were filtered, washed thoroughly with water, ethanol and then ether and dried *in vacuo* over P_4O_{10}.

4.2.3.2. Synthesis of $[Mn(L^1)(HL^1)]Ac$ (16)

To a solution of the HL^2 (2 mmol) in hot ethanol (25 ml) was added $Mn(Ac)_2\cdot 4H_2O$ (1 mmol) and heated under reflux for two hours and kept at room temperature (overnight). The complex formed was filtered, washed thoroughly with water, ethanol and then ether and dried *in vacuo* over P_4O_{10}.

4.2.3.3. Synthesis of $[MnL^3_2]\cdot 3H_2O$ (**18**)

To a solution of the HL^3 (2 mmol) in hot ethanol (25 ml) was added $Mn(ClO_4)_2\cdot 6H_2O$ (1 mmol) and heated under reflux for two hours and kept at room temperature (overnight). The complex formed was filtered, washed thoroughly with water, ethanol and then ether and dried *in vacuo* over P_4O_{10}.

4.2.3.4. Synthesis of $[Mn(HL^3)_2](SCN)_2\cdot MeOH$ (**19**)

To a solution of HL^3 (2 mmol) in hot ethanol (25 ml) was added $MnCl_2\cdot 4H_2O$ (1 mmol) and heated under reflux for two hours. The mixture was then cooled and stirred with KCNS for 30 minutes and kept at room temperature (overnight). The complex formed was filtered, washed thoroughly with water, ethanol and then ether and dried *in vacuo* over P_4O_{10}.

4.3. Physical Measurements

Elemental analyses of the ligands and the complexes were done on a Heracus elemental analyzer at CDRI, Lucknow, India and on a Vario EL III CHNS analyzer at SAIF, Kochi, India. The IR spectra were recorded on a Thermo Nicolet AVATAR 370

DTGS model FT-IR Spectrophotometer with KBr pellets at SAIF, Kochi. The far IR spectra were recorded using polyethylene pellets in the 500-100 cm^{-1} region on a Nicolet Magna 550 FTIR instrument at Regional Sophisticated Instrumentation Facility, Indian Institute of Technology, Bombay. Electronic spectra were recorded on a Cary 5000, version 1.09 UV-Vis-NIR spectrophotometer from a solution in DMF. The EPR spectra of the complexes were recorded in a Varian E-112 spectrometer using TCNE as the standard at SAIF, IIT, Bombay, India. The magnetic susceptibility measurements were carried out at the Indian Institute of Technology, Roorkee, at room temperature in the polycrystalline state on a PAR model 155 Vibrating Sample Magnetometer at 5 kOe field strength. The molar conductivities of the complexes in dimethylformamide solutions (10^{-3} M) at room temperature were measured using a direct reading conductivity meter.

4.4. X-Ray crystallography

Single crystals of compound **15** of X-ray diffraction quality were grown from its ethanol solution by slow evaporation at room temperature in air. The crystallographic data and structure refinement parameters are given in Table 4.1. The data collection and cell refinement were carried out using an ARGUS-MACH3 (Nonius, 1997) diffractometer with graphite monochromated Mo Kα (λ = 0.71073 Å) radiation on a single crystal of dimension 0.35×0.30×0.30 mm at the National Single Crystal X-Ray Diffraction Facility, IIT, Bombay, India. The unit cell dimensions and intensity data were measured at 293 K. The trial structure was solved using SHELXS-97 [5] and refinement was carried out by full-matrix least squares on F^2 (SHELXL-97) [5]. Molecular graphics employed were ORTEP-III [6] and PLATON [7].

4.5. Results and discussion

All the compounds are bis(thiosemicarbazone) complexes. Compound **17** exhibits orange color, while all others are brown. In the compounds **15**, **17** and **18**, the thiosemicarbazones deprotonate and chelate in thiolate form as proved by the IR spectral data. In **19**, the ligand moieties are in the thione form whereas in **16**, one of them is in the thione form and the other in the thiolate form. Elemental analyses and

conductivity data are in agreement with the general empirical formula $[MnL_2]$ for compounds **15**, **17** and **18**. Compound **16** is found to be [Mn(L)(HL)]OAc and **19** turned to be $[Mn(HL)_2](SCN)_2$.

Table 4. 1. Crystal refinement parameters of compound 15

Parameters	$[MnL^1_2]\cdot H_2O$ (**15**)
Empirical Formula	$C_{28}H_{26}Mn_1N_8O_3S_2$
Formula weight (M)	641.62
Temperature (T) K	293(2)
Wavelength (Mo Kα) (Å)	0.71073
Crystal system	Monoclinic
Space group	C 2/c
Lattice constants	
a (Å)	15.1640(12)
b (Å)	18.7930(15)
c (Å)	11.8960(11)
α (°)	90.00
β (°)	109.310(8)
γ (°)	90.00
Volume V ($Å^3$)	3199.4(5)
Z	8
Calculated density (ρ) (Mg m^{-3})	1.332
Absorption coefficient, μ (mm^{-1})	0.585
F(000)	1324
Crystal size (mm)	0.35 x 0.30x 0.30
Color, Nature	Brown, Block
Limiting Indices	0≤h≤18, -22≤k≤0, -14≤l≤13
Reflections collected	2855
Independent Reflections	2750 [R(int) = 0.0177]
Refinement method	Full-matrix least-squares on F^2
Data / restraints / parameters	2750/ 0 / 200
Goodness-of-fit on F^2	1.060
Final *R* indices [I > 2σ (I)]	R_1 = 0.0582, wR_2 = 0.1515
R indices (all data)	R_1 = 0.1229, wR_2 =0.1762
Largest difference peak and hole (e $Å^{-3}$)	0.703 and -0.280

The partial elemental analyses, molar conductivities and magnetic susceptibilities of the metal complexes are shown in Table 4.2. The room temperature magnetic moments of powdered samples of complexes **15–19** are consistent with

manganese(II) complexes where there are no significant exchange interactions between adjacent metal centers [8]. The molar conductivity values for 10^{-3} M DMF solutions of complexes **15**, **17**, and **18** suggest that these complexes are non-electrolytes and the values for **16** and **19** show that they are probably 1:1 and 2:1 electrolytes respectively [9].

Table 4. 2.
Magnetic susceptibilities, molar conductivities and partial elemental analyses of the complexes.

Complex	μ(B.M)	*λ_M	Found (Calc.)%			
			C	H	N	S
$[MnL^1_2].H_2O.EtOH$(**15**)	6.02	1.5	52.57(52.24)	4.75(4.97)	16.23(16.25)	9.34(9.30)
$[Mn(L^1)(HL^1)]OAc$(**16**)	5.62	69	52.85(52.55)	4.46(4.41)	16.42(16.34)	9.82(9.35)
$[MnL^2_2].3H_2O$(**17**)	5.33	18	53.78(53.32)	5.19(5.37)	16.93(16.58)	9.53(9.49)
$[MnL^3_2].3H_2O$(**18**)	5.56	12	44.67(44.95)	3.90(4.45)	14.76(14.98)	8.41(8.57)
$[Mn(HL^3)_2](SCN)_2.MeOH$(**19**)	5.81	138	49.99(50.05)	4.03(4.34)	19.19(18.83)	16.63(17.24)

*Molar conductivity of 10^{-3} M DMF solution, in $ohm^{-1}cm^2 mol^{-1}$

4.5.1. Infrared and electronic spectra

The shift in bands assigned in the spectra of ligands because of coordination are illustrated in Tables 4.3 and 4.4. A medium band in the range 3129-3158 cm^{-1} in the free ligands HL^1, HL^2 and HL^3 due to $\nu(^2N\text{-}H)$ vibration disappears in the spectra of complexes **15**, **17** and **18** providing a strong evidence for the ligand coordination around manganese(II) ion in the deprotonated thiol form [10]. In complexes **16** and **19** the $\nu(^2N\text{-}H)$ bands are present since they have the ligands in the thione form. The strong bands at 3310 and 3374 cm^{-1} in the spectra of HL^1 and HL^2 assigned to $\nu(^4N\text{-}H)$, shift to higher energies. The ν(C=N) bands of thiosemicarbazones are found to be shifted to lower frequencies in all complexes indicating the coordination *via* the azomethine nitrogen. The coordination of this nitrogen is also supported by a shift in ν(N–N) to higher frequencies [11]. In the spectra of the complexes **15**, **16**, **17** and **18,** the bands corresponding to the newly formed N=C bond $[\nu(^2N=^3C)]$ due to the enolization of the ligands are present at *ca.* 1600 cm^{-1}, while this band is absent in the spectrum of **19**.

Coordination *via* thiolate sulfur is indicated by the negative shift of two bands assigned to ν(C-S) and δ(C-S) vibrations. The out-of-plane and in-plane bending vibrations of the pyridine ring in uncomplexed ligands shift to higher frequencies on complexation confirming the coordination of ligands to metal *via* pyridine nitrogen [10]. The manganese-donor atom stretching frequencies [Table 4.4] in the ranges 402-420 cm^{-1}[$\nu(Mn\text{-}N_{imine})$], 352-381 cm^{-1} [ν(Mn-S)] and 248-288 cm^{-1}[$\nu(Mn\text{-}N_{py.})$] provide further evidence for the coordination of azomethine nitrogen, thione/thiolate sulfur and pyridyl nitrogen.

Table 4. 3. IR spectral assignments (cm^{-1}) of the ligands and the complexes.

Compound	ν(C=N)	ν(N=C)	ν(N-N)	ν/δ(C-S)	py(ip)	py(op)	$\nu(^2N\text{-}H)$	$\nu(^4N\text{-}H)$
HL^1	1584	---	1024	1334,837	613	401	3134	3310
$[Mn\,L^1_2]$**(15)**	1562	1607	1081	1296,836	646	409	---	3427
$[Mn(L^1)(HL^1)]$OAc**(16)**	1534	1598	1093	1296,832	654	408	3304	3411
HL^2	1586	---	1079	1324,897	622	406	3129	3374
$[Mn\,L^2_2]$**(17)**	1560	1592	1143	1300,837	632	409	---	3441
HL^3	1590	---	1035	1307,779	614	421	3158	---
$[Mn\,L^3_2]$**(18)**	1541	1596	1144	1301,774	635	457	---	---
$[Mn(HL^3)_2](SCN)_2$**(19)**	1574	1598	1132	1294,773	632	451	3434	---

Table 4. 4. Metal-ligand stretching frequencies (cm^{-1}) of the complexes.

Complex	$Mn\text{-}N_{azo}$	Mn-S	$Mn\text{-}N_{py}$
$[MnL^1_2]$**(15)**	402	364	248
$[Mn(L^1)(HL^1)]$OAc**(16)**	410	354	289
$[MnL^2_2]$**(17)**	411	381	279
$[MnL^3_2]$**(18)**	420	362	276
$[Mn(HL^3)_2](SCN)_2$ **(19)**	410	352	288

The strong band at 2054 cm^{-1} [ν(CN)] and a medium band at 481 cm^{-1} [δ(SCN)] indicates the presence of ionic thiocyanate in the complex **19** [12]. The spectrum of the acetate-containing complex **17** displays relatively strong bands at 1628 [ν_a(COO)] and 1397 cm^{-1}, [ν_s(COO)] indicating the ionic nature of the acetate in this compound [13].

Table 4. 5. Electronic spectral assignments of the ligands and the complexes

Compound	$\pi \rightarrow \pi^*$	$n \rightarrow \pi^*$	$^4T_{1g} \leftarrow {}^6A_{1g}$	$^4T_{2g} \leftarrow {}^6A_{1g}$
HL^1	42735,38760	30769	---	---
$[Mn\ L^1_2]$(**15**)	42841,37879	33898	18248	22936
$[Mn(L^1)(HL^1)]OAc$(**16**)	42194,37492	35481	18051	23810
HL^2	42194,36630	30960	---	---
$[Mn\ L^2_2]$(**17**)	41841,37453	33728	18903	23419
HL^3	43290,38610	30842	---	---
$[Mn\ L^3_2]$(**18**)	42194,38610	33003	18867	23148
$[Mn(HL^3)_2](SCN)_2$(**19**)	42118,38786	33416	18478	23542

Electronic transition intensities of octahedral manganese(II) complexes are very low since the transitions from the ground state $^6A_{1g}$ are doubly forbidden. The absorptions of the organic ligands tailing into the visible region obscure the very weak *d–d* absorption bands of the manganese(II) complexes. The broad band at *ca.* 23000 cm^{-1} typical of octahedral manganese(II) complexes due to the $^4T_{2g} \leftarrow {}^6A_{1g}$ transitions is observed for all the complexes. The very weak bands at *ca.*18000 cm^{-1} are assigned to $^4T_{1g} \leftarrow {}^6A_{1g}$ transitions. The electronic spectral assignments are summarized in Table 4.5.

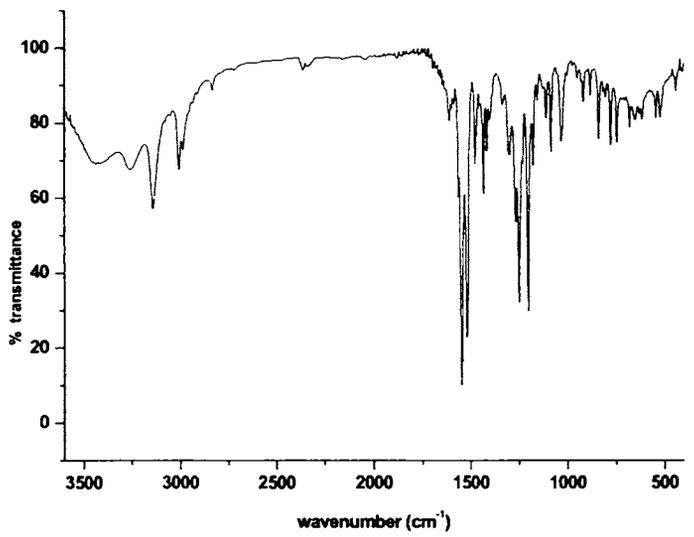

Fig. 4. 1. Infrared spectrum of $[MnL^1_2]$ (15)

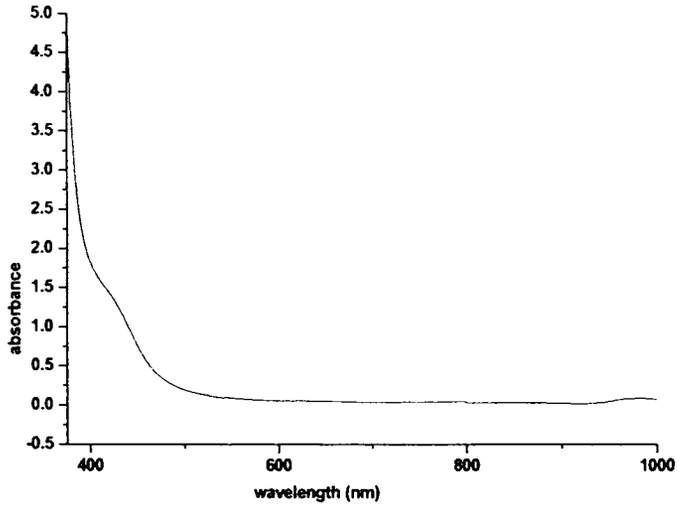

Fig. 4.2. Electronic spectrum of $[MnL^1_2]$ (15)

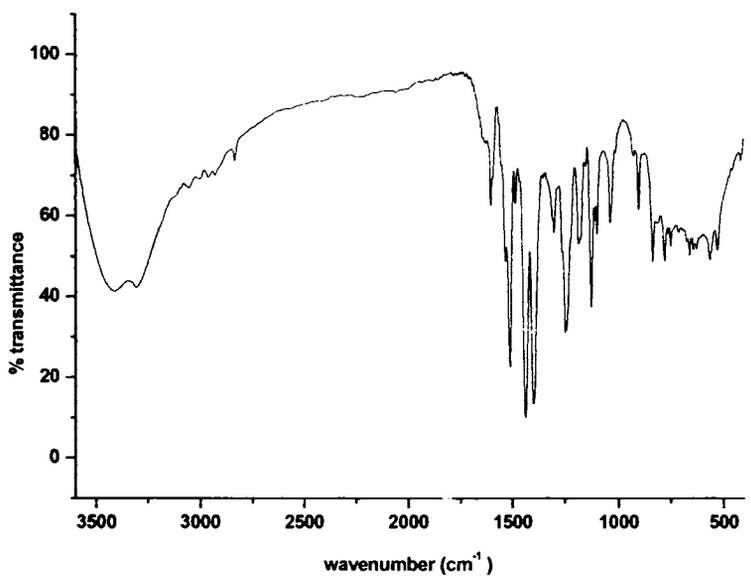

Fig. 4. 3. Infrared spectrum of $[Mn(L^1)(HL^1)]OAc$ (16)

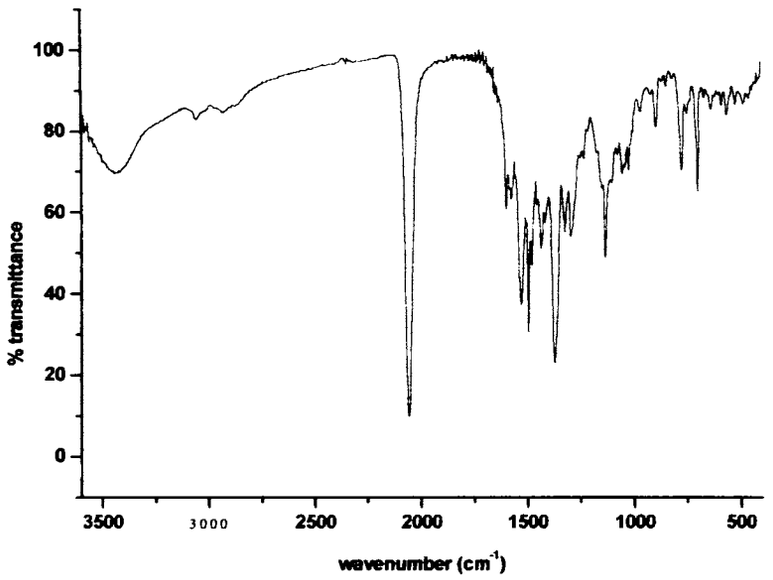

Fig. 4. 4. Infrared spectrum of $[Mn(HL^3)_2](SCN)_2$ (19)

4.5.2. EPR spectra

The spin Hamiltonian used to represent the EPR spectra of Mn(II) is given by

$$\hat{H} = g\beta HS + D[S_z^2\text{-}S(S+1)/3] + E(S_x^2 - S_y^2)$$

where H is the magnetic field vector, g is the spectroscopic splitting factor, β is the Bohr magneton, D is the axial zero field splitting term, E is rhombic zero field splitting parameter and S is the electron spin vector [14]. If D and E are very small compared to $g\beta HS$, five EPR transitions are expected. The solid state EPR spectra of the complexes **15**, **17** and **19**, at 298 K are characterized by broad signals with g values 1.99, 2.03 and 2.02 respectively. The signals of **16** and **18** were very broad due to dipolar interactions and random orientation of the Mn^{2+} ions [15]. In the spectra from DMF solutions at 77 K, a hyperfine sextet is observed with g values 1.98, 1.99, 1.99 and 1.98 and A values 98, 98, 100 and 100 G, respectively for **15**, **17**, **18** and **19**. The six hyperfine lines are due to the interaction of electron spin with the nuclear spin (^{55}Mn, I = 5/2). However, hyperfine splitting is not observed for **16**.

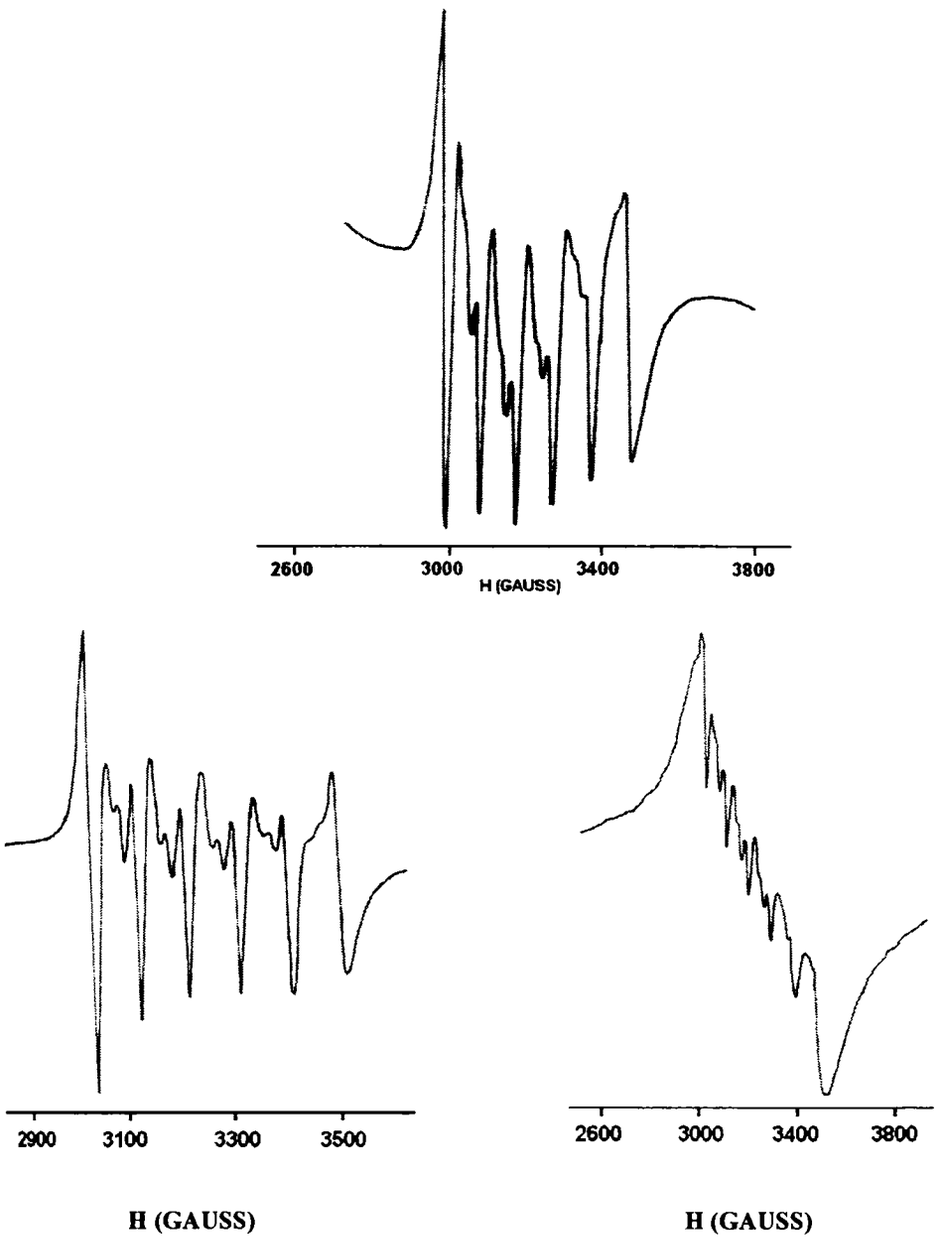

Fig. 4. 5. EPR spectra of 17 (top), 18 (left) and 19 in DMF at 77 K

The observed *g* values are very close to free electron spin value suggestive of the absence of spin orbit coupling in the ground state. The mixing of the nuclear

hyperfine levels with the zero field splitting factor produces low intensity forbidden lines with an average spacing of 38 G, lying between each of the two main hyperfine lines in the frozen solution spectra of the complexes [11].

4.5.3. Crystal structure of $[MnL^1_2]\cdot H_2O$ (15)

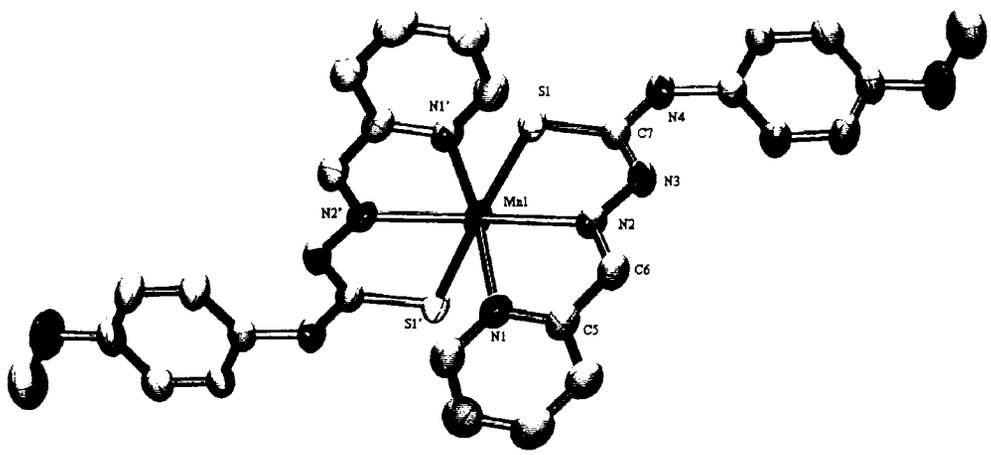

Fig. 4. 6. ORTEP diagram of $[MnL^1_2]\cdot H_2O$ in 25% probability ellipsoids. The hydrogen atoms and a water molecule are omitted for clarity.

Single crystal X-ray structural studies of compound **15** show a six coordinated Mn(II) center in a distorted octahedral geometry. The molecular structure of the compound along with atom numbering scheme is given in Fig. 4.6. The asymmetric unit contains one half of the molecule and the other half is generated by a two fold axis passing through the metal center. The Mn(II) center is coordinated in an N_4S_2 *meridional* manner by two anionic ligand moieties using pairs of *cis* pyridyl-*N*, *trans* azomethine-*N* and *cis* thiolate-*S* atoms. The coordination of sulfur occurs through deprotonation after enolization, confirmed by the partial single and double bond nature of C7-S1 [1.735(4) Å] and N3-C7 [1.316(5) Å] bond lengths (16).

The bond parameters (Table 4.6) show that the geometry around Mn(II) is distorted significantly from a perfect octahedron. The metal center is shared by four fused five membered chelate rings. The planes comprising Mn1, S1, C7, N2, N3 and Mn1, N1, C5, C6, N2, with a maximum deviation from the mean plane by 0.013(4) Å for N3 and –0.020(4) Å for C5 respectively, make an angle of 1.79(12)°. The mean plane of the bicyclic chelate rings Mn1, N1, C5, C6, N2, N3, C7, S1 having a maximum deviation of –0.059(4) Å for C5 atom makes a dihedral angle of 87.84(7)° with its counterpart. The Mn-$N_{azomethine}$, Mn-N_{py}, and Mn-S bond lengths are comparable with the previously reported manganese complexes [10, 11, 16].

The molecules are connected, in the crystal lattice, through an intermolecular hydrogen bond N4-H4...S1 [symmetry code: –x, -y, -z; with 2.62(6) Å of H...S distance and angle 148(5)°] interactions and make six membered rings leading to a three dimensional network (Figs. 4.7,4.8).

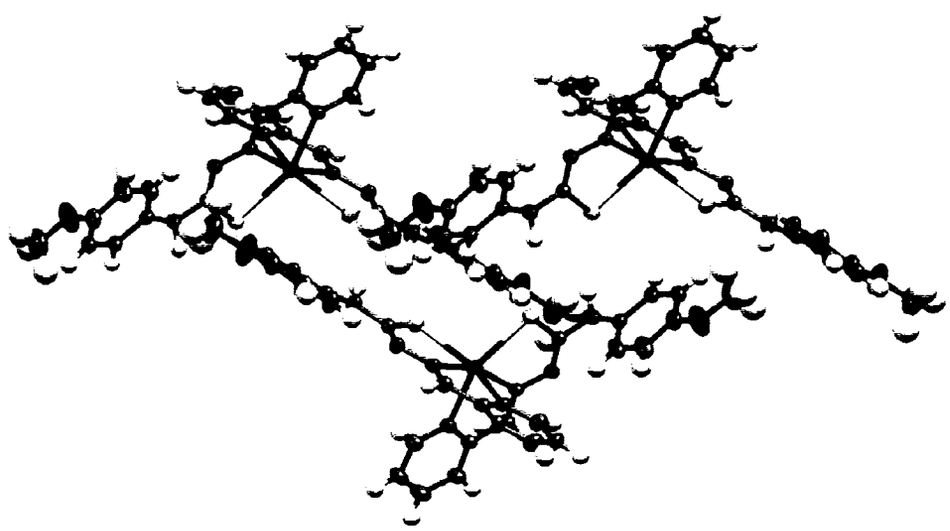

Fig. 4.7. The intermolecular hydrogen bonds in $[MnL^1_2]\cdot H_2O$ (15) with 25% probability ellipsoids.

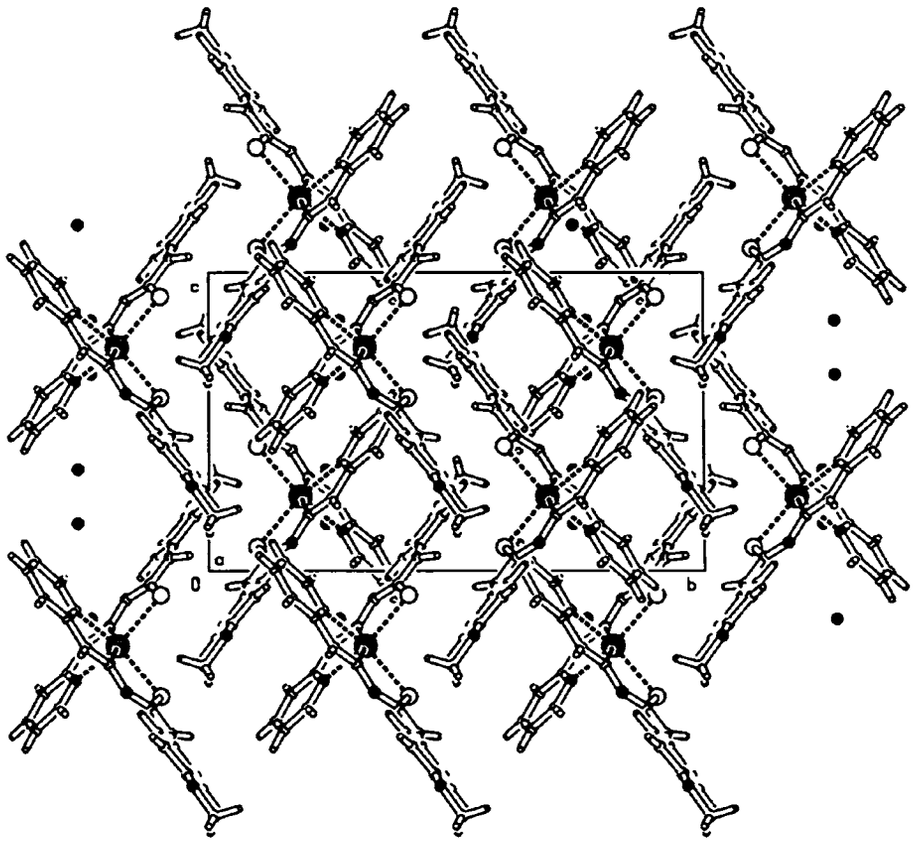

Fig. 4. 8. A view of the unit cell packing of the molecule 15 along the *a* axis

A weak intramolecular hydrogen bond C13-H13...N3 [with an H...N distance of 2.33 Å and an angle of 121°] stabilizes each molecule while π...π interactions between rings comprising N1, C1, C2, C3, C4 and C5 atoms [Cg(5)-Cg(5), symmetry code: ½-x, ½-y, -z; at a distance of 3.738(3) Å between ring centroids] reinforces the crystal structure cohesion in the packing (Fig. 4.8).

Table 4. 6. Selected bond lengths (Å) and bond angles (°) of $[MnL^1_2]\cdot H_2O$ (15)

Bond lengths (Å)		Bond angles (°)	
Mn(1)-N(2)	2.257(3)	N(2')-Mn(1)-N(2)	163.63(18)
Mn(1)-N(1)	2.293(4)	N(2')-Mn(1)-N(1)	96.44(13)
Mn(1)-S(1)	2.5349(13)	N(2)-Mn(1)-N(1)	71.78(13)
C(7)-S(1)	1.735(4)	N(2')-Mn(1)-N(1')	71.78(13)
N(1)-C(1)	1.317(6)	N(2)-Mn(1)-N(1')	96.44(13)
N(1)-C(5)	1.340(6)	N(1)-Mn(1)-N(1')	90.47(18)
N(2)-C(6)	1.291(5)	N(2')-Mn(1)-S(1)	117.10(9)
N(2)-N(3)	1.379(5)	N(2)-Mn(1)-S(1)	74.25(9)
N(3)-C(7)	1.316(5)	N(1)-Mn(1)-S(1)	146.00(10)
N(4)-C(7)	1.364(6)	N(1')-Mn(1)-S(1)	94.66(10)
N(4)-C(8)	1.419(6)	N(2')-Mn(1)-S(1')	74.25(9)
		N(2)-Mn(1)-S(1')	117.10(9)
		N(1)-Mn(1)-S(1')	94.66(10)
		N(1')-Mn(1)-S(1')	146.00(10)
		S(1)-Mn(1)-S(1')	99.46(6)
		C(7)-S(1)-Mn(1)	98.86(15)

Conclusion

This chapter deals with the syntheses and structural and spectral characteristics of five manganese(II) complexes of the three thiosemicarbazone ligands, viz., pyridine-2-carbaldehyde N(4)-*p*-methoxyphenyl thiosemicarbazone (HL^1), pyridine-2-carbaldehyde N(4)-phenylethyl thiosemicarbazone (HL^2) and pyridine-2-carbaldehyde N(4)-methyl, N(4)-phenyl thiosemicarbazone (HL^3). The complexes were characterized by partial elemental analyses, molar conductivity and magnetic susceptibility measurements, infrared, electronic and EPR spectral studies. All the complexes were assigned octahedral geometry based on analytical data. Single crystal X-Ray diffraction study of one complex supports the assignment.

References:

1. M. Devereux, M. McCann, V. Leon, V. McKee, R.J. Ball, Polyhedron 21 (2002) 1063.
2. B.J. Day, Drug Discovery Today 13 (9) (2004) 557.
3. M. Maneiro, M.R. Bermejo, M. Fondo, A.M. Gonzalez, J. Sanmartyn, J.C. Garcya-Monteagudo, R.G. Pritchard, A.M. Tyryshkin, Polyhedron 20 (2001) 711.
4. D. Huang, X. Zhang, C. Chen, F. Chen, Q. Liu, D. Liao, L. Li, L. Sun, Inorg. Chim. Acta 353 (2003) 284.
5. G.M. Sheldrick (1997) SHELXS97 and SHELXL97, Bruker AXS Inc., Madison, Wisconsin, USA.
6. L.J. Farrugia, J. Appl. Cryst. 30 (1997) 565.
7. A.L. Spek, J. Appl. Cryst. 36 (2003) 7.
8. M. Devereux, M. McCann, V. Leon, R. Kelly, D.O Sheaa, V. McKee, Polyhedron 22 (2003) 3187.
9. W.J. Geary, Coord. Chem. Rev. 7 (1971) 81.
10. V. Philip, V. Suni, M.R.P. Kurup, M. Nethaji, Spectrochim. Acta, Part A, 64 (2006) 171.
11. A. Sreekanth, M. Joseph, H. -K. Fun, M.R.P. Kurup, Polyhedron 25 (2006) 1408.
12. D.N. Sathyanarayana, Vibrational Spectroscopy, New Age International, New Delhi (2004) 400.
13. K. Nakamoto, Infrared and Raman Spectra of Inorganic and Coordination Compounds Wiley-Interscience, New York, 1986.
14. D.J.E. Ingram, Spectroscopy at Radio and Microwave Frequencies, second ed., Butterworth, London, 1967.
15. B.S. Garg, M.R.P. Kurup, S.K. Jain, Y.K. Bhoon, Transition Met. Chem. 13 (1988) 92.
16. A. Usman, I.A. Razak, S. Chantrapromma, H. -K. Fun, A. Sreekanth, S. Sivakumar, M.R.P. Kurup, Acta Cryst. C 58 (2002) m461.

Syntheses of Co(III) complexes and studies on their structural and spectral characteristics

5.1. Introduction

Cobalt (symbol Co, atomic number 27, atomic mass 58.933195(5) and electron configuration [Ar] $3d^7$ $4s^2$) is a hard, lustrous, silver-gray metal, and a chemical element. The word *cobalt* is derived from the German *kobalt*, from *kobold* meaning "goblin", a term used for the ore of cobalt by miners. Cobalt is not found as a free metal and is generally found in the form of ores. It is frequently associated with nickel, and both are characteristic ingredients of meteoric iron. Metallic cobalt commonly presents as a mixture of two crystallographic structures hcp and fcc with a transition temperature hcp→fcc of 722 K. Cobalt has wide applications in a) making of alloys [superalloys for parts in gas turbine aircraft engines, corrosion and wear-resistant alloys, high-speed steels], b) production of magnets and magnetic recording media, c) manufacture of catalysts for the petroleum and chemical industries, d) electroplating because of its appearance, hardness, and resistance to oxidation.

Swedish chemist Georg Brandt (1694–1768) is credited with isolating cobalt sometime between 1730 and 1737. In 1938, John Livingood and Glenn Seaborg discovered cobalt-60 (^{60}Co). It is a radioactive isotope of the metal that is used in radiotherapy. The ^{60}Co source is useful for about 5 years but even after this point is still very radioactive, and so cobalt machines have fallen from favor. There is a wide variety of cobalt compounds. Cobalt compounds are used in the production of pigments (cobalt blue and cobalt green) inks, and varnishes. They have been used for centuries to impart a rich blue color to glass, glazes, and ceramics. The +2 and +3 oxidation states are most prevalent, however cobalt(I) complexes are also fairly common. Cobalt compounds should be handled with care due to cobalt's slight toxicity. Powdered cobalt in metal form is a fire hazard.

Cobalt is ferromagnetic. The Curie temperature is 1388 K with 1.6 ~1.7 Bohr Magnetons per atom. Cobalt oxides CoO (Neel temperature 291 K) and Co_3O_4 (Neel temperature: 40 K) are antiferromagnetic at low temperature.

Cobalt in small amounts is essential to many living organisms, including humans. Cobalt is a central component of the vitamin, cobalamin or vitamin B-12.

Schiff bases and their transition metal complexes are of much interest in inorganic chemistry and have been studied extensively. Thiosemicarbazones and their metal complexes have been very promising compounds among Schiff bases, due to their beneficial biological applications [1]. Domag *et al.* [2] had reported that thiosemicarbazones possess antitubercular activity and after that, many papers on the pharmacology of these compounds appeared, indicating that they have wide inhibitory activity against smallpox [3] and several kinds of tumours [4]. They can also be used as pesticides [5] and fungicides [6]. Presence of various donor atoms and ability to change dentacity depending on the reaction conditions and starting reagents make thiosemicarbazones of various aldehydes and ketones a special category among organic ligands [7].

Cobalt(III) and various tridentate ligands form mainly mixed bis(ligand) complexes. Cobalt(III) complexes of the type $[CoL_2]X$ (X = Cl, SCN, N_3, NO_3 *etc.*, L = anion from the thiol form of the thiosemicarbazone ligand of the type, HL) which were proposed to be low-spin, diamagnetic and octahedral [8] have been reported. Extending these works further, we present in this chapter the synthesis and characterization of novel cobalt(III) complexes of the ligands HL^1, HL^2, HL^3 and H_2L^5.

5.2. Experimental

5.2.1. Materials

Cobalt(II) nitrate hexahydrate, cobalt(II) chloride hexahydrate, cobalt(II) perchlorate hexahydrate (Merck) were used as supplied and solvents were purified by standard procedures before use. **Caution!** Perchlorate complexes of metals with organic ligands are potentially explosive and should be handled with care.

5.2.2. Syntheses of ligands

The syntheses of thiosemicarbazone ligands have been discussed in Chapter 2.

5.2.3. Syntheses of complexes

All complexes were prepared by direct reaction between the ligand and the corresponding cobalt(II) salts. To a hot solution of 1 mmol of the thiosemicarbazone in methanol (20 ml), was added 0.5 mmol of the cobalt(II) salt. The mixture was refluxed for two hours and kept at room temperature. The compound formed was filtered, washed with water, methanol and ether. It was then dried *in vacuo* over P_4O_{10}. XRD quality single crystals of **20** and **23** were obtained by the slow evaporation of their methanol solutions.

5.2.4. Physical Measurements

Elemental analyses were carried out using a Vario EL III CHNS analyzer at SAIF, Kochi, India. Infrared spectra were recorded on a Thermo Nicolet, AVATAR 370 DTGS model FT-IR Spectrophotometer with KBr pellets. at SAIF, Kochi. Electronic spectra were recorded on a Cary 5000 version 1.09 UV-Vis-NIR Spectrophotometer from a solution in chloroform. The details regarding the various analytical methods have been given in Chapter 1.

5.2.5. X-Ray crystallography

The data of **20** was collected using a Bruker Smart Apex CCD diffractometer equipped with graphite monochromated Mo Kα (λ = 0.71073 Å) radiation, while the compound **23** was diffracted by CrysAlis CCD, Oxford Diffraction Ltd. with graphite monochromated Mo Kα (λ = 0.71073 Å) radiation at the National Single Crystal X-Ray Facility, IIT, Bombay, India. The trial structure was solved using SHELXS-97 [9] and refinement was carried out by full- matrix least squares on F^2 (SHELXL) [9]. Molecular graphics employed were ORTEP-III [10] and PLATON [11].

5.3. Results and discussion

The partial elemental analysis data and molar conductivities of the complexes are listed in Table 5.1. All the complexes are brown in color and soluble in solvents like methanol, ethanol, chloroform and DMF. They are found to be diamagnetic which confirms oxidation to cobalt(III) during preparation as has been found previously with

heterocyclic N(4)-substituted thiosemicarbazones and hence corresponds to d^6 ion in strong field [12]. The molar conductivities of 10^{-3} M DMF solutions of the complexes except **27** indicate that they are 1:1 electrolytes while **27** is a non-electrolyte [13]. The partial elemental analysis data and conductance measurement data are in consistence with the general formulation of the complexes except **27** as $[CoL_2]X$, where X = NO_3, Cl, Br and ClO_4 whereas **27** turns to be [Co(L)(HL)]. For the compounds **20**, **24**, **26** and **27**, the elemental analysis data matches with stoichiometry containing one molecule of water of crystallization/lattice water, two molecules in the case of **21** and **25**, whereas no water molecules are present in **22** and **23**.

Table 5.1. Partial elemental analyses and molar conductivities of the complexes

Compounds	Anal: Found (Calc.)%				Λ_M*
	C	H	N	S	
$[CoL^1_2]NO_3 \cdot H_2O$ (**20**)	47.89 (47.39)	3.85 (3.98)	18.05 (17.76)	9.12 (9.04)	86
$[CoL^1_2]Cl \cdot 2H_2O$ (**21**)	47.69 (47.97)	4.45 (4.31)	15.97 (15.98	9.23 (9.15)	78
$[CoL^1_2]ClO_4$ (**22**)	45.89 (46.13)	3.73 (3.59)	15.29 (15.37)	8.79 (8.80)	80
$[CoL^2_2]NO_3$ (**23**)	51.88 (52.40)	4.53 (4.40)	18.36 (18.33)	9.18 (9.33)	92
$[CoL^2_2]Cl \cdot 2H_2O$ (**24**)	52.78 (53.05)	4.37 (4.75)	16.21 (16.50)	9.44 (9.75)	67
$[CoL^3_2]Br \cdot 2H_2O$ (**25**)	46.98 (47.13)	4.56 (4.24)	15.75 (15.70)	9.04 (8.99)	89
$[CoL^3_2]ClO_4 \cdot H_2O$ (**26**)	46.58 (47.03)	4.06 (3.95)	15.82 (15.67)	9.08 (8.97)	75
$[Co(L^5)(HL^5)] \cdot H_2O$ (**27**)	56.50(57.13)	4.83(4.94)	12.36(12.48)	9.53 (9.53)	18

*Molar conductivity of 10^{-3} M DMF solution, in $ohm^{-1}cm^2 mol^{-1}$

5.3.1. Infrared spectra

The characteristic IR bands (50-4000 cm^{-1}) for the free ligands (HL^1, HL^2, HL^3 and H_2L^5) differ from those of their complexes (Table 5.2) and provide significant indications regarding the bonding sites of the ligands. Except for **27**, a medium band in the range 3129-3158 cm^{-1} in the free ligands due to $\nu(^2N\text{-}H)$ vibration disappears in the spectra of complexes providing a strong evidence for the ligand coordination around cobalt(III) ion in its deprotonated form. Bands ranging from 1600-1350 cm^{-1} suffer a significant shift in the spectra of complexes, which can be attributed to $\nu(C{=}C)$

and ν(C=N) vibration modes, and their mixing patterns are different from that in the spectra of ligands. Except for **27**, the positive shift of bands corresponding to ν(C=N) in the range 1584-1590 cm^{-1} in free ligands to 1602 -1614 cm^{-1} in complexes is consistent with coordination of azomethine nitrogen to the central Co(III) ion. However, compound **27** shows a negative shift in this frequency [14]. Medium bands *ca.* at 439-450 cm^{-1} corresponding to ν(Co-N) further support azomethine nitrogen coordination [15]. The enolization of the ligands and coordination of azomethine nitrogen is also evidenced from the increase in the ν(N—N) frequencies.

Table 5. 2. IR spectral data of the ligands and complexes (cm^{-1})

Compound	ν(C=N+N=C)	ν(N-N)	ν/δ(C-S)	py(ip)	py(op)	ν(^{2}N-H)	ν(^{4}N-H)
HL^1	1584	1024	1334,837	613	401	3134	3310
$[CoL^1_2]NO_3$ (**20**)	1604	1137	1315,827	617	408	----	3428
$[CoL^1_2]Cl$ (**21**)	1605	1132	1298,833	627	410	----	3402
$[CoL^1_2]ClO_4$ (**22**)	1602	1139	1303,826	620	412	----	3419
HL^2	1586	1079	1324,897	622	406	3129	3374
$[CoL^2_2]NO_3$ (**23**)	1605	1141	1315,892	630	416	----	3405
$[CoL^2_2]Cl$ (**24**)	1631	1137	1291,892	630	413	----	3426
HL^3	1590	1035	1307,779	614	421	3158	----
$[CoL^3_2]Br$ (**25**)	1603	1137	1292,770	632	453	----	----
$[CoL^3_2]ClO_4$(**26**)	1603	1137	1292,764	635	433	---	---
H_2L^5	1619	1003	1383,840	---	---	3250	3346
$[Co(L^5)(HL^5)]$ (**27**)	1601	1047	1385,842 1338,814	---	---	3259	3420

The bands in the range 1307-1383 and 779-897 cm^{-1} due to thioamide vibrations of the free ligands are shifted to lower values indicating coordination of sulfur to Co(III) ion [16]. For the complex **27**, two sets of bands are observed corresponding to C=S at 1385, 842 and at 1338, 814 cm^{-1}. This shows the coordination of one ligand moiety in the thione form and the other in the thiol form. Appearance of ν(^{2}N-H) band at 3259 cm^{-1} is another indication of the thione form. ν(O-H) band is absent in the spectrum showing the coordination of phenolic oxygen in the deprotonated form.

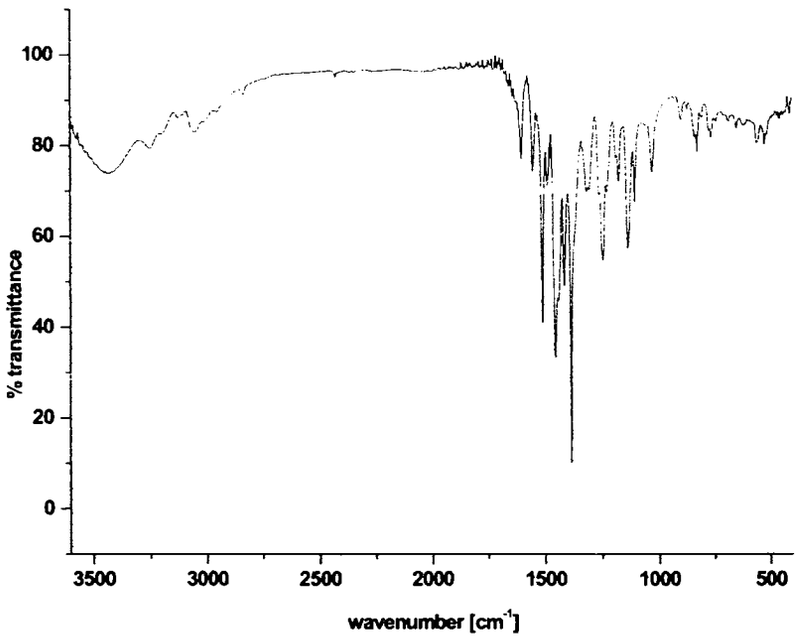

Fig. 5.1. IR spectrum of $[CoL^1_2]NO_3 \cdot H_2O$ (20)

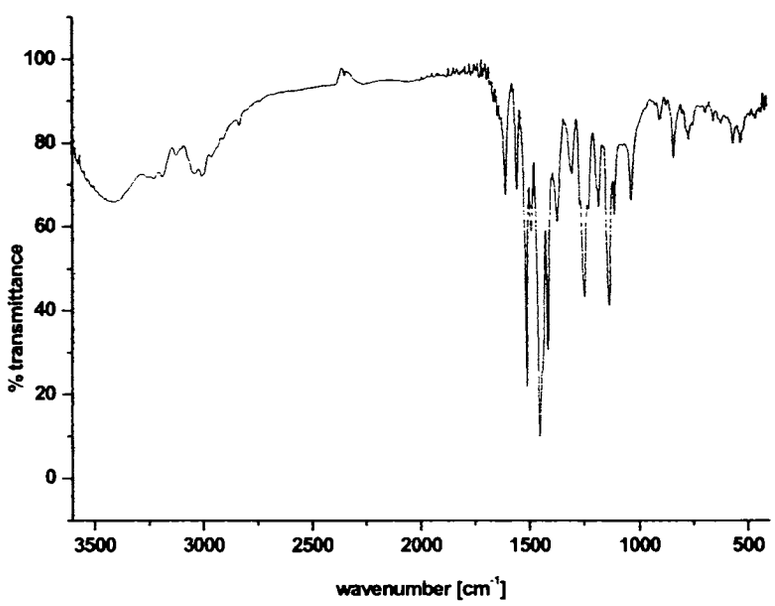

Fig. 5. 2. IR spectrum of $[CoL^1_2]Cl$ (21)

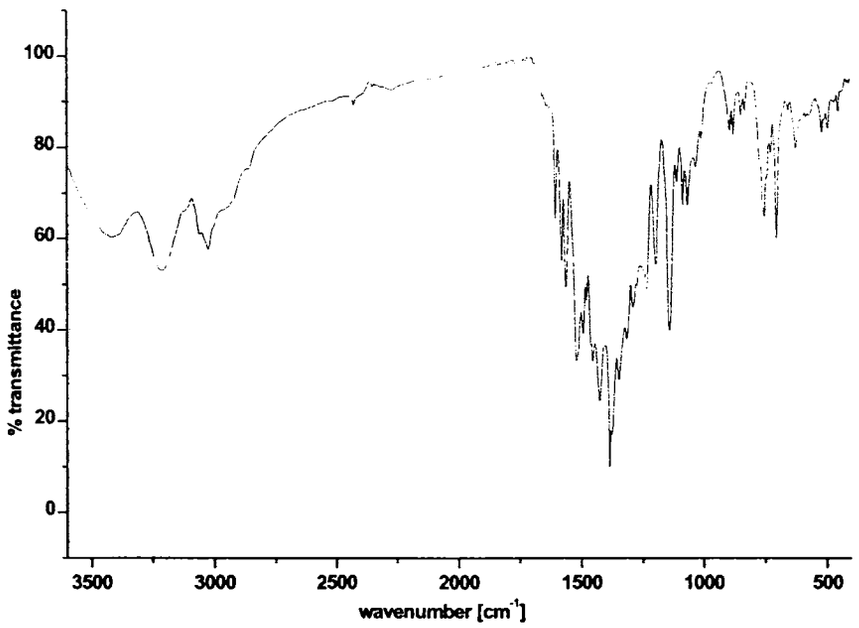

Fig. 5. 3. IR spectrum of $[CoL^2_2]NO_3$ (23)

Medium bands *ca.* at 375-385 cm^{-1} are assignable to ν(Co-S) [17]. A positive shift corresponding to out-of-plane bending vibrations of pyridine ring in the free ligands (613-622 cm^{-1}) to higher frequencies (617-635 cm^{-1}) in complexes is confirmative of pyridine nitrogen coordination to cobalt(III) ion [18]. Medium bands *ca.* at 255-268 cm^{-1} corresponding to $\nu(Co\text{-}N_{pyridyl})$ point towards the coordination of pyridyl nitrogen to the cobalt(III) ion [19].

The perchlorate complexes **22** and **26** show single broad bands at 1120 and 1123 cm^{-1} and strong bands at 620 and 625 cm^{-1}, indicating the presence of ionic perchlorate [20]. The bands at 1120 and 1123 cm^{-1} are assignable to $\nu_3(ClO_4)$ and unsplit bands at 620 and 625 cm^{-1} assignable to $\nu_4(ClO_4)$. Moreover, no bands assignable to ν_1 (930cm^{-1}) or ν_2 (460 cm^{-1}) are observed in its spectra. This along with unsplit ν_3 and ν_4 bands show exclusive presence of non-coordinated perchlorate group having C_{3v} symmetry and it is supposed to be descended from T_d symmetry due to lattice effects [21].

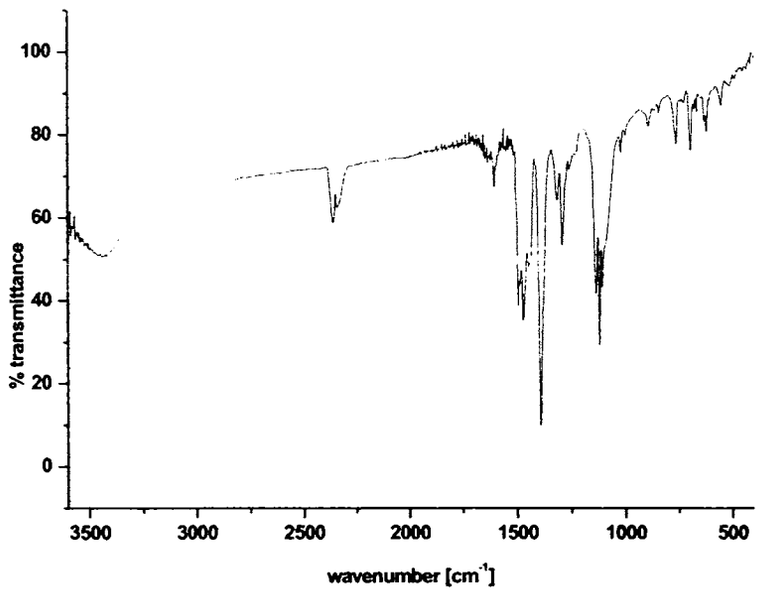

Fig. 5. 4. IR spectrum of $[CoL^3_2]ClO_4$ (26)

In the spectra of the complexes **20** and **23,** the absence of the combination bands ($\nu_1 + \nu_4$) in the region 1700-1800 cm^{-1} rules out the possibility for coordinated nitrato group. The bands *ca.* at 840 cm^{-1} (ν_2), 1384 cm^{-1} (ν_3) and 706 cm^{-1} (ν_4) for **20** and bands at 725, 1384 and 842 cm^{-1} for **23** clearly points out the uncoordinated nature of the nitrato group [22].

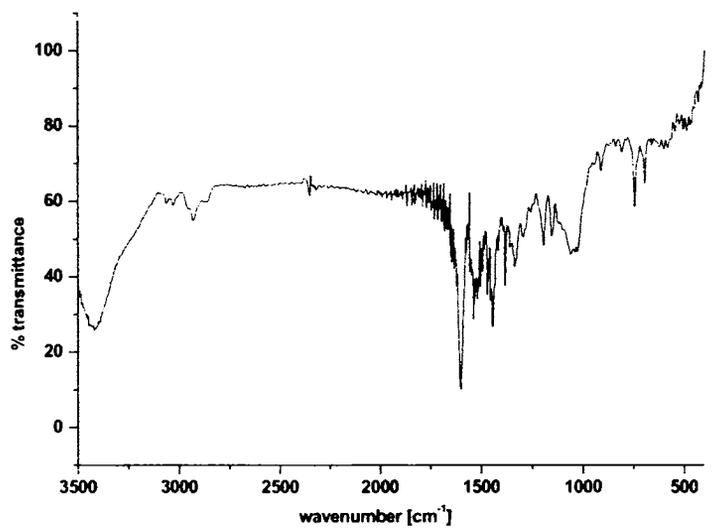

Fig. 5.5. IR spectrum of $[CoL^5(HL^5)](27)$

According to Stefov et al, coordinated water should exhibit bands at 825, 575 and 500 cm^{-1}. The absence of bands in these regions in the spectra of complexes **20**, **21**, **24**, **25**, **26** and **27** shows that the water molecules are not coordinated but are present as lattice water [23].

5.3.2. Electronic spectra

The electronic spectral assignments for the free ligands (HL^1, HL^2, HL^3 and H_2L^5) and their complexes are presented in Table 5.3. The electronic spectra of spin paired trivalent cobalt complexes of approximate O_h symmetry have the following assignments of *d-d* bands: v_1: $^1T_{1g} \leftarrow {}^1A_{1g}$; v_2: $^1T_{2g} \leftarrow {}^1A_{1g}$; v_3: $^3T_{1g} \leftarrow {}^1A_{1g}$; v_4: $^3T_{2g} \leftarrow {}^1A_{1g}$ [24]. The v_1 bands are assigned values ~ 19650-21050 cm^{-1} and the v_2 ~ 25000 cm^{-1}. The band assigned to v_2 is a combination band between it and the more intense $S \rightarrow Co^{III}$ charge-transfer bands. Very weak bands at ~16390-17950 cm^{-1} correspond to spin forbidden $^3T_{2g} \leftarrow {}^1A_{1g}$ transitions. The bands assigned are all spin allowed transitions. The band corresponding to $^3T_{1g} \leftarrow {}^1A_{1g}$ is weak and difficult to assign because it is spin forbidden. From the spectra it can be concluded that two well separated high energy bands corresponding to spin allowed singlet→singlet transitions have been observed with occasional presence of low energy spin forbidden bands.

Table 5. 3. Electronic spectra (cm^{-1}) of thiosemicarbazones and their complexes

Compound	$^1T_{1g} \leftarrow {}^1A_{1g}$	$^1T_{2g} \leftarrow {}^1A_{1g}$ + LMCT	$^3T_{2g} \leftarrow {}^1A_{1g}$	n→ π*	π→ π*
HL^1				30770	42730
$[CoL^1_2]NO_3 \cdot H_2O$ (**20**)	19700	24710	16550	30980	43210
$[CoL^1_2]Cl \cdot 2H_2O$ (**21**)	19650	24690	16390	30960	43100
$[CoL^1_2]ClO_4$ (**22**)	20110	25010	16800	31210	42990
HL^2				30960	42190
$[CoL^2_2]NO_3$ (**23**)	21050	24520	17790	31350	43860
$[CoL^2_2]Cl \cdot 2H_2O$ (**24**)	20620	25000	17510	29240	41670
HL^3				30950	42800
$[CoL^3_2]Br \cdot 2H_2O$ (**25**)	20580	25060	17950	31410	43210
$[CoL^3_2]ClO_4 \cdot H_2O$ (**26**)	20530	25000	17420	31400	43100
H_2L^5				29670	42020
$[Co(L^5)(HL^5)]$ (**27**)	20618	25020	18660	32200	42560

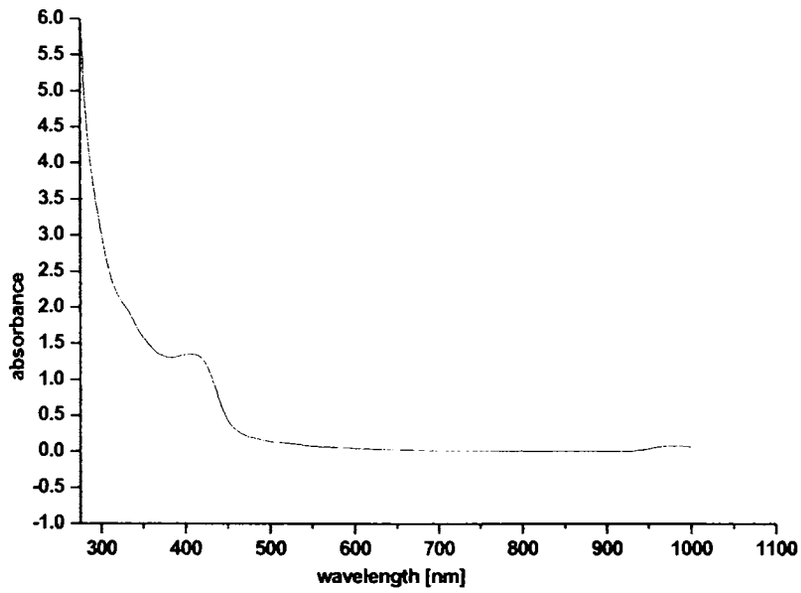

Fig. 5. 6. Electronic spectrum of $[Co(L^5)(HL^5)]$ (27)

5.3.3 Crystal structures of $[CoL^1{}_2]NO_3 \cdot H_2O$ (20) and *$[CoL^2{}_2] \cdot NO_3$ (23)*

The crystallographic data and structure refinement parameters for the compounds **20** and **23** are given in Table 5.4. The relevant bond lengths and bond angles of HL^3, $[CoL^1{}_2]NO_3 \cdot H_2O$ **(20)** and $[CoL^2{}_2]NO_3$ **(23)** are listed in Table 5.5. The asymmetric unit of **23** contains three molecules and only one of which is considered.

The molecular structures of the compounds along with atom numbering schemes are given in Figs 3 & 4. The metal centers in both the complexes possess octahedral geometry by two approximately planar tridentate monodeprotonated (L^-) ligands. The Co(III) ion is coordinated in a *meridional* fashion [25-27] using pairs of *cis* pyridyl nitrogen, *trans* azomethine nitrogen and *cis* thiolate sulfur atoms by two mononodeprotonated ligands. This results in four five membered chelate rings in both the complexes. The bond angles suggest the coordination geometries of both the complexes to be somewhat far from a perfect octahedron. The dihedral angle formed by the mean planes of the bicyclic chelate systems of each of the ligands is 89.75(13)° in **20** and 83.45° in **23**.

Table 5. 4. Crystal refinement parameters of compounds $[CoL^1_2]NO_3 \cdot H_2O$ and $[CoL^2_2]NO_3$

Parameters	$[CoL^1_2]NO_3 \cdot H_2O$ (**20**)	$[CoL^2_2]NO_3$ (**23**)
Empirical Formula	$C_{28}\ H_{26}\ Co\ N_9\ O_5\ S_2$	$C_{90}\ H_{90}\ Co_3\ N_{27}\ O_9\ S_6$
Formula weight (M)	691.63	2063.04
Temperature (T) K	293(2)	293(2)
Wavelength (Mo *Kα*) (Å)	0.71073	0.71073
Crystal system	Triclinic	Monoclinic
Space group	*P*-1	*P* 21
Lattice constants		
a (Å)	9.849(4)	14.7543(9)
b (Å)	13.193(5)	12.0675(18)
c (Å)	13.533(6)	27.424(8)
α (°)	60.879(7)	90.00
β (°)	79.885(8)	91.109(11)
γ (°)	86.595(8)	90.00
Volume V ($Å^3$)	1511.6(11)	4881.9(17)
Z	2	2
Calculated density (mg m^{-3})	1.520	1.403
Absorption coefficient (mm^{-1})	0.761	0.702
F(000)	712	2136
Color, Nature	Brown, Rod	Brown, Rod
Crystal size (mm)	0.24 x 0.16 x 0.08	0.30 x 0.25 x 0.20
θ Range for data collection	1.75 to 25.00	3.0986 to 29.9993
Limiting Indices	-11≤h≤11, -15≤k≤=15, -16≤=l≤16	-17≤h≤15, -14≤k≤14, -32≤l≤32
Reflections collected	10660	20242
Independent Reflections	5240 [R(int) = 0.0752]	15034 [R(int) = 0.0378]
Refinement method	Full-matrix least-squares on F^2	Full-matrix least-squares on F^2
Data / restraints / parameters	5240 / 0 / 408	15034/1/ 1216
Goodness-of-fit on F^2	1.034	0.784
Final *R* indices [1 > 2σ (I)]	R_1 = 0.0815, wR_2 = 0.1724	R_1 = 0.0478, wR_2 = 0.0773
R indices (all data)	R_1 = 0.1322, wR_2 = 0.1959	R_1 = 0.1131, wR_2 = 0.0900
Largest difference peak and hole (e $Å^{-3}$)	0.629 and -0.469	0.335 and -0.208

Each bicyclic chelate systems Co1, S1, N1, N2, N3, C5, C6, C7 and Co1, S1', N1', N2', N3', C5', C6', C7' are approximately planar as evidenced by the maximum deviation of –0.057(7) Å for C6 and 0.080(7) Å for C7' respectively for **20**, and 0.06297 Å for N1 and 2.12988 Å respectively for C7' for **23**. These results suggest that the distortion in octahedral geometry is more in **23** compared to **20**.

Table 5. 5 Selected bond lengths (Å) and bond angles (°) of the compounds

	$[CoL^1_2]NO_3 H_2O$ **(20)**	$[CoL^2_2]NO_3$ **(23)**
S(1)–C(7)	1.747(6)	1.776(8)
N(2)–C(6)	1.290(8)	1.305(6)
N(2)– N(3)	1.360(7)	1.336(6)
N(3)–C(7)	1.321(7)	1.329(6)
N(4)–C(7)	1.344(8)	1.324(6)
Co(1)–S(1)	2.232(2)	2.2348(17)
Co(1)–S(1')	2.2043(19)	2.2246(17)
Co(1)–N(1)	1.958(5)	1.963(5)
Co(1)–N(1')	1.956(5)	1.973(4)
Co(1)–N(2)	1.876(5)	1.889(4)
Co(1)–N(2')	1.885(5)	1.897(5)
C(6)–N(2)–N(3)	118.8(5)	120.3(5)
N(2)–N(3)–C(7)	111.6(5)	112.0(5)
N(4)–C(7)–N(3)	120.1(5)	116.4(6)
N(3)–C(7)–S(1)	123.3(5)	123.8(4)
N(4)–C(7)–S(1)	116.6(5)	119.8(5)
N(1)–Co(1)–N(1')	90.8(2)	90.10(18)
N(2)–Co(1)–N(2')	178.1(2)	178.4(2)
S(1)–Co(1)–S(1')	90.73(8)	92.24(7)

On complexation the ligand HL^2 undergoes structural reorientation to coordinate to the metal in an NNS manner in **23**. The azomethine nitrogen, was in *E* configuration with both pyridyl nitrogen and sulfur atoms in its thione form of ligand, now is in *Z* form with both the other donor atoms. The C-S bond length increases to 1.776(8) Å from 1.6849(13) Å seen in HL^2. The N3-C7 bond length also changes from 1.3587(16) Å to 1.329(6) Å due to enolization of the ligand for coordination after deprotonation. The Co-S, and Co-N bond lengths in both the complexes are comparable. The $Co\text{-}N_{azomethine}$ bond lengths are lesser compared to $Co\text{-}N_{pyridine}$, indicates former bonds are stronger than the latter.

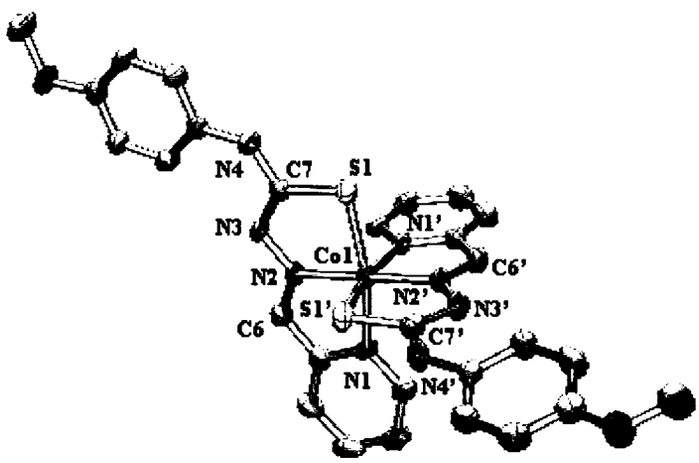

Fig. 5. 3. ORTEP diagram for the compound $[CoL^1_2]NO_3 \cdot H_2O$ (20) in 50% probability ellipsoids. Hydrogen atoms and nitrate ion are omitted for clarity.

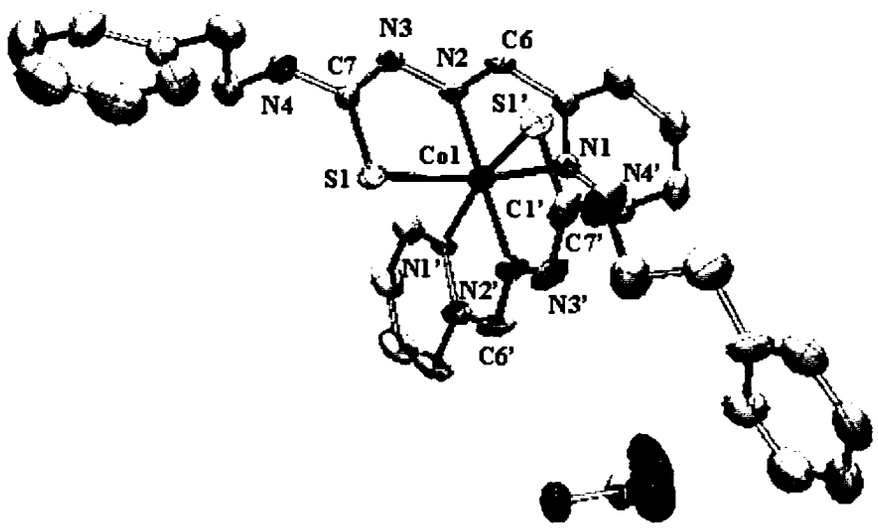

Fig. 5. 4. ORTEP diagram for the compound $[CoL^2_2]NO_3$ (23) in 25% probability ellipsoids. Hydrogen atoms are omitted for clarity.

The molecules of **20** and **23** are packed in a 'face to face' manner within the unit cell, as is evident from Fig. 5.5 for the case of **20**, resulted by diverse hydrogen

bonding and C-H...π ring interactions (Tables 5.6 & 5.7). The 'face to face' arrangement is along the *b* axis for the case of **20** and along the *c* axis for the case of **23** (Fig. 5.6). Since the latter contains three different molecules in the asymmetric unit large number of diverse interactions are present compared to that in **20.**

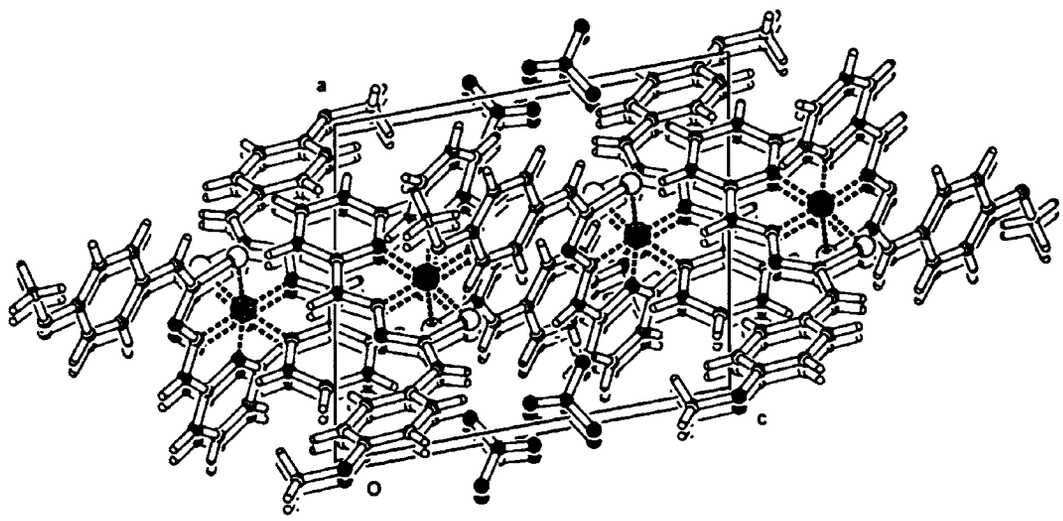

Fig. 5. 5. A view of the molecule $[CoL^1_2]NO_3 \cdot H_2O$ (20) along *b* axis showing face to face packing in the unit cell.

Table 5. 6. Interaction parameters of the compound 20

π----π interaction			
Cg(I)-Res(I)----Cg(J)	Cg-Cg(Å)	α (°)	β(°)
Cg(5)-[1]----Cg(7)[a]	3.6973	7.83	29.12
Cg(7)-[1]----Cg(5)[a]	3.6973	7.83	22.39
Cg(7)-[1]----Cg(7)[b]	3.6339	0.02	18.97
Eqivalent position codes : a= 1-x,-y,1-z; b= 1-x,-1-y,1-z			
Cg(5)= N(1),C(1),C(2),C(3),C(4),C(5)			
Cg(7)= C(8),C(9),C(10),C(11),C(12),C(13)			
CH----π interactions			
X-H(I)Res(1)----Cg(J)	H..Cg(Å)	X..Cg(Å)	X-H..Cg (°)
C(1)-H(1) [1]...Cg(2)[a]	2.81	3.0983	99
C(15)-H(15) [1]...Cg(1)[a]	2.88	3.1389	98
C(15)-H(15) [1]...Cg(3)[a]	2.87	3.1094	96
Equivalent position code; a= x,y,z			
Cg(1)= Co(1),S(1),C(7),N(3),N(2); Cg(2)= Co(1),S(4),C(21),N(7),N(6); Cg(3)= Co(1),N(1),C(5),C(6),N(2)			

Cg=Centroid, α=dihedral angles between planes I & J, β= angle Cg(1)-Cg(J)

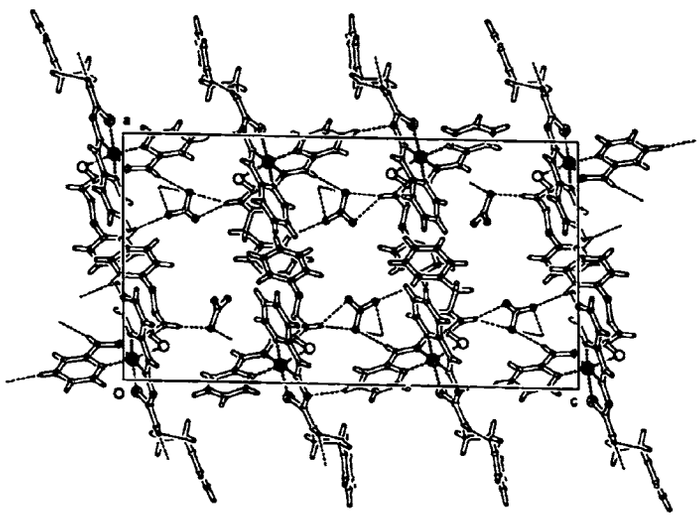

Fig. 5. 6. Unit cell packing of the compound 23 along b axis showing hydrogen bonding interactions.

Table 5.7. Interaction parameters of the compound 23

CH—π interactions			
X-H(I)Res(1)----Cg(J)	H..Cg (Å)	X..Cg (Å)	X-H..Cg (°)
C(1)–H(1) [1] -> Cg(1)[a]	2.88	3.1630	99
C(1)–H(1) [1] -> Cg(4)[a]	2.99	3.2167	96
C(1) -H(1) [1] -> Cg(2)[a]	2.93	3.1831	97
C(1)–H(1) [1] -> Cg(3)[a]	2.78	3.0836	100
C(2)–H(2) [1] -> Cg(15)[a]	2.90	3.4591	120
C(3)-H(3) [1] -> Cg(7)[b]	2.61	3.5363	171
C(16)-H(16) [2] -> Cg(10)[a]	2.96	3.1897	96
C(16)-H(16) [2] -> Cg(12)[a]	2.83	3.1076	99
C(16)-H(16) [2] -> Cg(9)[a]	2.88	3.1745	100
C(16) -H(16) [2] -> Cg(11)[a]	2.96	3.2015	97
C(17) -H(17) [2] -> Cg(7)[b]	2.92	3.4221	115
C(18) –H(18) [2] -> Cg(15)[b]	2.58	3.4932	168
C(31') -H(31') [3] -> Cg(17)[a]	2.93	3.2103	99
C(31') -H(31') [3] -> Cg(19)[a]	2.99	3.2095	95
C(32)-H(32) [3] -> Cg(24)[c]	2.79	3.5533	140
C(33)–H(33) [3] -> Cg(24)[b]	2.64	3.5568	168
C(31)–H(31) [3] -> Cg(18)[a]	2.95	3.2068	97
C(31)-H(31) [3] -> Cg(20)[a]	2.84	3.1071	98

Eqivalent position codes a = x,y,z; b = x,1+y,z; c = 1-x,1/2+y,-z
Cg(1)= Co1,S1,C7,N3,N2; Cg(2)= Co1,S1',C7,N3',N2 ; Cg(3)= Co1,N1,C5',C6,N2 ;
Cg(4)= Co1,N1,C5,C6,N2 ; Cg(7)= C10,C11',C12',C13,C14,C15.

Table 5.8. H-bonding interactions in compounds (Å), (°)

	Residue	D-H...A	D-H	H...A	D...A	D-H...A
HL^3	1	N3-H1N3...N1[a]	0.88	1.98	2.6768	135
	1	C6-H6...N2[b]	0.93	2.61	3.3540	137
$[CoL^1{}_2]NO_3$ H_2O **(20)**	1	N4'-H4'A...O3[c]	0.86	2.10	2.922(10)	159
	1	N4-H4A...O4[d]	0.86	2.12	2.964(9)	167
	1	C3'-H3'...O4[e]	0.93	2.46	3.350(10)	160
	1	C14'-H14'C...S1[f]	0.96	2.86	3.556(10)	131
	1	C4'-H4'...O1[g]	0.93	2.46	3.221(9)	139
	1	C6-H6...S1'[h]	0.93	2.71	3.477(7)	140
	1	C9-H9...N3[a]	0.93	2.24	2.845(10)	122
	1	C9-H9''...N3'[a]	0.93	2.36	2.929(10)	119
	1	N4-H4N...O5[i]	0.86	2.09	2.9152	160
	1	N4'-H4N'...O7[a]	0.86	2.16	2.9978	163
	1	N4'-H4N'...O9[a]	0.86	2.45	3.1914	145
	1	C3'-H3'...N7[j]	0.93	2.44	3.3499	166
	1	C6-H6...O1[j]	0.93	2.52	3.4235	164
	1	C8-H8A...S1[a]	0.97	2.60	3.0852	111
	1	C8-H8B...N3'[a]	0.97	2.40	2.8034	104
	1	C11'-H11'...O3[j]	0.93	2.58	3.8880	146
	2	N8-H8...O1[k]	0.86	2.25	3.0343	151
	2	N8-H8...O3[k]	0.86	2.41	3.1487	144
	2	N8'-H8N...O1[a]	0.86	2.22	3.0474	161
$[CoL^2{}_2]NO_3$ **(23)**	2	N8'-H8N...O2[a]	0.86	2.45	3.1740	143
	2	C18'-H18'...N11[a]	0.93	2.47	3.3572	160
	2	C21'-H21' ...O5[a]	0.93	2.42	3.3256	164
	2	C26' -H26'...O4[a]	0.93	2.46	3.3890	172
	2	C23-H23A...S2[a]	0.97	2.59	3.0969	112
	3	N12-H12B...O5[a]	0.86	1.99	2.8412	169
	3	N12-H12N...O8[l]	0.86	2.27	3.0763	156
	3	N12-H12N...O9[l]	0.86	2.53	3.2167	137
	3	C41' -H41'...O8[l]	0.93	2.51	3.4043	161
	3	C33-H33...N3[l]	0.93	2.48	3.3965	167
	3	C36-H36...O9[l]	0.93	2.54	3.4389	161
	3	C38-H38A...S3[a]	0.97	2.68	3.1332	109

D=donor, A=acceptor, Eqivalent position codes : a= x,y,z; b=-x,-y,1-z; c=1-x,1-y,1-z; d=-1+x,-1+y,z; e=2-x,1-y,-z; f=-x,1-y,-z; g=x,1+y,-1+z; h=1-x,-y,1-z; i= 1+x,y,z; j= 1-x,-1/2+y,1-z; k= -x,1/2+y,1-z; l= 1-x,1/2+y,-z

Conclusion

Syntheses and characterizations of eight cobalt(III) complexes of the ligands HL^1, HL^2, HL^3 and H_2L^5 are discussed in this chapter. In all the complexes, the thiosemicarbazones are coordinated in the deprotonated thiolate form. All complexes are assigned octahedral geometries at the metal centre by the coordination of two deprotonated ligand moieties. The single crystal X-ray studies of $[CoL^1_2]NO_3 \cdot H_2O$ and $[CoL^2_2]NO_3$, corroborate spectral characterization.

References

1. S.B. Padhye, G.B. Kauffman, Coord. Chem. Rev. 63 (1985) 127. and refs therein.
2. G.D. Domag, R.B. Chenich, F.M. Mietzch, H. Schmidt, Naturwissenschaften 33 (1946) 494.
3. D.J. Baaer, L.S. Vincent, C.H. Kempe, A.W. Downe, Lancet. 2 (1963) 494.
4. H.G. Petering, H.H. Buskirk, G.E.E. Underwood, Cancer Res. 64 (1964) 367.
5. C.W. Johnson, J.W. Joyner, R.P. Perry, Antibiot. Chemother. 2 (1952) 636.
6. D.X. West and C.S. Carlson, Transition Met. Chem. 15 (1990) 383.
7. N. M. Samus, V. I. Tsapkov, A.P. Gulya, Russian Journal of General Chemistry 74 (2004) 1428.
8. S. K. Chattopadhyay, M. Hossain, S. Ghosh, A. K.Guha, Transition Met. Chem.15 (1990) 473.
9. G. M. Sheldrick (1997) SHELXS97 and SHELXL97. Bruker AXS Inc., Madison, Wisconsin, USA.
10. L. J. Farrugia, J. Appl. Cryst. 30 (1997) 565.
11. A. L. Spek, J. Appl. Cryst. 36 (2003) 7.
12. R. P. John, A. Sreekanth, M. R. P. Kurup, S. M. Mobin, Polyhedron. 21 (2002) 2515.

13. W.J. Geary, Coord. Chem. Rev. 7 (1971) 81.
14. B S. Garg, M. R. P. Kurup, S. K. Jain, Y.K. Bhoon, Transition Met. Chem. 13 (1988) 309.
15. A. Sreekanth, U. L. Kala, C. R. Nayar, M. R. P. Kurup, Polyhedron, 23/1 (2004) 41.
16. P. Bera, R. J. Butcher, S. Chaudhuri, N. Saha, Polyhedron. 21 (2002) 1.
17. M.B. Ferrari, G.G. Fava, M. Lanfranchi, C. Pelizzi, P. Tarasconi, J. Chem. Soc., Dalton Trans. (1991) 1951.
18. D. F. Little, C. J. Long, Inorg. Chem. 7 (1968) 3401.
19. B. S. Garg, M. R. P. Kurup, S. K. Jain, Y. K. Bhoon, Transition. Met. Chem. 16 (1991) 111.
20. A.M. Bond, and R.L. Martin, Coord. Chem. Rev. 54 (1984) 23.
21. P. F. Rapheal, E. Manoj, M. R.P. Kurup, Polyhedron, 2006, in press.
22. D.N.Sathyanarayana, Vibrational Spectroscopy, New Age International, New Delhi (2004) 400.
23. V.Stefov, V.M.Petrusevski, B.Soptrajanov, J.Mol.Struct.293 (1993) 97.
24. R. Osterberg. Coord.Chem.Rev. 12 (1974) 309.
25. H.-S. Wang, L. Huang, Z.F. Chen, X.-W. Wang, J. Zhou, S.-M. Shi, H. Liang, K.B. Yu, Acta cryst. E60 (2004) m354.
26. S.K. Chattopadhyay, T. Banerjee, P. Roychaudhury, T.C.W. Mak, S. Ghosh, Transition Met. Chem. 22 (1997) 216.
27. D.X. West, M. A. Lockwood, A. Castineiras, Transition Met. Chem. 22 (1997) 447.

Syntheses of nickel(II) complexes and studies on their structural and spectral characteristics

6.1. Introduction

Nickel (Ni) is a transition element that is both siderophile (associates with iron) and chalcophile (associates with sulfur) having atomic number, 28 and atomic mass, 58.6934(2) g/mol. Nickel is a silvery white metal that takes on a high polish and is hard, malleable, and ductile. Nickel is one of the five ferromagnetic elements. The most common oxidation state of nickel is +2, though 0, +1, +3 and +4 Ni complexes are observed. Nickel-62 is the most stable nuclide of all the existing elements. Nickel is a very abundant natural element. The principal ore mineral is pentlandite: $(Ni,Fe)_9S_8$. The ionic radius of divalent nickel is close to that of divalent iron and magnesium, allowing the three elements to substitute for one another in the crystal lattices of some silicates and oxides. Chief use of nickel is in the nickel steels of different varieties. It is also widely used for many other alloys, such as nickel brasses and bronzes, and alloys with copper, chromium, aluminum, lead, cobalt, silver and gold.

The substituted derivatives of pyridine-2-carbaldehydethiosemicarbazone (HL) and their complexes with different metal ions have drawn special attention due to their interaction with enzymes such as ribonucleotide reductases, DNA polymerase and cell thiols Some reports show that labile four-coordinated nickel(II) complexes with tridentate thiosemicarbazone ligands exhibit antibacterial activities, whereas, six-coordinated nickel(II) complexes with thiosemicarbazone ligands show no activities against the test microorganisms [1]. We have prepared and characterized eight nickel(II) complexes of the ligands pyridine-2-carbaldehyde N(4)-*p*-methoxyphenyl thiosemicarbazone (HL^1), pyridine-2-carbaldehyde N(4)-phenylethyl thiosemicarbazone (HL^2), pyridine-2-carbaldehyde-N(4)-pyridyl thiosemicarbazone [HL^4] and salicylaldehyde-N(4)-phenylethyl thiosemicarbazone [H_2L^5]. In addition to

spectroscopic characterization of these eight Ni(II) complexes, this chapter describes the X-ray crystallography of two of them, *viz.*, $[NiL^1_2]$.DMSO (**28**) and $[Ni(HL^2)_2](ClO_4)_2$ (**32**).

6.2. Experimental

6.2.1. Materials

Nickel(II) nitrate hexahydrate, nickel(II) sulphate heptahydrate, nickel(II) acetate tetrahydrate and nickel(II) perchlorate hexahydrate (Merck) were used as supplied and solvents were purified by standard procedures before use. **Caution!** Perchlorate complexes of metals with organic ligands are potentially explosive and should be handled with care.

6.2.2. Syntheses and characterization of ligands

The syntheses and characterization of the thiosemicarbazone ligands HL^1, HL^2, and HL^3 have been described in Chapter 2.

6.2.3. Syntheses of complexes

6.2.3.1. Syntheses of $[NiL^1_2]\cdot 2H_2O$ (28), $[Ni(HL^2)_2](NO_3)_2\cdot H_2O\cdot EtOH$ (30), $[NiL^4NO_3]\cdot 3H_2O$ (34), $[Ni(H_2L^5)(HL^5)]NO_3$ (35)

To a solution of the respective ligand (1 mmol) in hot ethanol (25 ml) was added $Ni(NO_3)_2\cdot 6H_2O$ (1 mmol) and heated at reflux for two hours and kept at room temperature (overnight). The complex formed was filtered, washed thoroughly with water, ethanol and then ether and dried *in vacuo* over P_4O_{10}.

6.2.3.2. Synthesis of $[Ni_2L^2_2SO_4]\cdot 1\frac{1}{2}H_2O$ (29)

To a solution of the HL^2 (1 mmol) in hot ethanol (25 ml) was added a solution of $NiSO_4\cdot 7H_2O$ (1 mmol) in a mixture of ethanol (15 ml) and water (10 ml) and heated at reflux for four hours and kept at room temperature (overnight). The complex formed was filtered, washed thoroughly with water, ethanol and then ether and dried *in vacuo* over P_4O_{10}.

6.2.3.3. Syntheses of $[Ni(L^2)(HL^2)](Ac)\cdot 3H_2O$ (31) and $[NiL^4(Ac)]\cdot 2\frac{1}{2}H_2O$ (33)

To a solution of the respective ligand (1 mmol) in hot ethanol (25 ml) was added $Ni(Ac)_2\cdot 4H_2O$ (1 mmol) and heated at reflux for two hours and kept at room

temperature (overnight). The complex formed was filtered, washed thoroughly with water, ethanol and then ether and dried *in vacuo* over P_4O_{10}.

6.2.3.4. Synthesis of $[Ni(HL^2)_2](ClO_4)_2 \cdot 2H_2O$ (32)

To a solution of the HL^2 (1 mmol) in hot methanol (25 ml) was added $Ni(ClO_4)_2 \cdot 6H_2O$ (1 mmol) and heated at reflux for one hour and kept at room temperature (overnight). The complex formed was filtered, washed thoroughly with water, ethanol and then ether and dried *in vacuo* over P_4O_{10}.

6.3. Physical Measurements

Elemental analyses of the ligands and the complexes were done on a Heracus elemental analyzer at CDRI, Lucknow, India and on a Vario EL III CHNS analyzer at SAIF, Kochi, India. The IR spectra were recorded on a Thermo Nicolet AVATAR 370 DTGS model FT-IR Spectrophotometer with KBr pellets at SAIF, Kochi. The far IR spectra were recorded using polyethylene pellets in the 500-100 cm^{-1} region on a Nicolet Magna 550 FTIR instrument at Regional Sophisticated Instrument Facility, Indian Institute of Technology, Bombay. Electronic spectra were recorded on a Cary 5000, version 1.09 UV-Vis-NIR spectrophotometer from a solution in $CHCl_3$. The magnetic susceptibility measurements were carried out at the Indian Institute of Technology, Roorkee, at room temperature in the polycrystalline state on a PAR model 155 Vibrating Sample Magnetometer at 5 kOe field strength. The molar conductances of the complexes in dimethylformamide solutions (10^{-3} M) at room temperature were measured using a direct reading conductivity meter.

6.4. X-Ray crystallography

Single crystals of compounds **28** and **32** of X-ray diffraction quality were grown from their DMSO and methanol solutions respectively, by slow evaporation at room temperature in air. The crystallographic data and structure refinement parameters are given in Table 6.1. The data collection and cell refinement of **28**, were carried out using a ARGUS-MACH3 (Nonius, 1997) with graphite monochromated Mo Kα (λ =

0.71073 Å) radiation on a single crystal of **28** of dimension 0.25 × 0.20 × 0.15 mm at the National Single Crystal X-Ray Diffraction Facility, IIT, Bombay, India.

Table 6. 1. Crystal refinement parameters of compounds 28 & 32

Parameters	$[NiL^1_2]$·DMSO (**28**)	$[Ni(HL^2)_2](ClO_4)_2·2H_2O$ (**32**)
Empirical Formula	$C_{30}H_{32}N_8NiO_3S_3$	$C_{30}H_{36}N_8NiS_2Cl_2O_{10}$
Formula weight (M)	707.53	862.40
Temperature (T) K	293(2)	293(2)
Wavelength (Mo Kα) (Å)	0.71073	0.71073
Crystal system	Triclinic	Orthorhombic
Space group	*P*1	*Fddd*
Lattice constants		
a (Å)	10.2850(14)	10.6424(4)
b (Å)	10.6120(10)	44.668(3)
c (Å)	16.3600(11)	31.2715(15)
α (°)	108.467(6)	90.00
β (°)	93.263(8)	90.00
γ (°)	102.453(9)	90.00
Volume V ($Å^3$)	1638.6(3)	14865.7(13)
Z	2	16
Calculated density (*ρ*) (Mg m^{-3})	1.434	1.541
Absorption coefficient, *μ* (mm^{-1})	0.828	0.844
F(000)	736	7136
Crystal size (mm)	0.25 x 0.20x 0.15	0.78 x 0.28 x 0.19
Color, Nature	Brown, Rod	Brown, Block
Limiting Indices	-12<=h<=0, -12<=k<=12, -19<=l<=19	-10<=h<=12, -52<=k<=52, -37<=l<=37
Reflections collected	6090	54060
Independent Reflections	5739 [R(int) = 0.0452]	3287 [R(int) = 0.0425]
Refinement method	Full-matrix least-squares on F^2	Full-matrix least-squares on F^2
Data / restraints / parameters	5739/ 0 / 418	3272 / 0 / 287
Goodness-of-fit on F^2	1.026	1.401
Final *R* indices [I > 2σ (I)]	R_1 =0.0652, wR_2 = 0.1450	R_1 = 0.0983, wR_2 = 0.2459
R indices (all data)	R_1 = 0.1963, wR_2 =0.1815	R_1 = 0.1017, wR_2 = 0.2481
Largest difference peak and hole (e $Å^{-3}$)	1.241 and -0.802	0.763 and -0.909

The unit cell dimensions and intensity data were measured at 293 K. The single crystal of **32** of dimension 0.78 × 0.28 × 0.19 was diffracted by a Bruker Smart Apex2 CCD

area detector diffractometer equipped with graphite monochromated Mo Kα (λ = 0.71073 Å) radiation, at School of Physics, Universiti Sains Malaysia, Penang, Malaysia. The trial structures were solved using SHELXS-97 [2] and refinements were carried out by full-matrix least squares on F^2 (SHELXL-97) [2]. Molecular graphics employed were ORTEP-III [3] and PLATON [4].

6.5. Results and discussion

Compositions and empirical formulae of the eight nickel(II) complexes were determined by elemental analyses, magnetic susceptibility measurements, molar conductivity measurements, UV-Vis absorption spectra and FT-IR spectra. Molar conductivity measurements of the reported species show that **28**, **29**, **33**, and **34** are non-electrolytes and the remaining are cationic complexes, behaving as 1:1 (**30**, **31**, **35**) and 1:2 (**32**) electrolytes in10^{-3} M DMF solution. All the complexes except **35** are brown, **35** being green. The Ni(II) complexes **29**, **33** and **34** are diamagnetic indicating probable square planar geometry, while all others are paramagnetic with μ_{eff} = 2.85 - 3.09 BM for a normal spin free d^8 system. In the compounds **28**, **29**, **33** and **34**, the thiosemicarbazones deprotonate and chelate in thiolate form as evidenced by the IR spectra whereas in **30**, **32** and **35**, the thiosemicarbazones are in the thione form. The absence of the IR spectral band corresponding to ν(O-H) in **35** shows that the phenolic -OH group in H_2L^5 deprotonates and the oxygen atom coordinates with the metal. Infrared spectral evidences also support the presence one ligand in the thione form and the other ligand in the deprotonated thiolate form. in **31**. The stoichiometries of the complexes are presented in Table 6.2.

6.5.1. Infrared spectra

The shift in the relevant IR bands of the thiosemicarbazone ligands due to complexation with the Ni(II) ion is shown in the Table 6.3. Far infrared spectral data are given in the Table 6.4. In the IR spectrum of **30**, **32** and **35** bands in the 3204–3254 cm^{-1} region are due to the stretching frequency for ^{2}NH. Besides, no band due to the SH group is observed between 2600 and 2500 cm^{-1} in agreement with the thione form of the ligand in these complexes [5]. In the spectra of the complexes **28**, **29**, **33** and **34**,

Table 6. 2. Magnetic susceptibilities, molar conductivities and partial elemental analyses of the complexes.

Complex	μ(B.M)	*λ_M	Found (Calc.)%			
			C	H	N	S
$[NiL^1_2]\cdot 2H_2O$ (**28**)	2.88	5	51.13(50.54)	4.46(4.54)	16.50(16.84)	9.58(9.64)
$[Ni_2L^2_2SO_4]\cdot 1½H_2O$ (**29**)	Dia.	19	45.05(44.64)	4.68(4.12)	14.12(13.88)	11.49(11.92)
$[Ni(HL^2)_2](NO3)_2\cdot H2O\cdot EtOH$(**30**)	2.89	160	47.53(47.13)	4.43(4.94)	17.66(17.17)	8.43(7.86)
$[NiL^2(HL^2)]Ac\cdot 3H_2O$(**31**)	2.86	85	52.35(51.97)	5.07(5.45)	15.46(15.15)	8.19(8.67)
$[Ni(HL^2)_2](ClO_4)_2\cdot 2H_2O$ (**32**)	3.09	136	41.71(41.78)	4.07(4.21)	12.94(12.99)	7.56(7.44)
$[NiL^4Ac]\cdot 2½H_2O$ (**33**)	Dia.	2	40.34(40.12)	4.52(4.33)	16.48(16.71)	7.74(7.65)
$[NiL^4NO_3]\cdot 3H_2O$ (**34**)	Dia.	20	34.04(33.44)	4.19(3.74)	19.17(19.50)	7.52(7.44)
$[Ni(H_2L^5)(HL^5)]NO3$ (**35**)	2.85	68	53.85(53.49)	4.58(4.63)	13.54(13.65)	8.67(8.93)

*Molar conductivity of 10^{-3} M DMF solution, in $ohm^{-1}cm^2\ mol^{-1}$

Table 6. 3. Infrared spectral data (cm^{-1}) of thiosemicarbazones and the complexes

Compound	ν(C=N)	ν(N=C)	ν(N-N)	ν/δ(C-S)	py(ip)	py(op)	ν(^{2}N-H)	ν(^{4}N-H)
HL^1	1584		1024	1334,837	613	401	3134	3310
$[NiL^1_2]\cdot 2H_2O$ (**28**)	1566	1608	1133	1300,829	646	409	---	3440
HL^2	1586		1079	1324,897	622	406	3129	3374
$[Ni_2L^2_2SO_4]\cdot 1½H_2O$ (**29**)	1534	1624	1143	1338.894	670	438	---	3312
$[Ni(HL^2)_2](NO3)_2\cdot H2O\cdot EtOH$(**30**)	1575	---	1156	1302,886	637	425	3234	3428
$[NiL^2(HL^2)]Ac\cdot 3H_2O$(**31**)	1576	1600	1135	1310,891	637	417	---	3419
$[Ni(HL^2)_2](ClO_4)_2\cdot 2H_2O$ (**32**)	1570	---	1143	1310,886	637	425	3204	3424
HL^4	1593		1078	1298,929	614	412	3057	3310
$NiL^4Ac]\cdot 2½H_2O$ (**33**)	1537	1612	1126	1277,903	641	421	---	3411
$[NiL^4NO_3]\cdot 3H_2O$ (**34**)	1568	1608	1159	1260,897	640	416	---	3416
H_2L^5	1619		1003	1383,840	---	---	3250	3346
$[Ni(H_2L^5)(HL^5)]NO3$ (**35**)	1573	1600	1038	1329,809	---	---	3254	3428

$\nu(^4NH)$ vibrations appear in the range 3312-3440 cm^{-1}, but there is no band corresponding to stretching of the hydrazinic NH, consistent with deprotonation of the ligands in these complexes. The shift of the thiocarbonyl stretching and bending modes to lower frequencies in all the complexes is in accordance with the coordination through sulfur. The ν(Ni- S) bands in the 325 – 375 cm^{-1} region further confirms the sulfur coordination [6] A similar shift of ν(C=N) frequencies corroborates coordination of the azomethine nitrogen [7]. Additional evidence for coordination of the imine nitrogen is the presence of ν(Ni-/N) bands in the 417-/430 cm^{-1} range [8] A second band due to $\nu(^2C=^3N)$ is resolved in the spectra of **28**, **29**, **31**, **33** and **34** at *ca.* 1600cm^{-1}. Coordination of the pyridine nitrogen atom is clearly shown by the shift to higher frequencies of the deformation mode bands that appear in the ranges 613-622 and 401-412 cm^{-1} in the spectra of HL^1, HL^2 and HL^4 [9]. The ν(M- N) bands for the pyridyl nitrogen are assigned in the 211-272 cm^{-1} region, to confirm the coordination of pyridine nitrogen.

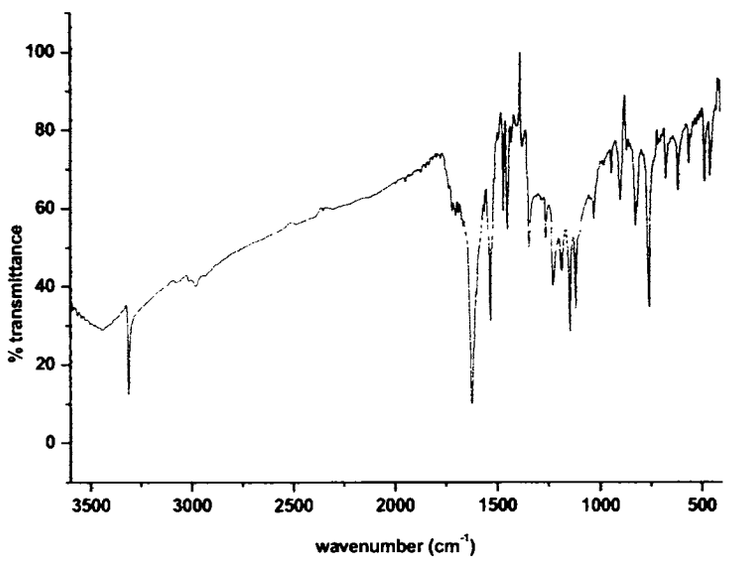

Fig. 6.1. Infrared spectra of $[Ni_2L^2{}_2SO_4]\cdot$ (29)

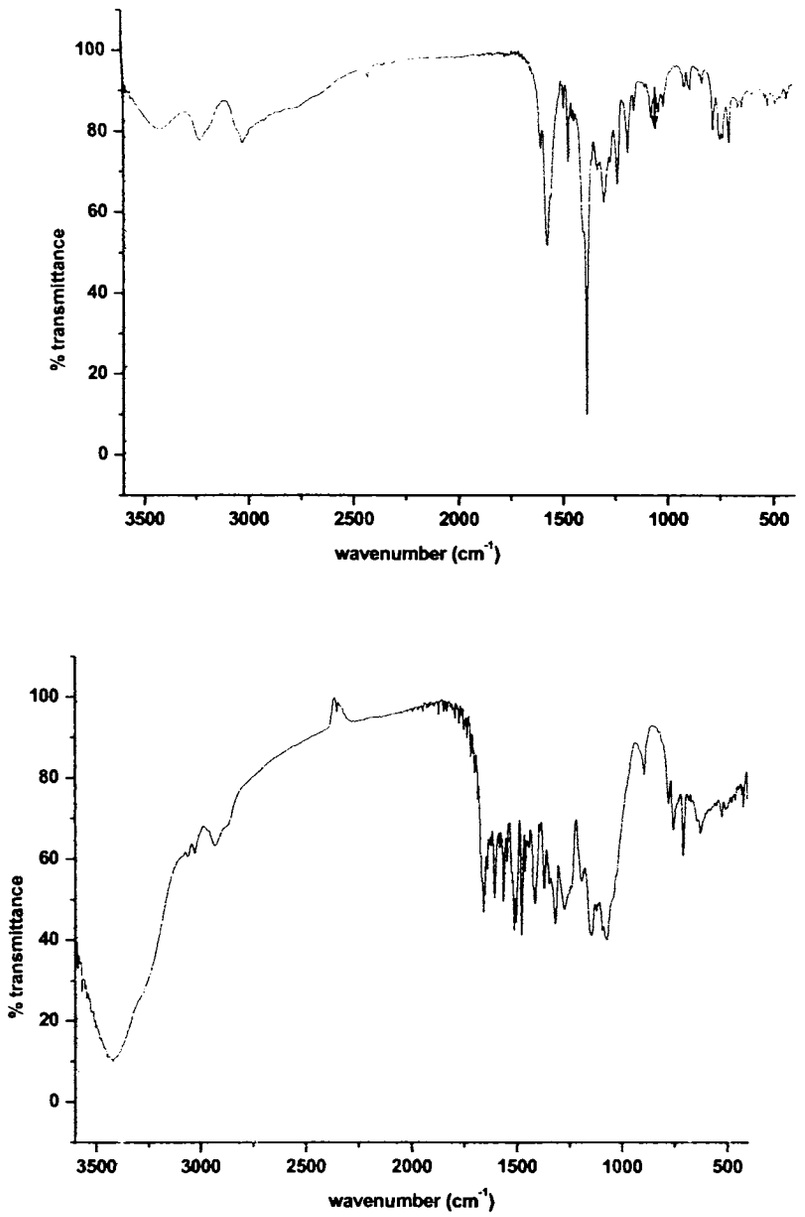

Fig. 6 .2. Infrared spectra of $[Ni(HL^2)_2](NO_3)_2$ (30) (top) and $[NiL^2(HL^2)]Ac$ (31) (bottom)

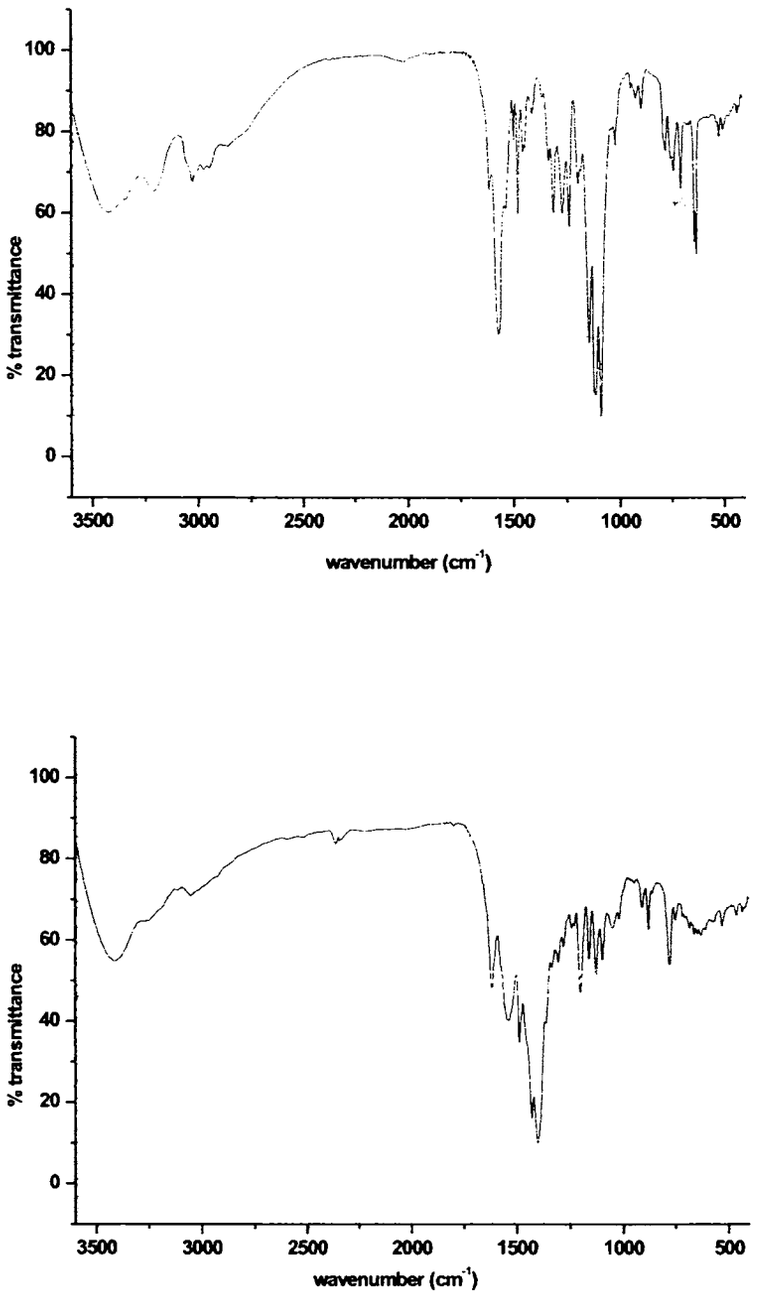

Fig. 6. 3. Infrared spectra of $[Ni(HL^2)_2](ClO_4)_2$ (32) (top) and $[NiL^4Ac]$ (33) (bottom)

The sulfato complex **29** exhibits the following vibrations: a medium band at 977 cm^{-1} due to ν_1, a medium band at 451 cm^{-1}due to ν_2, medium and weak bands at 1185, 1118 and 1023 cm^{-1}correspondingto ν_3, and weak band at 609 cm^{-1} due to ν_4, which are assigned to the bidentately coordinated sulfato group [10]

In the spectra of the complexes **30** and **35** the absence of the combination bands (ν_1+ ν_4) in the region 1700-1800 cm^{-1} rules out the possibility for coordinated nitrato group. The bands at *ca.* 830 (ν_2), 1380 (ν_3) and 700 cm^{-1} (ν_4) for these complexes clearly points out the uncoordinated nature of the nitrato group [11]

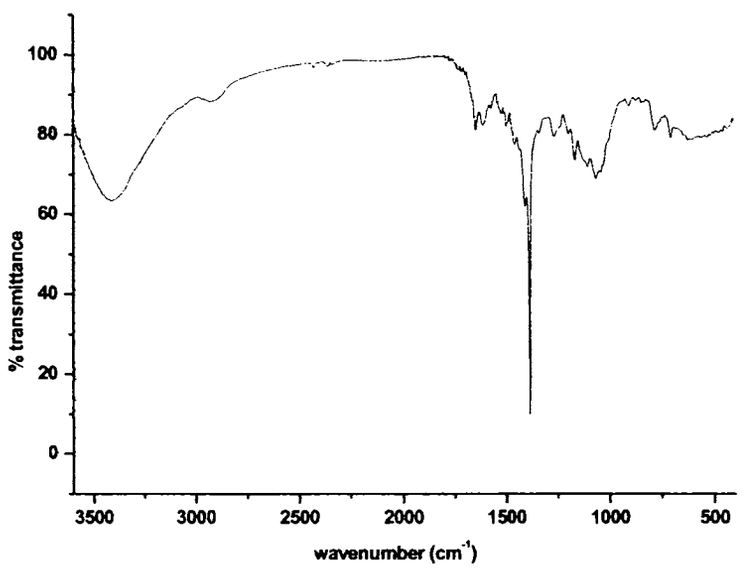

Fig. 6. 4. Infrared spectrum of [NiL^4NO_3] (34)

The nitrato complex **34** has two strong bands at 1260 and 1383 cm^{-1} with a separation of 123 cm^{-1} corresponding to ν_1 and ν_4 indicating the presence of a terminal monodentate nitrato group [12]. The ν_1+ν_4 combination bands considered as diagnostic for the monocordinated nitrato group are observed at 1713 and 1738 cm^{-1}.

The spectrum of the acetate-containing complex **31** displays relatively strong bands at 1559 [ν_a(COO)] and 1417 cm^{-1}, [ν_s(COO)] indicating the ionic nature of the acetate in this compound [12]. The bands at 1570 [ν_a(COO)] and 1400 cm^{-1}[ν_s(COO)] support the unidentate nature of acetate group in **33** [13].

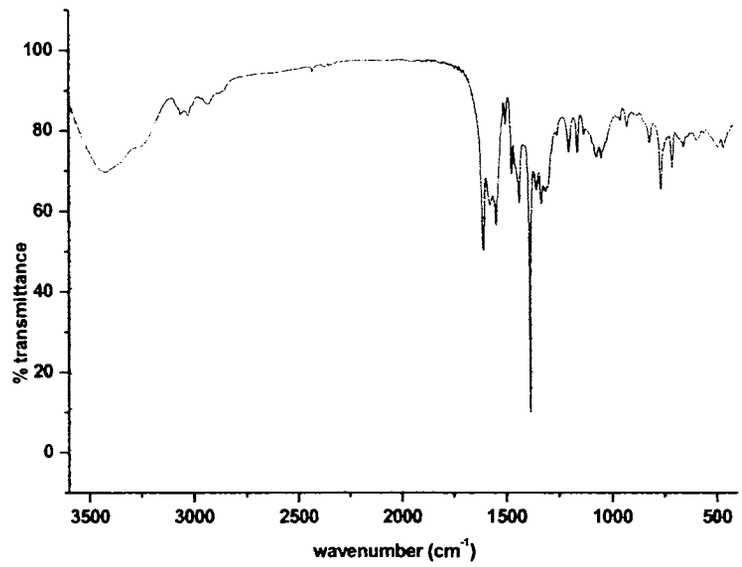

Fig. 6. 5. Infrared spectrum of $[Ni(H_2L^5)(HL^5)]NO_3$ (35)

The perchlorate complexes **32** show single broad bands at 1122 cm^{-1} and strong bands at 637 and 624 cm^{-1}, indicating the presence of ionic perchlorate. The bands at 1122 cm^{-1} are assignable to $\nu_3(ClO_4)$ and, a medium band at 915 cm^{-1} may be assigned to $\nu_1(ClO_4)$ of the perchlorate ion [14].

6.5.2. Electronic spectra

The electronic spectral data of the ligands and the complexes in $CHCl_3$ solutions are listed in the Table 6.5. The high-energy $\pi \rightarrow \pi^*$ transition *ca.*42000 cm^{-1} are not significantly altered on complex formation. The $n \rightarrow \pi^*$ transitions associated with the azomethine functions of the thiosemicarbazone moieties are shifted to higher energy for the complexes.

Table 6. 4. Metal-ligand stretching frequencies (cm^{-1}) of the complexes

Compound	νNi-$N_{azo.}$	νNi-N_{py}	νNi-S
$NiL^{1}_{2}]\cdot 2H_2O$ (**28**)	417	245	372
$[Ni_2L^{2}_{2}SO_4]\cdot 1½H_2O$ (**29**)	425	228	358
$[Ni(HL^{2})_2](NO3)_2\cdot H2O\cdot EtOH$(**30**)	430	248	375
$[NiL^{2}(HL^{2})]Ac\cdot 3H_2O$(**31**)	412	271	325
$[Ni(HL^{2})_2](ClO_4)_2\cdot 2H_2O$ (**32**)	427	211	371
$NiL^{4}Ac]\cdot 2½H_2O$ (**33**)	428	220	345
$[NiL^{4}NO_3]\cdot 3H_2O$ (**34**)	427	225	355
$[Ni(H_2L^{5})(HL^{5})]NO3$ (**35**)	425	272	325

Table 6. 5 Electronic spectral data (cm^{-1}) of the complexes

Compound	π→π*	n→π*	C T	d -d
HL^{1}	42730,38760	30770	---	---
$[NiL^{1}_{2}]\cdot 2H_2O$ (**28**)	41800,37880	32360	22620	11590
HL^{2}	42190,36630	30960	---	---
$[Ni_2L^{2}_{2}SO_4]\cdot 1½H_2O$ (**29**)	42200,38310	33010	22320	17010
$[Ni(HL^{2})_2](NO3)_2\cdot H2O\cdot EtOH$(**30**)	42120,38610	32220	22570	11856
$[NiL^{2}(HL^{2})]Ac\cdot 3H_2O$(**31**)	41600,37910	33110	22108	18907
$[Ni(HL^{2})_2](ClO_4)_2\cdot 2H_2O$ (**32**)	42300,37740	33070	22422	18182
HL^{4}	41840,35840	29500	---	---
$NiL^{4}Ac]\cdot 2½H_2O$ (**33**)	42200,35910	32104	22226	---
$[NiL^{4}NO_3]\cdot 3H_2O$ (**34**)	41900,38020	32210	22070	---
H_2L^{5}	42020,33560	29670	---	---
$[Ni(H_2L^{5})(HL^{5})]NO3$ (**35**)	42700,34170	32500	22320	11830

The ground state of Ni(II) in an octahedral coordination is $^3A_{2g}$. Electronic spectral bands of hexacoordinate compounds of nickel(II) can be assigned to the three spin allowed transitions $^3T_{2g}(F) \leftarrow {}^3A_{2g}(F)$ (ν_1), $^3T_{1g}(F) \leftarrow {}^3A_{2g}(F)$ (ν_2) and $^3T_{1g}(P) \leftarrow {}^3A_{2g}(F)$ (ν_3) in the increasing order of energy with molar absorptivities generally below 20. The ν_3 band is often masked by the high-intensity charge transfer bands [9]. The energy of the ν_1 is equal to 10 Dq as seen from the energy diagram. It is found that the spectra of the octahedral complexes **28**, **30**, **31**, **32**, and **35** do not resolve to get all the three bands possible. The bands at *ca.*12000 cm^{-1} are assigned to ν_1 and the bands at *ca.*17000 – 19000 cm^{-1} are assigned to ν_2 The ν_3 is presumably obscured by the weak charge transfer bands at *ca.* 23000 cm^{-1} [15].

Diamagnetism in Ni(II) complexes is a consequence of eight electrons being paired in the four low-lying *d* orbitals, the upper orbital being $d_{x^2-y^2}$. The four lower orbitals are often so close in energy that individual transitions from them to the upper *d* level cannot be distinguished resulting in a single absorption band. The very weak band at *ca.* 19000 cm^{-1} corresponds to the *d-d* bands of the complexes **29**, **33** and **34**. A weak shoulder at *ca.*23000 cm^{-1} is assigned to charge transfer transition [16].

6.5.3. Crystal structures of 28 & 32

The Ni(II) centers in both the complexes possess octahedral geometry by the coordination of the mono deprotonated form of the ligand HL^1 in $[NiL^1_2]\cdot 2H_2O$ (**28**) and the neutral ligand HL^2 in $[Ni(HL^2)_2](ClO_4)_2\cdot 2H_2O$ (**32**). The molecular structures of **28** and **32** along with atom numbering schemes are given in Figs. 6.6 and 6.7. The Ni(II) ion in compound **28** is coordinated in a *meridional* fashion [7,16,17] using pairs of *cis* pyridyl nitrogen, *trans* azomethine nitrogen and *cis* thiolate sulfur atoms by two monoanionic ligands. In compound **32**, two molecules of the neutral ligand HL^2 are coordinated in the *meridional* fashion [18] using pairs of *cis* pyridyl nitrogen, *trans* azomethine nitrogen and *cis* thione sulfur atoms. Heterocyclic thiosemicarbazones show a strong tendency for this *meridional* coordination and is seen in most of their octahedral metal complexes, resulting in two bicyclic chelate systems. In **28**, the bicyclic chelate systems Ni1, S1, C7, N3, N2, C6, C5, N1 and Ni1, S2, C21, N7, N6,

C20, C19, N5 are approximately planar as evidenced by the maximum deviation of 0.093(7) Å for C6 and 0.092(5) Å for N5 respectively. Similarly in **32**, the bicyclic chelate system Ni1, S1, C7, N3, N2, C6, C5, N1 is approximately planar with a maximum deviation of -0.089(9) Å for C7. The dihedral angle formed by the mean planes of the bicyclic chelate systems of each of the ligands is 87.13(12)° in **28**, and 86.58(15)° in **32**. The bond lengths Ni-$N_{azomethine}$, Ni-N_{py}, and Ni-S in both the complexes increases in that order as in similar compounds [7,17,18,19]. In compound **28** the trans angles N1-Ni1-S1, N5-Ni1-S2 and N2-Ni1-N6 are 159.19(15), 158.88(16) and 173.1(2)° respectively, while in compound **32** these angles N1-Ni1-S1 and N2-Ni1-N2a are 158.8(2) and 174.9(4)° respectively. These factors suggests considerable distortion from an octahedral geometry around Ni(II) center in both the complexes.

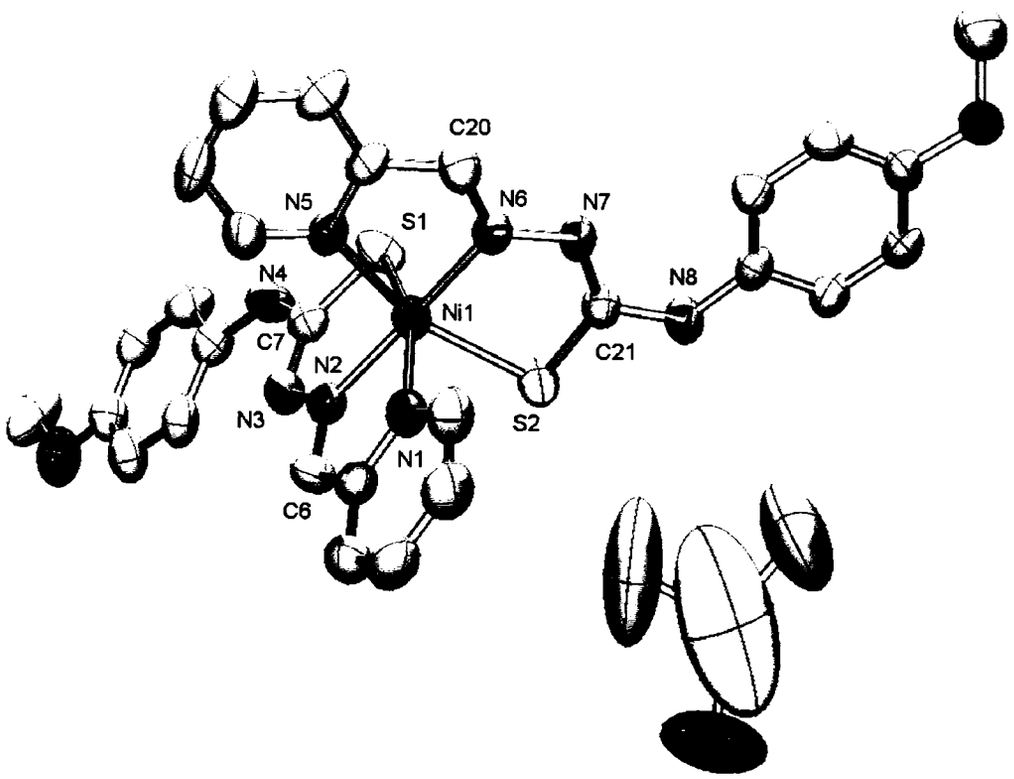

Fig. 6. 6. ORTEP diagram of *28* in 50% probability ellipsoids.

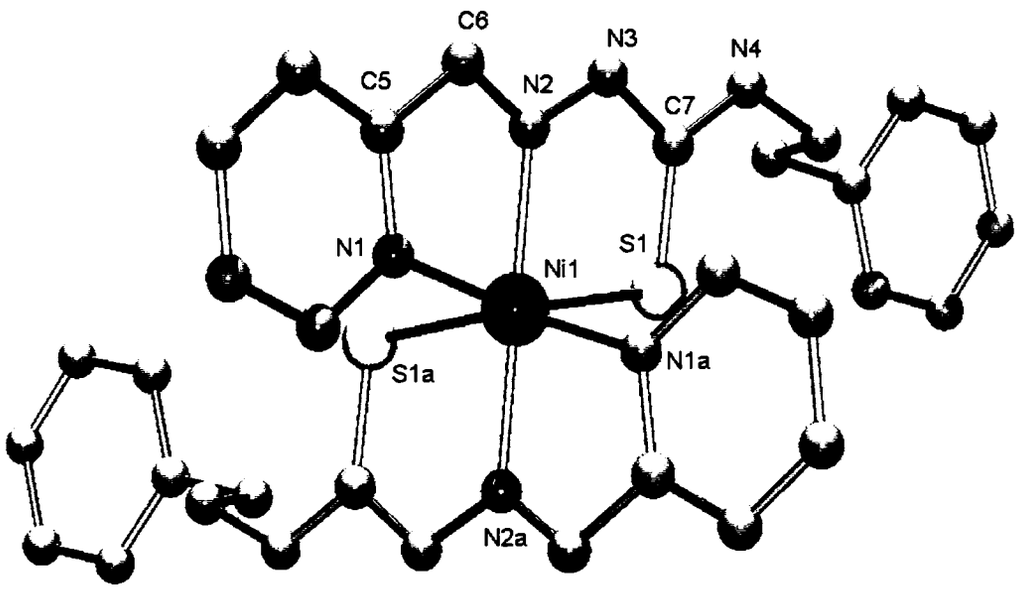

Fig. 6.7. Molecular structure of *32*. All hydrogen atoms and anions are omitted for clarity

In compound **32**, the ligand HL^2 undergoes structural reorientation to coordinate to the metal in an NNS manner. The azomethine nitrogen, was in *E* configuration with both pyridyl nitrogen and thione sulfur atoms in its metal free form of ligand, is now in *Z* form with pyridine nitrogen and sulfur atoms. The C-S bond length increases slightly by 0.0141(16) Å and the N3-C7 bond length remains almost same on coordination, in agreement with the coordination *via* thione form of the ligand. In complex **28,** the C-S {1.707(6) Å for C7-S1 and 1.737(6) Å for C21-S2} and C-N {1.331(7) Å for N3-C7 and 1.320(7) Å for C21-N7} bond lengths are consistent with partial single and double bond character confirming the coordination *via* thiolate sulfur after deprotonation. The Ni-$N_{azomethine}$ bond lengths are less compared to Ni-$N_{pyridine}$ in complexes **28** and **32**, indicating the higher strength of former bond than the latter. The Ni-S bond length in complex **32** is higher compared to that **28** (Table 6.6).

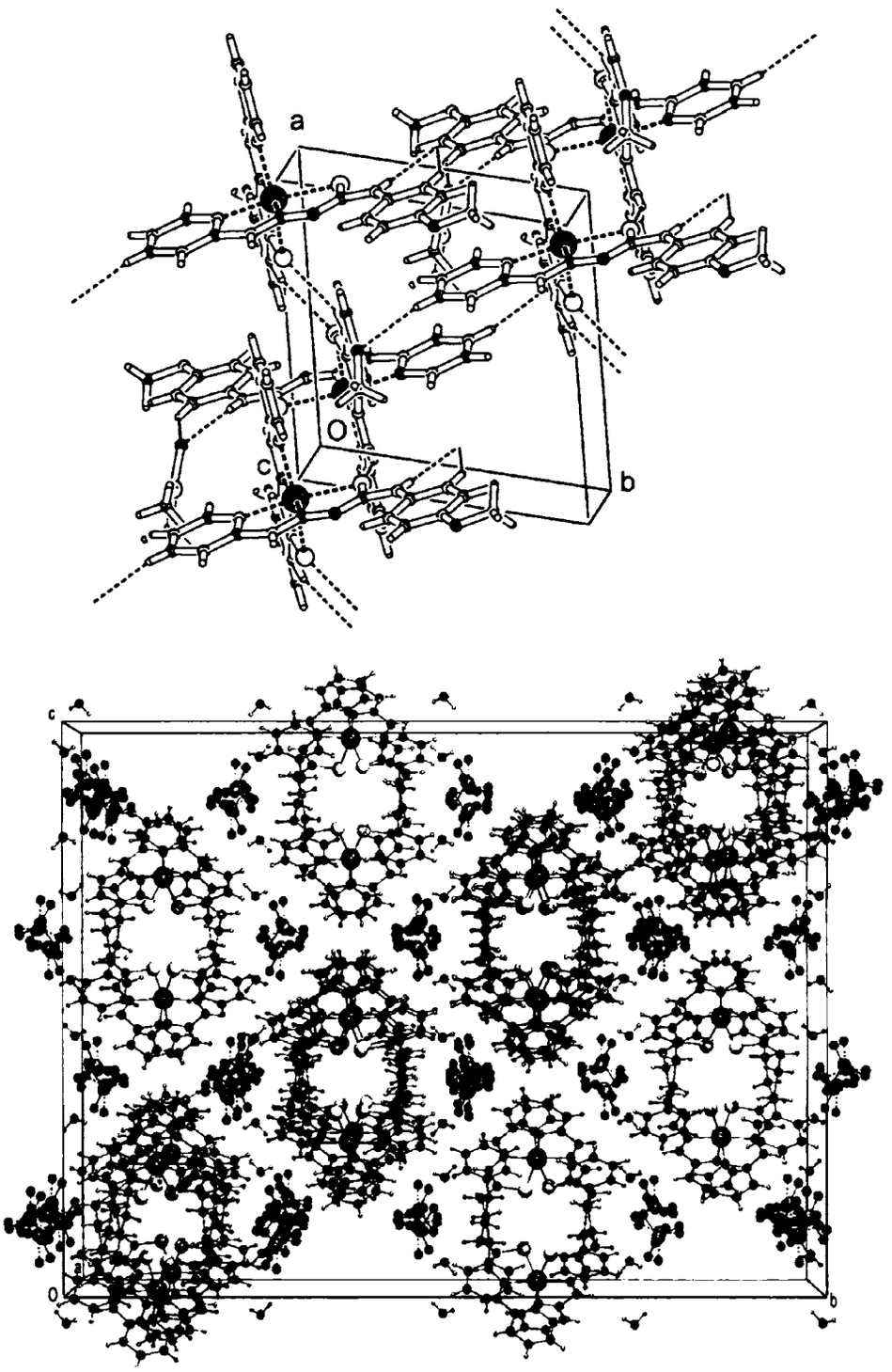

Fig. 6. 8. A view of the packing of 28 showing hydrogen bonding interactions (top) and a view of the unit cell packing of 32 (bottom) along the *a* axis showing ABABAB packing along the *c* axis.

The molecules of **32** are packed in a 'face to face' ABABAB... manner along the *c* axis within the unit cell, as seen in Fig. 6.8, as a result of diverse hydrogen bonding and C-H...π ring interactions (Table 6.8).However, no significant π...π interactions are found in the packing.

In complex **28** the molecules are connected by various hydrogen bonding interactions (Fig. 6.8) and are packed in the lattice in a 'face to face' arrangement along the *a* axis by making use of π...π and C-H...π ring interactions. Relevant hydrogen bonding π...π and C-H...π ring interactions of the compound **28** are given in Table 6.7.

Table 6 .6.
Selected bond lengths (Å) and bond angles (°) of HL^2, $[NiL^1_2]$·DMSO (*28*) and $[Ni(HL^2)_2](ClO_4)_2·2H_2O$ (*32*)

	HL^2	1	5
S(1)–C(7)	1.6849(13)	1.707(6)	1.699(9)
S(2)–C(21)		1.737(6)	
N(2)–C(6)	1.2837(15)	1.291(7)	1.288(11)
N(6)–C(20)		1.269(8)	
N(2)– N(3)	1.3783(14)	1.364(6)	1.362(10)
N(6)–N(7)		1.369(7)	
N(3)–C(7)	1.3587(16)	1.331(7)	1.359(12)
N(7)–C(21)		1.320(7)	
N(4)–C(7)	1.3401(16)	1.379(8)	1.331(12)
N(8)–C(21)		1.364(8)	
Ni(1)–S(1)		2.3893(19)	2.441(2)
Ni(1)–S(2)		2.404(2)	
Ni(1)–N(1)		2.105(5)	2.094(8)
Ni(1)–N(5)		2.107(5)	
Ni(1)–N(2)		2.031(5)	2.036(7)
Ni(1)–N(6)		2.024(5)	
C(6)–N(2)–N(3)	114.37(10)	118.9(5)	120.8(7)
N(2)–N(3)–C(7)	120.47(10)	110.9(5)	119.5(7)
N(4)–C(7)–N(3)	116.16(10)	117.0(6)	115.2(8)
N(3)–C(7)–S(1)	119.25(8)	127.9(5)	121.6(7)
N(4)–C(7)–S(1)	124.59(9)	115.1(5)	123.2(7)
N(1)–Ni(1)–N(5)		90.15(19)	

N(1)–Ni(1)–N(1a)		93.6(4)
N(2)–Ni(1)–N(6)	173.1(2)	
N(2)–Ni(1)–N(2a)		174.9(4)
S(1)–Ni(1)–S(2)	96.40(7)	
S(1)–Ni(1)–S(1a)		95.61(12)
S(1)–Ni(1)–N(1)	159.19(15)	158.8(2)
S(1)–Ni(1)–N(5)	92.05(14)	
S(1)–Ni(1)–N(2)	80.37(15)	81.3(2)
S(1)–Ni(1)–N(2a)		102.2(2)
S(1)–Ni(1)–N(6)	104.99(15)	
N(1)–Ni(1)–N(2)	78.8(2)	77.5(3)
N(1)–Ni(1)–N(2a)		99.0(3)
N(1)–Ni(1)–N(6)	95.7(2)	
N(1)–Ni(1)–S(2)	88.77(15)	
N(1)–Ni(1)–S(1a)		89.3(2)
N(2)–Ni(1)–N(5)	97.1(2)	
N(2)–Ni(1)–S(2)	103.38(15)	
S(2)–Ni(1)–N(5)	158.88(16)	
S(2)–Ni(1)–N(6)	80.63(16)	
N(5)–Ni(1)–N(6)	78.5(2)	

Table 6. 7.
Interaction parameters of $[NiL^1_2]$·DMSO (*28*)

π----π interactions			
Cg(I)-Res(I)----Cg(J)	Cg-Cg(Å)	α °	β °
Cg(5) [1] ----Cg(7)[a]	3.670(4)	3.73	24.38
Cg(6) [1] ----Cg(8)[b]	3.707(4)	3.23	27.61
Cg(7) [1] ----Cg(5)[c]	3.670(4)	3.73	21.67
Cg(8) [1] ----Cg(6)[b]	3.706(4)	3.23	24.48
CH----π interactions			
X-H(I)Res(1)----Cg(J)	H..Cg(Å)	X..Cg(Å)	X-H..Cg (°)
C(1)-H(1) [1]...Cg(2)[d]	2.92	3.243(8)	102
C(15)-H(15) [1]...Cg(1)[d]	2.99	3.328(8)	103
C(23)-H(23) [1]...Cg(1)[e]	3.00	3.813(8)	147

Cg(1)= Ni(1), S(1), C(7), N(3), N(2); Cg(2)= Ni(1), S(2), C(21), N(7), N(6); Cg(5)= N(1), C(1), C(2), C(3), C(4), C(5); Cg(6)= N(5), C(15), C(16), C(17), C(18), C(19); Cg(7)= C(8). C(9), C(10), C(11), C(12), C13); Cg(8)= C(22), C(23), C24), C(25), C(26), C(27)

Hydrogen bonding interactions				
D-H...A	D-H (Å)	H...A (Å)	D...A (Å)	D-H...A (°)
N(4)-H(104)...O(3)[f]	0.76(6)	2.25(7)	2.961(12)	156(8)
N(8)-H(108)...S(2)[e]	0.76(6)	2.66(6)	3.375(7)	158(6)
C(3)-H(3)...O(2)[g]	0.93	2.55	3.420(9)	155
C(9)-H(9)...N(3)	0.93	2.30	2.898(9)	121
C(13)-H(13)...O(3)[f]	0.93	2.52	3.308(13)	143
C(20)-H(20)...S(1)[b]	0.93	2.82	3.691(7)	157
C(27)-H(27)...N(7)	0.93	2.26	2.862(8)	122

D=donor, A=acceptor; Eqivalent position codes : a= -x, 1+y, z; b= -x, -y, -z; c= x, -1+y, z; d= x. y, z; e= 1-x, -y, -z; f=-1+x,-1+y,z; g=1-x,1-y,-z

Table 6.8. Interaction parameters of $[Ni(HL^2)_2](ClO_4)_2 \cdot 2H_2O$ (32)

CH----π interactions			
X-H(I)Res(1)----Cg(J)	H..Cg(Å)	X..Cg(Å)	X-H..Cg (°)
C(1)-H(1A) [1]...Cg(1)[a]	2.95	3.274(10)	102
C(1)-H(1A) [1]...Cg(3)[b]	2.95	3.274(10)	102

Cg(1)= Ni(1), S(1), C(7), N(3), N(2); Cg(3)= Ni(1), S(1a), C(7a), N(3a), N(2a).

Hydrogen bonding interactions					
Res	D-H...A	D-H (Å)	H...A (Å)	D...A (Å)	D-H...A (°)
1	N4-H1N4...O3B	1.03	2.20	3.171(19)	156
3	O1W-H1W1...N3	0.84	2.20	2.784(10)	127
3	O1W-H2W1...O3B	0.87	2.18	2.823(19)	131
1	N3-H3B...O1W	0.86	1.96	2.784(10)	160
1	C2-H2A...O2B[c]	0.93	2.46	3.37(3)	165
1	C3-H3A...O2B[d]	0.93	2.55	3.26(3)	134
1	C8-H8A...S1	0.97	2.77	3.110(9)	102
1	C15-H15A...O4B	0.93	2.59	3.43(3)	150

D=donor, A=acceptor, Res= Residue; Eqivalent position codes : a= 3/4-x, -1/4-y, z; b= x, y, z; c= 1-x, -1/4+y, -1/4+-z; d=3/4+x,-y, -1/4+z.

Conclusion

This chapter describes the syntheses of three square planar and five octahedral Ni(II) complexes of the ligands HL^1, HL^2, HL^4 and H_2L^5 and their characterizations by partial elemental analyses, molar conductivity and magnetic susceptibility

measurements, IR and electronic spectral studies. Crystal structures of $[NiL^1{}_2]\cdot DMSO$ and $[Ni(HL^2)_2](ClO_4)_2$ confirm the distorted geometries of the octahedral complexes.

References

1. N.C. Kasuga, K. Sekino, M. Ishikawa, A. Honda, M. Yokoyama, S. Nakano, N. Shimada, C. Koumo, K. Nomiya, J. Inorg. Biochem. 96 (2003) 298.
2. G.M. Sheldrick (1997) SHELXS97 and SHELXL97 Bruker AXS Inc., Madison, Wisconsin, USA.
3. L.J. Farrugia, J. Appl. Cryst. 30 (1997) 565.
4. A.L. Spek, J. Appl. Cryst. 36 (2003) 7.
5. M.B. Ferrari, F. Bisceglie, G. Pelosi, M. Sassi, P. Tarasconi, M. Cornia, S. Capacchi, R. Albertini, S. Pinelli, J. Inorg. Biochem. 90 (2002) 113.
6. G. DeVoto, M. Massacesi, R. Pinna, G. Ponticelli, Spectrochim.Acta, Part A 38 (1982) 725.
7. I. Garcý'a, E. Bermejo, A K. El Sawaf, A. Castineiras, D.X. West, Polyhedron 21 (2002) 729.
8. R. Roy, M. Chaudhury, S.K. Mondal, K. Nag, J. Chem. Dalton Trans. (1984) 1681.
9. D.K. Rastoh, K.C. Sharma, J. Inorg. Nucl. Chem. 36 (1974) 2219.
10. V. Philip, V. Suni, M.R.P. Kurup, M. Nethaji, Polyhedron 25 (2006) 1931.
11. P. F. Rapheal, E. Manoj, M. R.P. Kurup, E.Suresh, Polyhedron 2006, in press.
12. K. Nakamoto, Infrared and Raman Spectra of Inorganic and Coordination Compounds, 5th ed., Wiley-Interscience, New York, 1997.
13. P.S.N. Reddy, B.V. Agarwala, Synth. React. Inorg. Met-org. Chem. 17 (1987) 585.
14. P. F. Rapheal, E. Manoj, M. R.P. Kurup, Polyhedron, 2006, in press.
15. S. Chandra, L.K. Gupta, Spectrochim. Acta Part 62 A (2005) 1089.

16. D.N. Sathyanarayana, Vibrational Spectroscopy, New Age International, New Delhi (2004) 251.
17. N.C. Kasuga, K. Sekino, C. Koumo, N. Shimada, M. Ishikawa, K. Nomiya, J. Inorg. Biochem. 84 (2001) 55.
18. K.A. Ketcham, I. Garcia, E. Bermejo, J.K. Swearingen, A K. El Sawaf, E. Bermejo, A. Castineiras, D.X. West, Polyhedron 21 (2002) 859.
19. A. Sreekanth, S. Sivakumar, M. R. P. Kurup, J. Mol. Struct. 655 (2003) 47.

Syntheses of zinc(II) complexes and studies on their structural and spectral characteristics

7.1 Introduction

Zinc, the 23rd most abundant element in the Earth's crust, is mainly produced from the ore sphalerite (zinc sulfide) which contains roughly 40-50% zinc. Other minerals from which zinc is extracted include smithsonite (zinc carbonate), hemimorphite (zinc silicate), and franklinite (a zinc spinel). Zinc is the fourth most common metal in use, trailing only iron, aluminium, and copper. It is a bluish pale gray metal with atomic mass 65.409(4) g/mol and it melts at 692.68 K and boils at 1180 K. Smelting and extraction of impure forms of zinc was being accomplished as early as 1000 AD in India and China. By the end of the 14th century, the Hindus were aware of the existence of zinc as a metal separate from the seven known to the ancients. Strabo mentions it as *pseudo-arguros,* "mock silver". Zinc alloys must have been used for centuries, as brass goods dating to 1000–1400 BC have been found in Israel and zinc objects with 87% zinc have been found in prehistoric Transylvania. The manufacture of brass was known to the Romans by about 30 BC.

Zinc is an essential element, necessary for sustaining all life. In the human body, generally, 2-3 g of zinc is present and about 15 mg per day is necessary for the maintenance of healthy condition. It is estimated that about 3000 proteins in the human body contain zinc. It stimulates the activity of approximately 100 enzymes, which are substances that promote biochemical reactions in the body [1]. In addition, there are over a dozen types of cells in the human body that secrete zinc ions. Brain cells in the mammalian forebrain, cells in the salivary gland, prostate, immune system and intestine are the main types that secrete zinc. Zinc supports a healthy human immune system [2], is needed for wound healing [3], helps maintain the sense of taste and smell [4] and is needed for DNA synthesis. Zinc also supports normal growth and development during pregnancy, childhood and adolescence [5].

Functions of zinc in living systems may be summarized as follows:1) formation, growth and metabolism of cells; 2) healing of wounds; 3) activation and

secretion of hormones; 4) maintenance of neurotransmission system, ability of memory, normal carbohydrate and lipid metabolism, stability of retina and crystalline lens, sensitivity in taste and smell; 5) stabilization of cellular membranes; 6) maintenance and activation of immune system; 7) maintenance of normal alcohol metabolism; 8) reduction of hazardous effect of heavy metals. In these functions, zinc plays an essential role as zinc-containing enzymes in many cases or complexes formed with some components in biological systems.

Advantageous features of zinc in the above-mentioned functions and its applications for medical use are well explained by the following basic physicochemical aspects of zinc ion and its complexes. 1) Zinc ion has a small radius and acts as a Lewis acid and hence it can play an advantageous role as a catalyst in hydrolysis reactions. 2) The stability of zinc complexes with some ligands present in living system is satisfactorily high but not too high, so that zinc is reactive in complexation. This means high probability of ligand-exchange reactions in zinc complexes in living systems. Irving-Williams stability order applicable to various divalent metal complexes with common ligands shows that the stability of zinc complexes is generally lower than that of copper and is comparable to that of nickel and much higher than that of calcium or magnesium. 3) The bivalent state is stable because of the fully occupied $3d$ orbital, and it is maintained even in highly oxidizing and reducing environments. 4) Fairly high affinity is shown towards the main coordinating atoms such as sulphur, nitrogen, and oxygen. This means high flexibility in the structure, coordination mode, and coordination number of the complexes produced [6].

The electron configuration [Ar] $3d^{10}$ $4s^2$ provides a filled (n-1) d state for zinc. In view of the stability of the filled d sublevel, the element shows few of the characteristics of transition metals despite its position in the d-block of the periodic table. It resembles other transition metals in the formation of stable complexes with O, N and S-donor ligands and with ions like cyanide, halide etc. The d^{10} configuration affords no crystal field stabilization, which implies that the stereochemistry of a Zn^{2+} complex depends on the size and polarizing power of this ion. Because of this versatility towards different kinds of ligands and its flexibility towards coordination number ranging from two to six, the zinc(II) ion provides various types of chelate

complexes. Among theses complexes, some have attracted special attention as model compounds for the active sites of zinc-containing enzymes [7,8] and their functions strongly depend upon the coordination environment around the zinc ion. Therefore, for understanding or creating functional zinc complexes, it is important to consider the relationship of the coordination characteristics peculiar to the zinc ion. Heterocyclic carbaldehyde thiosemicarbazones have been extensively investigated for activity against various bacterial and viral infections [9,10]. Biological activity of thiosemicarbazones is found to increase on complexation with transition metals [11], higher activity being incorporated with substitution at N(4) position [12]. These observations were the impetus for us to build an N(4)-substituted thiosemicarbazone moiety on pyridine-2-carbaldehyde and synthesize zinc(II) complexes to study the coordinating behavior. In this chapter we describe the structural and spectral studies of five new Zn(II) complexes of the ligands HL^1 and HL^2.

7.2. Experimental

7.2.1. Materials

Zinc(II) nitrate hexahydrate, zinc(II) chloride, zinc(II) bromide and zinc(II) sulphate heptahydrate (Merck) were used as supplied. The solvents were purified by standard procedures before use.

7.2.2 Syntheses of ligands

Syntheses of the ligands HL^1 and HL^2 have been described earlier in Chapter 2.

7.2.3 Syntheses of complexes

7.2.4 Synthesis of $[Zn(HL^1)Cl_2]$ (36)

To a solution of 0.429 g (1.5 mmol) HL^1 in 15 ml hot methanol was added 10 ml of a methanolic solution of 0.204 g (1.5 mmol) $ZnCl_2$. The mixture was heated under reflux for one hour and cooled. The complex formed was filtered, washed thoroughly with water, methanol and then ether and dried *in vacuo* over P_4O_{10}. Crystals suitable for X-ray analysis were obtained by slow evaporation of a solution of the compound in methanol.

7.2.5 Synthesis of $[Zn(HL^1)_2](NO_3)_2$ (37)

To a solution of 0.429 g (1.5 mmol) HL^1 in 20 ml hot ethanol was added 10 ml of an ethanolic solution of 0.446 g (1.5 mmol) $Zn(NO_3)_2 \cdot 6H_2O$. The mixture was stirred for four hours. The complex formed was filtered, washed thoroughly with water, ethanol and then ether and dried *in vacuo* over P_4O_{10}.

7.2.6 Synthesis of $[Zn(L^2)Br] \cdot C_2H_5OH$ ***(38)***

To a solution of 0.427 g (1.5 mmol) HL^2 in 20 ml hot ethanol was added 10 ml of an ethanolic solution of 0.338 g (1.5 mmol) $ZnBr_2$. The mixture was heated under reflux for three hours and cooled. The complex formed was filtered, washed thoroughly with ethanol and then ether and dried *in vacuo* over P_4O_{10}.

7.2.7 Synthesis of $[Zn_2(L^2)_2SO_4] \cdot 2H_2O$ ***(39)***

To a solution of 0.568 g (2 mmol) HL^2 in 20 ml hot ethanol was added a suspension of 0.575 g (2 mmol) $ZnSO_4 \cdot 7H_2O$ in a mixture of 10 ml of methanol and 10 ml of ethanol. The mixture was stirred for 15 minutes. The complex formed was filtered, washed thoroughly with water, ethanol and then ether and dried *in vacuo* over P_4O_{10}.

7.2.8 Synthesis of $[Zn(HL^2)Cl_2]$ ***(40)***.

To a solution of 0.427 g (1.5 mmol) HL^2 in 20 ml hot methanol was added 10 ml of a methanolic solution of 0.204 g (1.5 mmol) $ZnCl_2$. The mixture was stirred for 15 minutes. The complex formed was filtered, washed thoroughly with water, methanol and then ether and dried *in vacuo* over P_4O_{10}.

7.3 Physical Measurements

Elemental analyses were carried out using a Vario EL III CHNS analyzer at SAIF, Kochi, India. Infrared spectra were recorded on a Thermo Nicolet AVATAR 370 DTGS model FT-IR spectrophotometer with KBr pellets at SAIF, Kochi, India. Electronic spectra were recorded on a Cary 5000, version 1.09 UV-Vis-NIR spectrophotometer from a solution in chloroform. Molar conductance measurements of the solutions of complexes in methanol (10^{-3} M) at room temperature were done using a digital conductivity meter at DAC, CUSAT, Kochi.

Table 7.1. Crystal refinement parameters of compound (36)

Parameters		
Empirical formula	$C_{14}H_{14}Cl_2N_4OSZn$	
Formula weight	422.62	
Diffractometer used	Siemens P4	
Radiation used, Wavelength	MoKα, 0.71073 Å	
Crystal system, Space group	Monoclinic, C2/c	
Unit cell dimensions	a = 31.737(5) Å	α= 90°.
	b = 7.727(1) Å	β= 118.58(1)°.
	c = 16.200(2) Å	γ = 90°.
Volume	3488.7(8) $Å^3$	
Z, Calculated Density	8, 1.609 mg/m^3	
Absorption coefficient	1.841 mm^{-1}	
F(000)	1712	
Crystal size	0.18 x 0.11 x 0.08 mm	
Max. and min. transmission	0.881 0.455	
Theta range for data collection	2.52 to 24.01°.	
Scan type	2θ-θ	
Scan speed	Variable, 2.0° to 45.0°/min. in ω	
Scan range (ω)	1.10° plus Kα separation	
Background measurement	Stationary crystal and stationary counter at the beginning and end of scan, each for 25.0% of total scan time	
Index ranges	$-36\le h\le 0$, $-8\le k\le 0$, $-16\le l\le 18$	
Reflections collected	2724	
Independent reflections	2676 [R(int) = 0.0543]	
Refinement method	Full-matrix least-squares on F^2	
Data / restraints / parameters	2676 / 0 / 208	
Goodness-of-fit on F^2	1.010	
Weighting scheme	$1/[\sigma^2(Fo^2)+(0.0555P)^2+0.00P]$,	
$P=(\max(F_o^2,0)+2*F_c^2)/3$		
Data to parameter ratio	12.86:1	
Final R indices, 1707 reflections [$I>2\sigma(I)$]	R_1 = 0.0524, wR_2 = 0.1052	
R indices (all data)	R_1 = 0.0994, wR_2 = 0.1232	
Largest diff. peak and hole	0.596 and -0.570 $e.Å^{-3}$	

7. 4 X-Ray crystallography

Single crystals of compound **36** for X-ray analysis were grown by slow evaporation of methanol solution of the complex. A brown shining crystal of **36** was mounted on a glass fibre with epoxy cement. The crystallographic data and structure refinement parameters for the compound are given in Table 7.1. The data were collected using a Siemens P4 CCD diffractometer equipped with graphite monochromated Mo Kα (λ = 0.71073 Å) radiation at temperature 293 K. The trial structure was solved using SHELXS-97 and refinement was carried out by full- matrix least squares on F^2 (SHELXL). Molecular graphics employed was ORTEP-III and PLATON.

7. 5 Results and discussion

The colors and partial elemental analysis data of the complexes are listed in Table 7.2. Molar conductivity measurements show that except **37** all of them are non-electrolytes, **37** being a 2:1 electrolyte. From the elemental analysis, the compounds **36** and **40** were assigned the empirical formulae *[Zn(HL^1)Cl$_2$]* and *[Zn(HL^2)Cl$_2$]* respectively, while **37**, **38** and **39** were assigned the formulae *[Zn(HL^1)$_2$](NO$_3$)$_2$*, *[Zn(L^2)Br]·C$_2$H$_5$OH* and *[Zn$_2$(L^2)$_2$SO$_4$]·2H$_2$O* respectively. The complexes **36**, **37** and **40** have ligands in the thione form, whereas **38** and **39** have ligands coordinated in the thiolate form as evidenced by the IR spectra. The complexes are found to be diamagnetic as expected for a d^{10} Zn(II) system.

Table 7. 2
Stoichiometries, partial elemental analyses, colors and molar conductivities of the complexes

Complex	Color	*λ_M	Found (Calc.)%			
			C	H	N	S
[Zn(HL^1)Cl$_2$] (**36**)	Yellow	64	40.15(39.78))	3.26(3.34)	13.24(13.26)	7.27(7.59)
Zn(HL^1)$_2$](NO$_3$)$_2$ (**37**)	Yellow	166	43.66(44.13)	3.88(3.70)	18.14(18.38)	8.29(8.42)
[Zn(L^2)Br]·C$_2$H$_5$OH (**38**))	Yellow	56	42.68(43.01)	4.28(4.46)	11.85(11.80)	7.20(6.75)
[Zn$_2$(L^2)$_2$SO$_4$]·2H$_2$O (**39**)	Yellow	43	43.24(43.43)	4.41(4.13)	13.25(13.51)	11.82(11.60)
[Zn(HL^2)Cl$_2$] (**40**)	Yellow	63	42.82(42.86)	3.70(3.83)	13.27(13.32)	7.74(7.62)

*10^{-3} M in DMF and expressed as ohm^{-1} cm^2 mol^{-1}

7.5.1 Infrared spectra

IR spectral assignments of the ligands HL^1 and HL^2 and the complexes are listed in the Table 5. The ν(S-H) band at 2570 cm^{-1} is absent in the IR spectra of these ligands but $\nu(^2N\text{-}H)$ bands are present at 3134 and 3129 cm^{-1} respectively for HL^1 and HL^2, indicating that the ligands remain as the thione tautomers in the solid state [19]. The bands corresponding to $\nu(^4N\text{-}H)$ appear at 3310 cm^{-1} for HL^1 and at 3374 cm^{-1} for HL^2. In the spectra of the complexes **36** and **37**, the $\nu(^2N\text{-}H)$ and $\nu(^4N\text{-}H)$ bands appear at 3214, 3211 cm^{-1} and 3448, 3439 cm^{-1} respectively indicating the coordination of the HL^1 in the thione form in these complexes [15]. In the spectra of **36**, **37** and **40**, the bands corresponding to the newly formed N=C bond $[\nu(^2N=^3C)]$ due to the enolization of the ligands are absent, while these bands are present at 1587 and 1590 cm^{-1} in the spectra of the complexes **38** and **39**. This observation combined with the shift of ν(N-N) frequency from 1079 cm^{-1} to 1058 and 1064 cm^{-1} in **38** and **39** respectively, supports the enolization of HL^2 into the thiolate form during coordination with the metal to form these complexes. The azomethine N band appearing at 1584 cm^{-1} in the spectrum of HL^1 is shifted to lower frequency of 1559 cm^{-1} in **36** and **37**, corroborating the coordination of azomethine nitrogen in these complexes [20]. The azomethine N band appearing at 1586 cm^{-1} in the spectrum of HL^2 is red shifted to 1567, 1566 and 1568 cm^{-1} in **38**, **39** and **40**, evidencing the coordination of azomethine nitrogen in these complexes also. In the far IR spectra of the complexes, the bands at 415-410 cm^{-1} assignable to $\nu(Zn\text{-}N_{azo})$ further confirms the coordination of the metal through azomethine nitrogen [14]. The bands at 1334 and 837 cm^{-1} in the spectrum of HL^1 and the bands at 1324 and 897 cm^{-1} in the spectrum of HL^2 are assigned to the C-S stretching and bending modes of vibrations. These bands also shift to lower energies showing thione sulfur coordination [21] in **36**, **37** and **40** and thiolate sulfur coordination in **38** and **39**. The bands at 325-380 cm^{-1} assignable to ν(Zn-S) in the far IR spectra of the complexes is consistent with sulfur coordination [14]. The out-of-plane and in-plane pyridine ring deformation bands observed at 401 and 613 cm^{-1} for HL^1 and at 406 and 622 cm^{-1} for HL^2 are shifted to higher frequencies in all the complexes showing the coordination of the pyridyl nitrogen [22]. This fact is further

supported by the appearance of bands at *ca.*198-228 cm^{-1} assigned to $\nu(Zn\text{-}N_{py})$, in the far IR spectra [23].

In the far IR spectra of **36**, **38** and **40**, the bands at 285 -220 cm^{-1} respectively assignable to ν(Zn-Cl) and ν(Zn-Br) show the presence of terminally coordinated chlorine and bromine.

Table 7. 3. Infrared spectral assignments (cm^{-1}) of thiosemicarbazones and their complexes

Compound	ν(C=N)	$\nu(^2N=^3C)$	ν(N-N)	ν/δ(C-S)	py(ip)	py(op)	$\nu(^2N\text{-}H)$	$\nu(^4N\text{-}H)$
HL^1	1584	----	1024	1334,837	613	401	3134	3310
$[Zn(HL^1)Cl_2]$ (**36**)	1559	----	1025	1302,832	640	412	3214	3448
$[Zn(HL^1)_2](NO_3)_2$(**37**)	1559	----	1029	1301,830	639	412	3211	3439
HL^2	1586	----	1079	1324,897	622	406	3129	3374
$[Zn(L^2)Br]\cdot EtOH$(**38**)	1567	1587	1058	1303,892	63.6	408	----	3422
$[Zn_2(L^2)_2SO_4]\cdot 2H_2O$(**39**)	1566	1590	1064	1311,885	620	410	----	3427
$[Zn(HL^2)Cl_2]$ (**40**)	1568	----	1056	1307,891	636	416	3270	3425

In the spectrum of the complex **37**, the absence of the combination bands ($\nu_1+\nu_4$) in the region 1700-1800 cm^{-1} rules out the possibility for coordinated nitrato group. The bands at 837 $cm^{-1}(\nu_2)$, 1385 $cm^{-1}(\nu_3)$ and 712 $cm^{-1}(\nu_4)$ clearly points out the uncoordinated nature of the nitrate group [24].

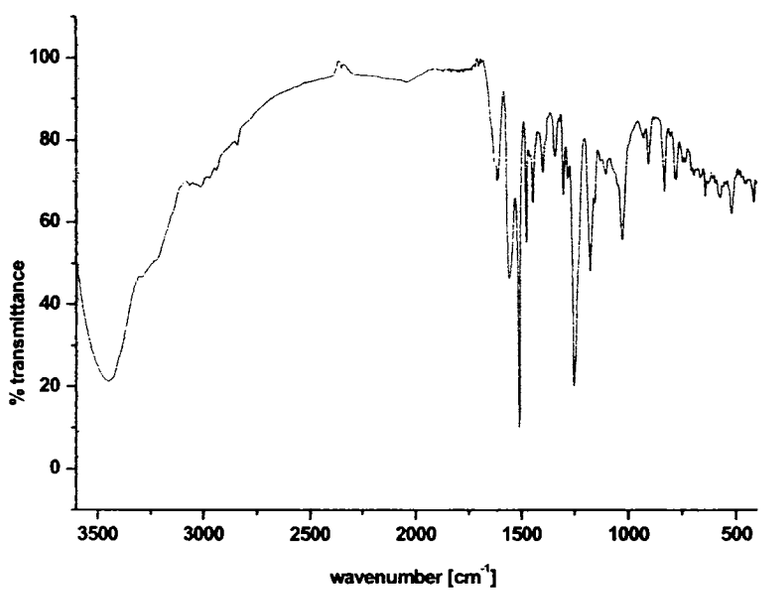

Fig. 7. 1. IR spectrum of $[Zn(HL^1)Cl_2]$ (36)

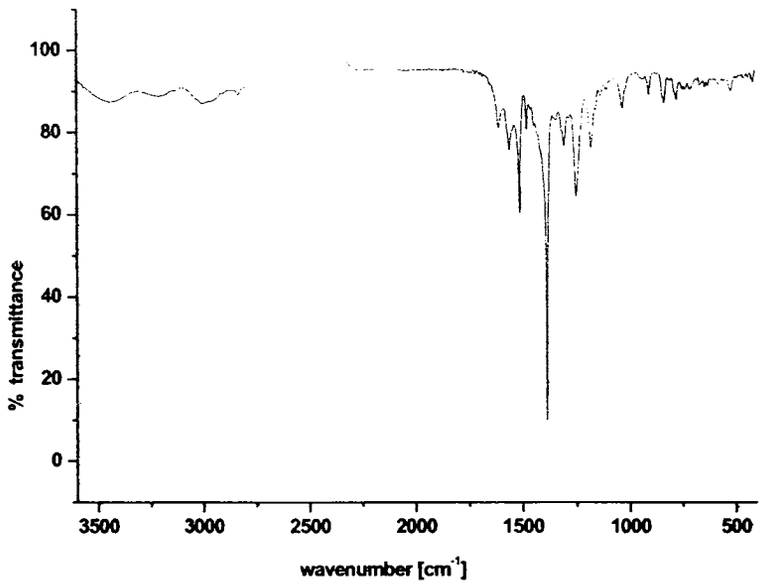

Fig. 7. 2. IR spectrum of $[Zn(HL^1)_2](NO_3)_2$ (37)

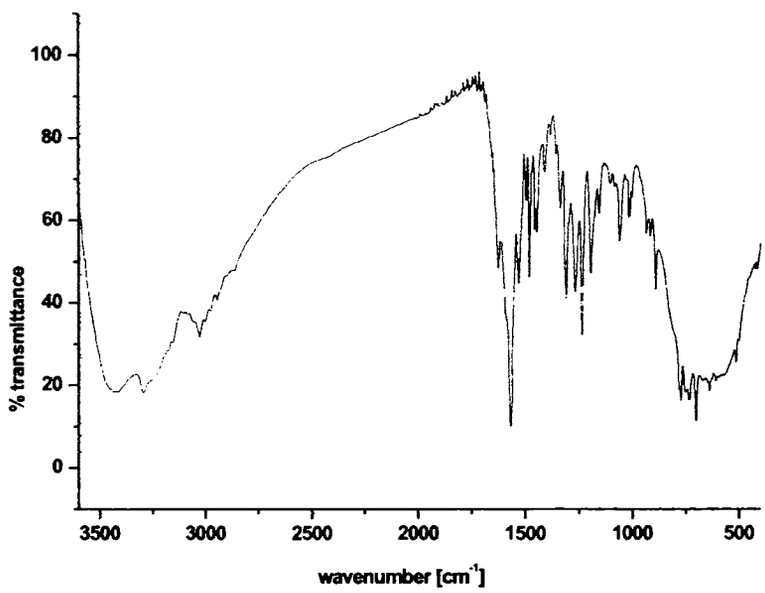

Fig. 7. 3. IR spectrum of $[Zn(L^2)Br]\cdot EtOH$ (38)

The IR spectrum of the complex **39** shows bands at 1198, 1119 and 1033 cm^{-1} that can be attributed to the ν_3 vibrations of the bridging bidentate sulphato group with

C_{2v} symmetry. The appearance of medium bands at 620 and 451 cm^{-1} and a weak band at 988 cm^{-1} assigned to ν_4, ν_2 and ν_1 vibrations is also in support of a bridging bidentate sulfato group [24,25]. According to Stefov *et. al*, coordinated water should exhibit bands at 825, 575 and 500 cm^{-1}. The absence of bands in these regions in the spectrum of **39** shows that the water molecules are not coordinated but are present as lattice water [26].

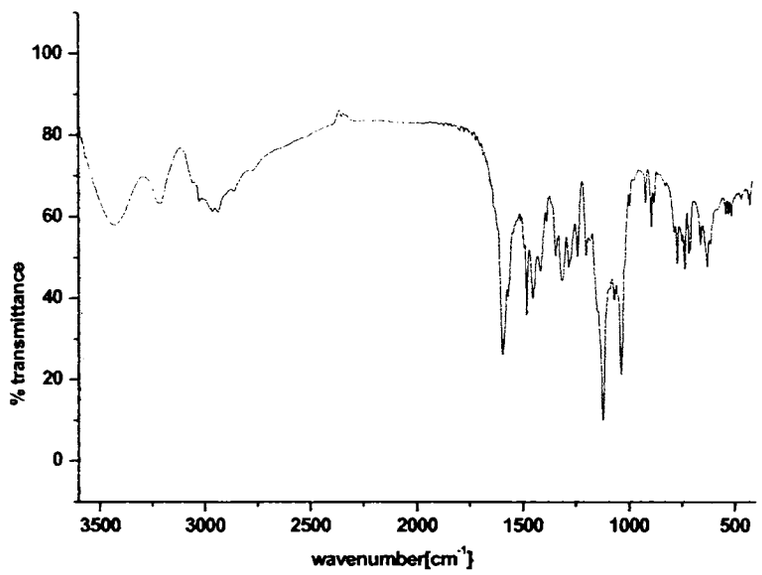

Fig. 7. 4. IR spectrum of $[Zn_2(L^2)_2SO_4]$ (39)

7.5.2 Electronic spectra

The electronic spectral assignments of the two ligands and the complexes are given in the Table 7.6. The electronic spectrum of the ligand HL^1 recorded in chloroform shows bands at 42730 and 30770 cm^{-1} assignable to $\pi \rightarrow \pi^*$ transitions of the phenyl ring and the thiosemicarbazone moiety [27] and $n \rightarrow \pi^*$ transitions of the azomethine and thioamide functions respectively. For HL^2, these bands appear at 42190 and 30960 cm^{-1}. The energy of these bands are slightly shifted on complexation. The complexes **36**, **37** and **40** show two $\pi \rightarrow \pi^*$ bands in the range 41490 – 40320 and 36900 - 35840 cm^{-1}. The $n \rightarrow \pi^*$ bands of these complexes are observed in the range 30960-28740 cm^{-1}, the shift showing donation of a lone pair of electrons to the metal by the coordination of azomethine nitrogen [28,29]. In the spectra of **38** and **39**, the bands appear at 42550, 42020 ($\pi \rightarrow \pi^*$) and 30390, 30960

($n \rightarrow \pi^*$) cm^{-1}. Spectra of all the complexes lack charge transfer bands. No appreciable absorptions occurred below 20000 cm^{-1} indicating the absence of *d-d* bands, which is in accordance with the d^{10} configuration of the Zn(II) ion.

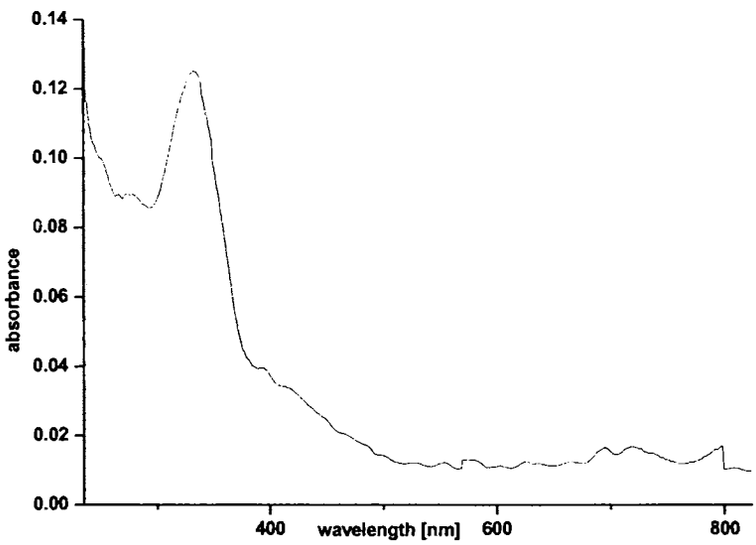

Fig. 7. 5. Electronic spectrum of $[Zn(HL^1)Cl_2]$ (36)

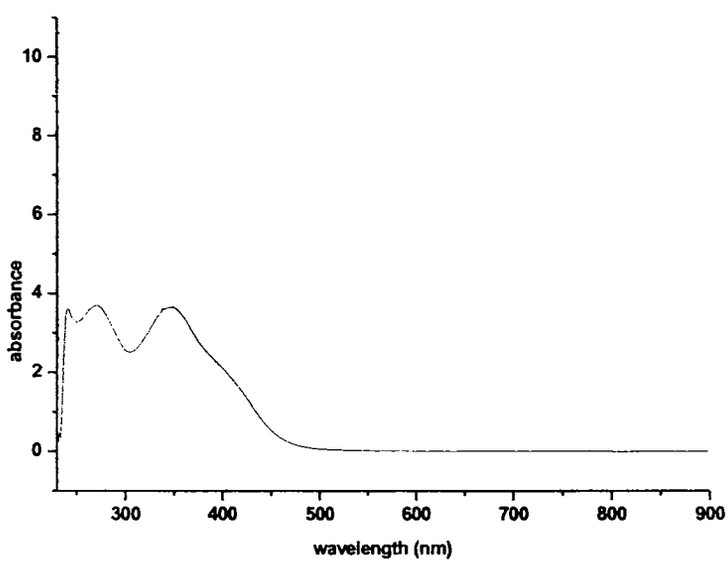

Fig. 7. 6. Electronic spectrum of the $[Zn(HL^1)_2](NO_3)_2$ (37)

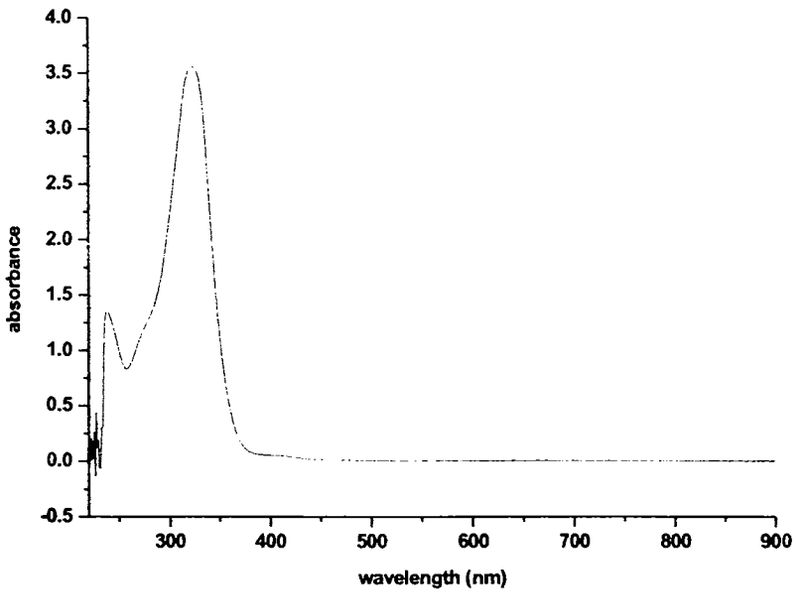

Fig. 7. 7. Electronic spectrum of $[Zn_2(L^2)_2SO_4]$ (39)

Table 7. 4. Electronic spectra (cm^{-1}) of thiosemicarbazones and their complexes

Compound	$\pi \rightarrow \pi^*$	$n \rightarrow \pi^*$
HL^1	42730	30770
$[Zn(HL^1)Cl_2]$ (**36**)	40320, 35840	29940
$[Zn(HL^1)_2](NO_3)_2$ (**37**)	41490, 36900	28740
HL^2	42190	30960
$[Zn(L^2)Br].C_2H_5OH$ (**38**)	42550	30390
$[Zn_2(L^2)_2SO_4].2H_2O$ (**39**)	42020	30960
$[Zn(HL^2)Cl_2]$ (**40**)	40650, 36360	30030

7.5.3 Crystal structure of $[Zn(HL^1Cl_2]$ (1)

The single crystal X-ray diffraction study of compound **36** indicates a five coordinate distorted square pyramidal geometry at the metal centre. The molecular structure of the compound along with atom numbering scheme is given in Fig. 7.8. The Zn(II) centre is coordinated by pyridine nitrogen N1, iminyl nitrogen N2 and thione sulfur S1 from the ligand HL^1 and by the chloro atom Cl1 form the basal plane (with a maximum deviation of -0.2392(1) Å for N2), while the second chloro atom Cl2 takes the apical position. The coordination of the ligand to metal results in two five membered rings involving Zn1. Of these, sulfur-involving ring is slightly puckered

and the other one is almost planar. The ligand HL^1 acts as a neutral ligand and the compound **36** is similar in several respects with the complex $[Zn(HAmpip)Br_2]$ where Ampip is 2-pyridine formamide 3-piperidyl thiosemicarbazone [13]. A deviation from square pyramid towards trigonal bipyramid is evidenced from the τ value of 0.187, comparable to 0.15 and 0.17 values seen in both the metal centres of $[Zn(Amhexim)(OAc)]_2$ [14] and a value of 0.25 as in $[Zn(HAmpip)Br_2]$ [13]. The Zn1 is displaced 0.5793(1) Å from the basal plane toward the Cl2 atom further indicating the distortion from square pyramid geometry. The thiosemicarbazone moiety comprising atoms C6, N2, N3, C7, S1 and N4 has a mean plane deviation of 0.037(6) Å for C6 and make angles of 8.4(3)° with the mean plane of pyridine ring and 9.0(3)° with the mean plane of phenylene ring.

Fig. 2

A list of relevant bond parameters of **36** is presented in Table 7.5. As in other 2-pyridine thiosemicarbazones, Zn-N_{im}, Zn-N_{py} and Zn-S bond lengths increase in that order [15]. However the Zn1-N1 distance is only slightly greater [0.006(7) Å] than Zn1-N2 distance and indicates both Zn1-N bonds are almost equal in strength.

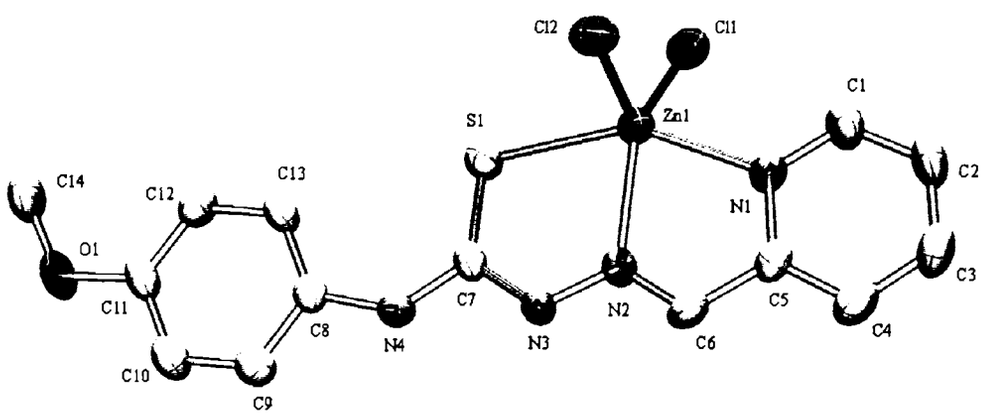

Fig. 7. 8. ORTEP diagram for the compound *[Zn(HL^1)Cl$_2$] (36)* in 50% probability ellipsoids. Hydrogen atoms are omitted for clarity

The Zn1-N1 distance is comparable with that in $[Zn(Amhexim)(OAc)]_2$ [14] and $[Zn(HAmpip)Br_2]$ [13]. However the Zn-N2 bond length is slightly greater [from

0.042(9) Å to 0.132(6) Å] than that found in [Zn(HAmpip)Br_2] [13]), [Zn(Amhexim)(OAc)]$_2$ [14], [Zn(Am4M)(OAc)]$_2$ [15], [Zn(PzAm4M)$_2$] [16] and [Zn(Ishexim)$_2$)] [17]. The bond length 1.673(6) Å of C7-S1 is slightly lesser than that [1.6895(18) Å] in pyridine-2-carbaldehyde thiosemicarbazone [18] confirms the coordination through thione sulfur.

The other bond lengths C7-N4, C7-N3, N3-N2 and N2-C6 are also comparable with the corresponding N(4)-unsubstituted thiosemicarbazone [18]. Interestingly, the C8 atom is in *cis* form with S1-(C8-N4-C7-S1) dihedral angle of -2.6(10) °) about N4-C7 bond. The intramolecular hydrogen bond C13-H13...S1 facilitates this *cis* form

Table 7. 5. Selected bond lengths and angles of the compound (36)

Bond lengths (Å)		Bond angles (°)	
Zn(1)-N(2)	2.170(5)	N(2)-Zn(1)-N(1)	74.01(18)
Zn(1)-N(1)	2.176(5)	N(2)-Zn(1)-Cl(1)	138.69(14)
Zn(1)-Cl(1)	2.2368(17)	N(1)-Zn(1)-Cl(1)	94.38(14)
Zn(1)-Cl(2)	2.3183(18)	N(2)-Zn(1)-Cl(2)	107.85(13)
Zn(1)-S(1)	2.5194(18)	N(1)-Zn(1)-Cl(2)	100.48(14)
S(1)-C(7)	1.673(6)	Cl(1)-Zn(1)-Cl(2)	113.26(6)
N(2)-C(6)	1.281(7)	N(2)-Zn(1)-S(1)	77.29(13)
N(2)-N(3)	1.351(6)	N(1)-Zn(1)-S(1)	149.89(14)
N(3)-C(7)	1.366(7)	Cl(1)-Zn(1)-S(1)	101.24(7)
N(4)-C(7)	1.338(7)	Cl(2)-Zn(1)-S(1)	96.76(7)
N(4)-C(8)	1.431(7)	C(7)-S(1)-Zn(1)	98.6(2)
		C(1)-N(1)-Zn(1)	126.7(4)
		C(5)-N(1)-Zn(1)	115.3(4)
		C(6)-N(2)-Zn(1)	118.0(4)
		N(3)-N(2)-Zn(1)	120.5(4)
		N(4)-C(7)-N(3)	111.7(5)
		N(4)-C(7)-S(1)	126.5(5)
		N(3)-C(7)-S(1)	121.8(4)

The packing of the molecule, shown in Fig 7.9 along the *c* axis, is interesting in many aspects. The main intermolecular hydrogen bonds are given in Table 7.6. The apical chlorine atom Cl2 is involved in intermolecular hydrogen bond with H3A-N3 and H4A-N4 of a second molecule (symmetry code; -x, 1-y, -z) and vice-versa. Similarly the oxygen atom O1 makes intermolecular hydrogen bond with H14A-C14 of a third molecule (symmetry code; -1/2-x, -1/2-y, -z) and vice versa, thus forming a C-H...O dimer ring. These mutual hydrogen bonds cohesion forms bimolecular network. Another intermolecular hydrogen bond C4-H4B...Cl1 (symmetry code; x, -

1-y, z-1/2) along with very weak π ... π stacking interactions (Table 7.6) involving phenyl and pyridyl rings reinforces the close packing.

Table 7. 6. H-bonding and π...π interactions in compound (36)

D-H...A	H...A (Å)	D...A (Å)	D-H...A(°)
N(3)-H(3A)...Cl(2)[a]	2.38	3.1663	152
N(4)-H(4A)...Cl(2)[a]	2.54	3.3298	154
C(4)-H(4B)...Cl(1)[b]	2.79	3.5034	135
C(13)-H(13A)...S(1)	2.59	3.2466	128
C(14)-H(14A)...O(1)[c]	2.48	3.3525	151
π... π	Cg...Cg (Å)	α(°)	β(°)
Cg(3)-Cg(4)[d]	4.6100	2.80	40.46
Cg(3)-Cg(4)[a]	3.7465	2.80	21.05
Cg(4)-Cg(3)[d]	4.6100	2.80	43.23
Cg(4)-Cg(3)[a]	3.7465	2.80	20.79

Cg(3)=N1,C1,C2,C3,C4,C5; Cg(4)= C8,C9,C10,C11,C12,C13.
D,donor; A, acceptor; Cg, centroid; α, dihedral angle between planes I and J; β, angle Cg(I)-Cg(J).
Equivalent position codes: (a) -x, 1-y, -z; (b) x, 1-y, -1/2+z; (c) -1/2-x, -1/2-y, -z; (d) -x, -y, -z.

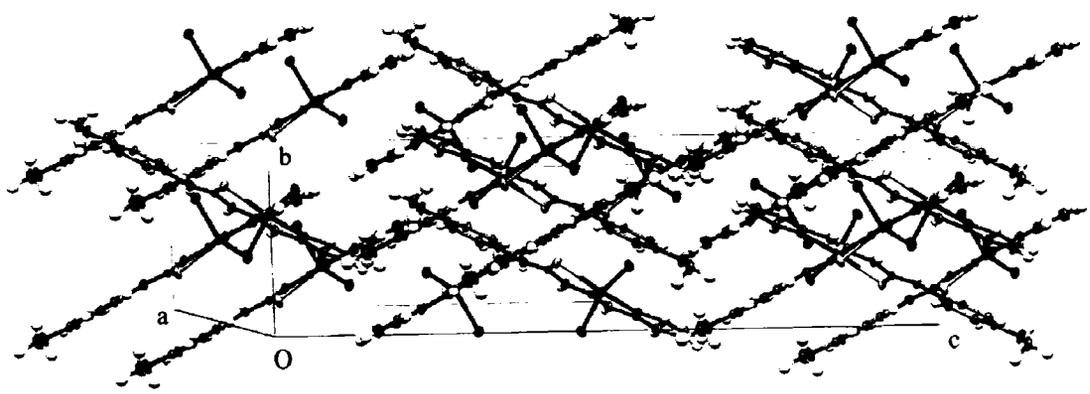

Fig. 7. 9. Packing diagram of the compound *[Zn(HL^1)Cl$_2$]* (36) along the c axis.

Conclusion

This chapter describes the syntheses and physico-chemical characterizations of five zinc(II) complexes of HL^1 and HL^2 by means of partial elemental analyses, molar

conductivity measurements, electronic, and infrared spectral studies. In the complexes of HL^1, the thiosemicarbazones are coordinated in the thione form, while complexes of HL^2 were formed through the coordination of both thione and thiol forms. The structure of the compound $[Zn(HL^1)Cl_2]$ has been solved by single crystal X-ray diffraction and was found to be distorted square pyramidal.

References:

1. H.H. Sandstead, J. Lab. Clin. Med. 124 (1994) 322.
2. N.W. Solomons, Nutr. Rev. 56 (1998) 27.
3. C.A. Heyneman, Ann. Pharmacother 30 (1996) 186.
4. A.S. Prasad, F.W. Beck, S.M. Grabowski, J. Kaplan, R.H. Mathog, Proc. Assoc. Am. Physicians 109 (1997) 68.
5. K Simmer, R.P. Thompson, Acta Paediatr. Scand. Suppl. (1985).
6. T. Matsukura, H. Tanaka, Biochemistry 65 (2000) 817.
7. G. Parkin, Chem. Commun. 1971 (2000).
8. M. Doring, M. Ciesielski, O. Walterand, H. Gorls, Eur. J. Inorg. Chem. (2002) 1615.
9. P. Malatesta, G. P. Accinelli, G. P. Quaglia, Ann. Chim. Rome 49 (1959) 397.
10. J. C. Logan, M. P. Fox, J. H. Morgan, A. M. Makohon, C. J. Pfau, J. Gen. Virol. 28(1975) 271.
11. D. X. West, A. E. Liberta, S. B. Padhye, R. C. Chikate, P. B. Sonawane, A. S. Kumbhar, R. G. Yerande, Coord. Chem. Rev. 123 (1993) 49.
12. D. L. Klayman, J .F. Bartosevich, T.S Griffin, C.J. Manson, J.P. Scovill, J. Med. Chem. 22 (1979) 885.
13. K. A. Ketcham, J. K. Swearingen, A. Castineiras, I. Garcia, E. Bermejo, D.X. West, Polyhedron 20 (2001) 3265.
14. E. Bermejo, A.Castineiras, I.G- Santos , D. X. West, Z. Anorg. Allg. Chem. 630 (2004) 1097.

15. I. Garcia, E. Bermejo, A. K. El Sawaf, A. Castineiras, D. X. West, Polyhedron 21 (2002) 729.
16. E. Labisbal, A. S- Pedrares, A. Castineiras, J. K. Swearingen, D. X. West, Polyhedron 21 (2002) 1553.
17. E. Labisbal, A. Sousa, A. Castineiras, J. A.G- Vazquez, J. Romero, D. X. West, Polyhedron 19 (2000) 1255.
18. Z. M. Jin, L Shen, L. He, H. Guo, H. T. Wang, Acta Cryst. E 59 (2003) o1909.
19. Y-P. Tian, W-T. Yu, C-Y. Zhao, M-H. Jiang, Z-G. Cai, H.- K. Fun, Polyhedron 21 (2002) 1217.
20. R.P.John, A. Sreekanth,V. Rajakannan, T.A. Ajith, M.R.P. Kurup, Polyhedron 23 (2004) 2549.
21. D. X. West, A. C.Whyte, F. D. Sharif, H. Gebremedhin, A. E. Liberta, Transition Met. Chem. 18 (1993) 238.
22. D. X. West, I. S. Billeh, J. P. Jasinski, J. M. Jasinski, R. J.Butcher, Transition Met. Chem. 23 (1998) 209.
23. K. Nakamoto, Infrared and Raman Spectra of Inorganic and Coordination Compounds, 5th ed., Wiley-Interscience, New York.
24. D. N. Sathyanarayana, Vibrational Spectroscopy, New Age International, New Delhi (2004) 400.
25. M. Joseph, V.Suni, M. R. P. Kurup, M. Nethaji, A. Kishore, S. G. Bhat, Polyhedron 23 (2004) 3069.
26. V.Stefov, V.M. Petrusevski, B. Soptrajanov, J. Mol. Struct. 293 (1993) 97.
27. A. Castineiras, E. Bermejo, D. X. West, L. J. Ackerman, J. V. Martinez, S. H. Ortega, Polyhedron 18 (1999) 1469.
28. N.C. Bhardwaj, R.V. Singh, Proc. Indian Acad. Sci. (Chem. Sci.) 106 (1994) 15.
29. E.W. Ainscough, A.M. Brodie, J. Ranford, J.M. Waters, J. Chem Soc., Dalton Trans. (1997) 279.

The discovery of *cis*-dichlorodiammine platinum(II) [cisplatin] and its subsequent use as a drug in the treatment of several human tumours stimulated the development of modern medicinal inorganic chemistry. Thiosemicarbazones (hydrazinecarbothioamides) are a family of compounds with beneficial biological activity *viz.*, anticancer, antitumour, antifungal, antibacterial, antimalarial, antifilarial, antiviral and anti-HIV activities. The biological activity depends on the parent aldehyde or ketone, presence of a bulky group at the terminal nitrogen and presence of an additional potential bonding site. The ability of thiosemicarbazone molecules to chelate with traces of metals in the biological system is believed to be a reason for their activity. Many thiosemicarbazone ligands and their complexes have been prepared and screened for their antimicrobial activity against various types of fungi and bacteria. The results prove that the compounds exhibit antimicrobial properties and it is important to note that in some cases metal chelates show more inhibitory effects than the parent ligands. The increased lipophilicity of these complexes seems to be responsible for their enhanced biological potency.

Adverse biological activities of thiosemicarbazones have been widely studied in rats and in other animal species. The parameters measured show that copper complexes caused considerable oxidative stress and zinc complexes behaved as antioxidants.

Thiosemicarbazones have applications in analytical field also. Some of the thiosemicarbazones produce highly colored complexes with metal ions. These complexes have been proposed as analytical reagents that can be used in selective and sensitive determinations of metal ions. Ferrocene derivatives containing thiosemicarbazone side chain have been used in positron annihilation lifetime (PAL) measurements.

Presence of C=N, make thiosemicarbazones exist as *E* and *Z* stereoisomers, the *E* isomer predominating in the mixture. This may be due to the fact that, the *trans* arrangement places the amine and azomethine nitrogen atoms in relative positions more suitable for intramolecular hydrogen bonding. Presence of NH-C=S group in

thiosemicarbazones can bring about thione–thiol tautomerism. In solution, thiosemicarbazones exist as an equilibrium mixture of thione and thiol forms. In most of the cases, thiosemicarbazones coordinate as bidentate ligands *via* azomethine nitrogen and thione/thiolate sulfur. When additional coordination functionality is present , they coordinate in a tridentate manner.

The work presented in this thesis aims on the syntheses of some novel thiosemicarbazone ligands and their transition metal complexes together with their physico-chemical characterization. The coordination geometries have been confirmed by X-Ray diffraction studies. The thesis is divided into seven chapters.

Chapter 1 deals with an extensive literature survey relating the history, applications and recent developments in the field of thiosemicarbazones and their transition metal complexes. A brief introduction to the various analytical methods is also furnished.

The discussion presented in Chapter 2 begins with the details regarding the syntheses of four N-N-S donor ligands *viz.*, pyridine-2-carbaldehyde N(4)-*p*-methoxyphenyl thiosemicarbazone (HL^1), pyridine-2-carbaldehyde N(4)-phenylethyl thiosemicarbazone (HL^2), pyridine-2-carbaldehyde N(4)-methyl, N(4)-phenyl thiosemicarbazone (HL^3), pyridine-2-carbaldehyde N(4)-pyridyl thiosemicarbazone (HL^4) and one O-N-S donor ligand, salicylaldehyde-N(4)-phenylethyl thiosemicarbazone (H_2L^5). They were characterized by partial elemental analyses, IR, electronic, and ^1H NMR spectral techniques. X-ray diffraction studies of the ligands HL^2 and HL^3 corroborate the spectral characterization. Single crystals of an interesting intermediate product (HL^4A) could be isolated during the synthesis of HL^4 and its structure was solved by X-ray diffraction.

Chapter 3 describes the syntheses and physico-chemical characterizations by partial elemental analyses, conductivity and room temperature magnetic susceptibility measurements and IR, electronic and EPR spectral studies of fourteen copper(II) complexes of the four NNS donor ligands and the ONS donor ligand. Of these, seven complexes are found to be binuclear, while the remaining are monomeric. The X-Ray

crystal structure determination of compound $[CuL^3Cl]_2$ reveals that the dimer consists of two square pyramidal Cu(II) centers linked by two chlorine atoms.

Chapter 4 deals with the syntheses and physico-chemical characterizations of five manganese(II) complexes of HL^1, HL^2 and HL^3. The coordination behavior was assessed by IR and electronic spectroscopy. EPR spectra of the complexes showed six-line hyperfine splitting with forbidden transitions. The structure of the compound $[MnL^1_2]\cdot H_2O$ was solved by single crystal X-Ray diffraction and is found to be distorted octahedral.

Syntheses and spectral characterizations of eight cobalt(III) complexes of the ligands HL^1, HL^2, HL^3 and H_2L^5 are discussed in Chapter 5. In all the complexes, the thiosemicarbazones are coordinated in the deprotonated thiolate form. All complexes are assigned octahedral geometries at the metal centre. The single crystal X-ray diffraction studies of $[CoL^1_2]NO_3$, and $[CoL^2_2]NO_3$ corroborate spectral characterization.

Chapter 6 includes syntheses and spectral characterizations of three square planar Ni(II) complexes and five octahedral Ni(II) complexes of the ligands HL^1, HL^2, HL^4 and H_2L^5. Crystal structures of $[NiL^1_2]\cdot DMSO$ and $[Ni(HL^2)_2](ClO_4)_2$ confirm the distorted geometries of the octahedral complexes.

Chapter 7 describes the syntheses and physico-chemical characterizations of five zinc(II) complexes of HL^1 and HL^2 by means of partial elemental analyses, molar conductivity measurements and spectral studies. In the complexes of HL^1, the thiosemicarbazones are coordinated in the thione form, while complexes of HL^2 were formed through the coordination of both thione and thiol forms. The structure of the compound $[Zn(HL^1)Cl_2]$ has been solved by single crystal X-Ray diffraction and was found to be distorted square pyramidal.